Distribution and impacts of contamination by natural and artificial radionuclides in attic dust and urban soil samples from two former heavy industrial Hungarian cities: A case study from Salgótarján and Ózd

by

Davaakhuu Tserendorj
Lithosphere Fluid Research Lab, Institute of Geography and Earth Sciences
Eötvös Loránd University, Budapest
PhD thesis
DOI: 10.15476/ELTE.2023.268

submitted to the
PhD Program of Environmental Earth Sciences, Doctoral School of Environmental Sciences
Eötvös Loránd University, Budapest
Director: Imre Jánosi†, DSc, Tamás Turányi, DSc
Program leader: Csaba Szabó, PhD, Zoltán Szalai, PhD

Supervisor:
Csaba Szabó, PhD
Lithosphere Fluid Research Lab, Institute of Geography and Earth Sciences,
Eötvös Loránd University, Budapest

Consultants:
Katalin Zsuzsanna Szabó, PhD
Nuclear Security Department, Centre for Energy Research, Centre for Energy Research
Péter Völgyesi, PhD
Nuclear Security Department, Centre for Energy Research, Centre for Energy Research

Budapest, August 2023

Table of contents

Lists of Acronyms and Abbreviations

ATSDR	Agency for Toxic Substances and Disease Registry
EPA	Environmental Protection Agency
HPGE	High Purity Germanium Detector
HDPE	High density Polyethylene
FOREGS	Forum of European Geological Surveys (now EuroGeoSurveys)
GEMAS	Geochemical Mapping of Agricultural Soils of Europe
IAEA	International Atomic Energy Agency
NORM	Naturally Occurring Radioactive Materials
PTE	Potential Toxic Elements
TENORM	Technologically Enhanced Naturally Occurring Radioactive Materials
UCC	Upper continental crust
UNSCEAR	Unite Nations Scientific Committee on the Effects of Atomic Radiation
WW2	World War 2

UNITS

Bq kg^{-1}	Becquerel per kilogram
Cps	Count per second
G	giga-annum (10^9 years)
mg kg^{-1}	µg/g = g/t = m/m %

List of figures

List of tables

1. Introduction and objectives

Radioactivity has become a major concern over the years because of its association with impact on public health (UNSCEAR, 2010). The primordial radionuclides (^{238}U (^{226}Ra), ^{232}Th and ^{40}K) are present in various degrees in all environmental spheres as naturally occurring radioactive materials (NORM). Human interventions (e.g., coal mining, coal-fired power plants, and related process) utilize, recover and dispose of these materials thereby creating technologically enhanced naturally occurring radioactive materials (TENORM), which can cause extra and enhanced radiation exposures (EPA, 2006). Furthermore, artificial radionuclides (e.g., ^{137}Cs) have been released through nuclear weapon tests (from the 1940s to 1980s) and major nuclear accidents such as Chernobyl, 1986, and Fukushima, 2011 (UNSCEAR, 2010). Studies of environmental liabilities (e.g., contaminated areas, waste basins) provide valuable knowledge about radiation risk assessment associated with exposure and dose (Ahmad et al., 2019).

The combustion of coal in coal-fired power plants (CFPP) leads to an increase in the concentration of primordial radionuclides in the by-productions (e.g., coal ash), which are released to the atmosphere and fall to the ground and onto surface water, resulting in a modification of the natural radioactivity background levels in surface soils. From the 1960s, numerous studies all over the world (e.g., Poland, China, Brazil) have been proposed to focus on contamination around CFPP (e.g., Eisenbud & Petrow, 1964; Bem et al., 2002; Flues et al., 2002; Lu et al., 2012; Papaefthymiou et al., 2013; Charro et al., 2013a, b; Tanić et al., 2016). Furthermore, in Ajka (a former industrial city in Hungary), several studies of radionuclide impact on soil samples around the local CPFF have been conducted (Papp et al., 2002; 2003; Zacháry et al., 2016). Considerably elevated activity concentration of ^{238}U and ^{226}Ra in soil were reported from the deposition of fly ash and other by-productions due to the prolonged use of local U-rich brown coal (Szabó, 1992). Most of these studies performed radioactivity measurements on surface soils around the local CFPP.

During coal combustion, the natural radionuclides concentrate in the residual by-products (e.g., coal ash) provide up to ten times greater activity concentration than the burnt coal (IAEA, 2003). A part of this by-product (< 100 μm grain size fraction) can easily be emitted to the atmosphere from spoil dumps and CFPP chimneys; this can then, reach residential areas through several transfer pathways (namely, in the atmosphere and water and via the food chain) in the biosphere (UNSCEAR, 2010). Therefore, spoil dumps are considered a potential risk to humans, since they can lead to increase in beyond the background level of natural radioactivity levels in the environment. Hence, it is obvious that dust particles emitted from CFPPs are

capable of entering houses through active and passive ventilation portals (e.g., open windows, cracks, and vents) and may then accumulate inside, together with house and street dust, especially in the undisturbed areas such as attics thus, the term attic dust (Cizdziel et al., 1999, 2000; Gosar et al., 2006). Since attic dusts are less subjected to environmental degradation (e.g., sunlight effects, decomposition by microbial influence, chemical weathering, ventilation, precipitation), they can be preserved in long-term deposits (Coronas et al., 2013). Accordingly, attics may be considered areas of long-term dynamic accumulation of material, influenced over decades only by the natural movement of air, penetration of the dust indoors (resupply), and settling on solid surfaces (Cizdziel et al., 2000); they should, therefore, be considered potential sources of radiation risk within urban areas (Cizdziel & Hodge, 2000). Undisturbed archived attic dust, which has recorded long-term pollution, has been used as a monitoring factor for certain highly potential toxic elements (e.g., Pb, Cd, As) (Cizdziel & Hodge, 2000; Davis & Gulson, 2005; Ilacqua et al., 2003; Sajn, 2005; Gosar et al., 2006; Völgyesi et al., 2014a; Balabanova et al., 2011; 2017; Painecur et al., 2022) and polycyclic aromatic hydrocarbons (Coronas et al., 2013; Wheeler et al., 2020) that suspected dominantly emitted from contamination sources to the ambient environment. Analysis of certain radionuclides (e.g., ^{137}Cs and ^{239}Pu) (Cizdziel et al., 1998, 1999; Tserendorj et al., 2022) has demonstrated that attic dust accumulates and preserves valuable information about changes in the degree of pollution of both global and local environments. Additionally, attic dust should also be considered a material hazardous to human health, particularly in areas with documented long-term pollution (e.g., heavy industrial zones and areas with extensive coal burning reflected by high levels of potential toxic elements (PTE) and the occurrence of specific PTE-bearing particles) (Gabersek & Gosar, 2022). Despite these, the presence of natural radionuclides in attic dust has not been studied yet. This fact makes it necessary to examine whether attic dust should be regarded as a cause of concern over the course of decades, and, if so, to what extent. In 1986, during the largest nuclear accident, in Chernobyl (now Ukraine, at the time a part of the Union of Soviet Socialist Republics), up to 85 PBq (1 PBq = 10^{15} Bq) of ^{137}Cs activity were released into the atmosphere (UNSCEAR, 2000a) over vast areas of Europe. The rate of the initial ^{137}Cs deposition, as is characteristic of this material, was strongly dependent on meteorological conditions during the first days after the event. A high level of radionuclide fallout was deposited mostly over the territory of what is today Belarus, northern Ukraine, and the European part of Russia (De Cort et al., 1998). Due to the changes in wind direction, the contaminated air masses were then transported rather towards the west and north-west,

reaching Poland and the Scandinavian countries. In the following days, however, the wind patterns changed substantially to southerly and eastern southeasterly, reaching this part of Europe, i.e., the area under consideration in this study (IAEA, 2006). Therefore, deposition rates from the radioactive cloud were not constant during its dispersal, especially in terms of wet deposition associated with rainfall at that time (De Cort et al., 1998; Beresford et al., 2016). From the atmosphere, ^{137}Cs adsorbs on precipitation and returns to lithosphere (i.e., pedosphere) or hydrosphere by wet and dry deposition as a component of radioactive fallout. The total activity of ^{137}Cs deposited in the present territory of Hungary attributable to Chernobyl was 0.15 PBq (De Cort, M. et al., 1998). As for the geographic distribution, slightly higher levels of ^{137}Cs activity were found in the northern and north-western parts of Hungary (1.35 – 2.15 Bq cm^{-2}) than over other areas (0.13 – 0.94 Bq cm^{-2}) based on 86 field (in situ) gamma-spectrometry measurements (De Cort, M. et al., 1998). Similar findings were reported by Szerbin et al. (1999) based on an additional 19 measurements. Activity concentrations of ^{137}Cs activity in the undisturbed upper 30 cm of soils in Pest County (Central Hungary) ranged between 0.5 and 61.1 $\pm$ 2.2 Bq kg^{-1} (Szabó et al., 2012). As reported by De Cort et al. (1998), airborne gamma radiation surveys were performed between 1963 and 1973 over Europe just prior to the Chernobyl accident, and at that time, the estimated total activity of ^{137}Cs was 20 kBq/m^2, and the activity concentration in Hungary was estimated at 2.5-3.0 kBq/m^2.

In the absence of washout effects, the ^{137}Cs became attached to airborne particles and was transported over distances of thousands of kilometres and depleted by dry deposition all over Europe (Balonova et al., 1996; De Cort et al., 1998). Both dry and wet deposition were affected by local surface properties, such as aerodynamic roughness, as determined by local surface topography and land cover (Van der Perk et al., 2002). Those aerosol and dust particles to which ^{137}Cs adhered were also capable of entering houses (e.g., through open windows, vents and cracks) in residential areas and accumulated inside and remained undisturbed in areas that are not easily accessible for regular cleaning, like attics (Ilacqua et al., 2003). In addition, deposition processes and activity within urban territories contributed to radionuclide redistribution and shifting atmospheric deposition, especially over the longer term. For this reason, undisturbed archived attic dust containing records of long-term pollution has been used as a monitoring factor for potential toxic elements (e.g., heavy metal(loid)s; (Davis & Gulson, 2005; Gosar et al., 2006).

Furthermore, anthropogenic activities (mining, manufacturing, industrial activities, etc.) have resulted in widespread metal(loid) contamination in urban areas that threatens the well-being

of residents and the environment. City areas covered by such contaminated soil include places where residents spend significant time for recreation (like parks and playgrounds). Hence, the investigation of such media is one of the most common ways to estimate the risk of the population. The principal increase in potentially toxic elements (PTE) occurs after their usage in various industrial products (e.g., pipes, steel, glass, paint, batteries, ammunition, etc.) due to their chemical and physical characteristics. The continuous accumulation of heavy metal(loid) contaminants changes the physical, chemical and biological properties of soils. The behaviour of PTE in the soil is controlled by various environmental parameters, including pH and redox potential, presence of Fe and Mn oxyhydroxides as well as organic material, etc. (Wu, et al., 2017). Additionally, the analysis of the radionuclides in urban soils and, more precisely in agricultural and forest soils (e.g., Charro et al., 2013b), is highly important given the direct connection between the soil and vegetation.

The goals of this thesis are to determine and identify the possible degree of enrichment and spatial distribution of U, Th, K and Cs and the levels of activity of three primordial radionuclides (^{226}Ra, ^{232}Th and ^{40}K) and one artificial nuclear fission production (^{137}Cs radionuclide) through the examination of samples of attic dust (undisturbed) and urban soil (disturbed) from two former industrial cities of Hungary, namely Salgótarján and Ózd. The overall objectives of this research are the following:

1. To compare the potential U, Th, K and Cs contamination of attic dust and urban soils locally (within cities) and regionally (between cities) in Hungary.
2. Evaluate the degree of enrichment and contamination of ^{226}Ra, ^{232}Th, ^{40}K and ^{137}Cs in attic dust and urban soils and determine their possible local sources. Determining the presence of radionuclides in attic dust, which provides information about any potential risk of and the pathway for the radionuclide contamination through urban areas. This study also offers a new perspective on and strengthens approaches to radionuclide studies of attic dust in the future.
3. Of particular interest in the case of ^{137}Cs is that, given its special origin, is the goal of obtaining a better understanding of the pathways of contamination in urban environments by means of attic dust.
4. To examine the influence of local sources and spatial distribution of the contaminants via the use of widely accepted statistical techniques and geostatistical mapping tools based on kriging.

5. To assess the risk to the population living in former industrialised areas (i.e., located near coal-fired power plants, iron and steel works, etc.) on the basis of estimating the dose rate and the annual outdoor effective dose in both cities.

2. Theoretical background to elemental synthesis and the origin of radioactivity

The elements and their isotopes present in our solar system and in other stellar systems are the products of energetic nuclear processes, which occurred in various astrophysical environments, beginning with the "Big Bang", the event that initiated the expansion of our Universe. In a general sense, the word "nucleosynthesis" refers to the different energetic astrophysical processes involved in the formation of the nuclides known to us (White, 2018). Tracking the current expansion of the universe back in spacetime, we see that the fusion of the primordial protons, and the subsequent stages of the fusion process (deuterium, helium-3, tritium, and helium-4, giving rise to the release of energy ($E = mc^2$), led to the formation of rapidly changing populations of subatomic particles, such as neutrinos, annihilating electron-antielectron, and neutrons, and energetic particle interactions such as neutron and proton capture and spallation, in a highly dynamic and energetic environment. This fusion resulted in the not only the formation of the products mentioned above, but also a small proportion of lithium-7. The nucleosynthesis of the remaining elements continued and continues today massive stars and supernova explosions, as well as spallation processes resulting from collisions between pre-existing nuclei and cosmic rays.

Radioactive decay is the result of a spontaneous change within the nucleus of an atom; it results in the emission of particles (alpha and beta particles) or and in many cases electromagnetic radiation (gamma rays). This decay is behind three phenomena: 1/ the emission of high energy radiation that may be harmful to living organism exposed to it, 2/ the release of decay energy that accounts for the internal heating of Earth's core, and 3/ the generation of daughter nuclides can be used for geochronology (White, 2018; Gilmore et al., 2008; Lilley et al., 2001). There are various reasons why naturally unstable isotopes were found in the environment:

1) Long-lived isotopes: some radioactive nuclides that have very long half-lives were created during the formation of the solar system (~ 4.6 billion years ago) and nuclear energy production for civil and defence purposes (including the whole fuel cycle from uranium mining, fuel fabrication, reactor operation, reprocessing, etc), the fabrication of nuclear weapons, radioisotope production, and their use in industrial processes, e.g., industrial radiography,

sterilisation, medical diagnostics; further, it was these that were involved in reactor accidents, and which are present in the re-entry into the atmosphere of satellites, some of which carry on board small fission reactors (De Cort et al., 1998). Furthermore, a significant number of nuclear tests were carried out between 1945 and 1964, but after Limited Test Ban Treaty, test were conducted mainly underground (or underwater), in all types of settings: ~25 % in the atmosphere, 75 % underground and 3 % underwater; Prăvălie, 2014). Approximately 90 % of these tests were conducted in the northern hemisphere, especially by the USA, Russia (USSR), and China, and the other 10 % (~ 208 tests) in the southern hemisphere by France and the UK (Prăvălie, 2014). Consequently, the northern hemisphere is more contaminated than the southern as a result of the presence of large quantities of radioactive isotopes (e.g., ^{3}H, ^{14}C, ^{90}Sr, ^{137}Cs) released into the atmosphere in fallout (UNSCEAR, 2000b). It is important to note that NPP catastrophes like Chernobyl (1986) was caused by elevated radiation in the northern hemisphere. Therefore, environment has always been radioactive and certain level of radioactivity, and this natural radiation accounts for up to ~80 % of the annual dose received by the population, whereas medical procedures are the source of most of the remaining ~20 %. Less than 1% of exposure is due to the fallout from past testing of nuclear weapons or the generation of electricity in nuclear power plants, as well as from coal power plants (Cinelli et al., 2019). Although public concern about radioactivity is mainly focussed on man-made sources of radiation, particularly nuclear facilities, by far the largest contribution to public exposure is natural in origin, being present because of long-lived isotopes and their decay processes.

2.1 Exposure pathways of external and internal radiations

Radionuclides may be subjected to biogeochemical processes and this, together with transportability, can influence the environment through bioaccumulation, with the results being hazardous to the environment and humans (Ahmad et al., 2019). Primordial radionuclides are present in the atmosphere, having either terrestrial or cosmogenic origin, and can be inhaled directly by humans or removed from the air by other pathways. These particles can be washed out from the atmosphere when air currents cannot keep them suspended, or during precipitation, and may be deposited in water, on the soil, or on any kind of surface. These particles may subsequently return to the atmosphere by resuspension, which occurs when wind or some other natural or human activity generates clouds of dust containing these radionuclides, or through water evaporation (Cinelli et al, 2019). Thus, we can see that our environment causes an external radiation dose to the human organism due to cosmic radiation and radiation from

terrestrial radionuclides present in soil, rocks and building materials etc. (UNSCEAR, 2010; Cinelli et al, 2019). Furthermore, it should be noted that radionuclides are easily absorbed into the food chain through these processes. Plants are capable of absorbing radionuclides just as well as minerals. Animals consume plants and water, and therefore any radionuclides found in these sources will end up in their bodies. Subsequently, water, plants and animals will be consumed by humans, and natural radionuclides enter the human organism, causing internal exposure (UNSCEAR, 2010; Cinelli et al, 2019). We are exposed to radiation in our everyday lives without realising it because radiation dose limits have historically focused exclusively on human health protection. The unit of radiation exposure doses a person receives is given in Sieverts (*Sv*), and the larger effects of radiation to which the human body is exposed, the higher the value. An estimated value of world-wide average annual public exposure to natural radiation sources remains at 2.4 mSv y^{-1} (UNSCEAR, 2010). Despite this, radiation exposure can also vary depending on local geology, as also on altitude, with a range between 1 and 10 mSv y^{-1}, and indeed even going as high as 50 mSv y^{-1} (e.g., Brazil and Sudan average exposures up to about ~40 mSv y^{-1}) (Link 1). Exposure to increased levels of radiation can be harmful to human health, and radiation can also can ionise or excite atoms while passing through the tissues thereby altering the structure of the cells. The effects of radiation can be divided into two ways, deterministic and stochastic. Deterministic effects are characterised by a threshold beneath which no cell damage is to be observed, while above it, cell damage increases with dose rate (mSv). Radiation effects may result in acute radiation exposure syndrome immediately after irradiation, and yet induce no cancer (Cinelli et al., 2019). The stochastic effects of ionising radiation are chance events, with the probability of the effect increasing with dose rate, but severity of the effect is independent of the dose received. It is primarily to this kind of effect that cancer risk and genetic disorders are related (Cinelli et al., 2019). There is no threshold in stochastic effects; whether there are any noticeable effects in the human body as result of radiation exposure depends on the type of radiation exposure (i.e., internal or external, whole-body or local, and which area of body was exposed in the event of local exposure, furthermore, the radiation dose rate and exposure period (Link 2). Although ^{238}U (^{226}Ra) and ^{232}Th are α emitters and are characterised as radiotoxic isotopes, usually only relatively low doses are likely to be received from any pure ^{238}U and ^{232}Th sources because of their long half-life. Additionally, the estimated global average annual per capita effective dose due to atmospheric nuclear weapons testing was highest in 1963 (0.11 mSv y^{-1}), and subsequently declined to less than 0.006 mSv in 1990s. Because of this, radiation exposure

from man-made sources is still primarily caused by nuclear tests conducted some decades ago (UNSCEAR, 2010).

2.2 Geochemistry of elements studied and their radionuclides

2.2.1 Uranium (U, ^{226}Ra)

Uranium (U) is a refractory lithophile metallic element in the actinide series of the periodic table, with atomic number 92, and an atomic weight of 238.0289. The specific gravity of U is 18.95 g/cm^3, which makes it the fourth in line with respect to density after Pt, Au, Os and W. Uranium is a pyrophoric metal when finely ground. It is malleable, ductile and slightly paramagnetic (White, 2018).

In nature, the two common valence states are tetravalent (+IV) under reducing and hexavalent (+VI) under oxidising conditions. Uranium is highly mobile and soluble under near-surface oxidising conditions. Under most conditions, U geochemistry is controlled by redox conditions, pH, carbonate concentrations and sorption capacity. On the surface of the Earth (i.e., in an oxidative environment), U is present predominantly in U^{6+} in the form of UO_2^{2+} (uranyl ion) and its associated hydroxyl complexes for low pH values, which is also the most stable and mobile form. In anaerobic conditions, it can reduce to the U^{4+} state in $U(OH)_4$ and $U(OH)_3$ where it is insoluble and therefore far less mobile than U^{6+} (Bourdon et al., 2003), or it will react with sulfide, forming a solid phase. At neutral pH, U^{4+} can precipitate as UO_3*$2H_2O$. Under saturated conditions, U^{6+} can readily adsorb to iron (III) oxyhydroxides (ferrihydrite, goethite, hematite) and clay minerals (Singh, 2010).

Isotopes and decay series: Naturally occurring uranium isotopes are ^{238}U ($T_{1/2}$ = 4.468 $\pm$ 0.0048 G years, 99.2745 % of total U mass) and ^{235}U ($T_{1/2}$ = 0.70381 $\pm$ 0.00096 G years, 0.720 % of total U mass). Both decay in their own ways through extended and complex radioactive decay series, ending in stable ^{206}Pb and ^{207}Pb (Figure 1), respectively. Furthermore, ^{234}U ($T_{1/2}$ = 245, 250 $\pm$ 490 years, 0.0055 % of total natural U) is a decay product of ^{238}U, and its natural abundance is a reflection of the radioactive equilibrium with ^{238}U. Additionally, with a mass number ranging from 227 to 240 several U isotopes (e.g., ^{231}U) exist, though, their short half-lives exclude any natural occurrence (Vivo et al., 1984). The ^{238}U-series terminates in the stable isotope ^{206}Pb, and during this decay (Figure 1), eight alpha particles are released. The ^{235}U decay series ends in the stable isotope ^{207}Pb, and seven alpha particles are released (Figure 1). If the decay chain is undisturbed, it reaches a steady state called secular equilibrium, and the abundance of short-lived intermediate nuclides is then controlled by their half-lives ($T_{1/2}$). However, this secular equilibrium can be perturbed by physical or chemical processes (e.g.,

crystallisation/precipitation, water-rock interaction, or nuclear properties) that lead to a fractionation between isotopes of the U decay (White, 2018). This disintegration (decay) probability is a fundamental property of an atomic nucleus and remains equal over time (Lilley, 2001; Gilmore, 2008). This type of alpha decay is related to heavy nuclei with, Z $\geqslant$ 82 (Lilley, 2001), which emit nucleus $({}^{4}_{2}He)^{+}$ during decaying. Radium-226 to ^{222}Rn (${}^{226}_{88}Ra \rightarrow {}^{222}_{86}Rn + {}^{4}_{2}He + Q$) is accompanied α energy release of 4.484 MeV (Figure 1). A fixed quantity of energy, Q, equal to the difference in mass between the initial nuclides and final products, is released. This energy must be shared between the Rn and He in a definite ratio because of the conservation of momentum (Gilmore, 2008).

Radium has no stable or long-lived isotopes and exists in nature only because it is continually produced by radioactive decay, ultimately of U and Th. Its longest-lived and consequently most abundant isotope, ^{226}Ra ($t_{1/2}$ = 1599 years; common valences: 2^{+}), is part of the ^{238}U decay series chain and the daughter of ^{230}Th (Figure 1). Concentrations in the silicates of the Earth's crust listed here assume ^{226}Ra is in secular radioactive equilibrium with ^{238}U; other isotopes are orders of magnitude less abundant. Based on the extent of radioactive disequilibrium between parent and daughter nuclides, Ra isotopes, like other nuclides in the U-series decay chain, can be useful geochronological tools particularly useful in magmatic processes (White, 2018). The radionuclide ^{226}Ra is a natural component of the environment, and may also be of anthropogenic origin, coming mainly from phosphate and potassium fertilisers, radioactive waste, luminising wastes, coal combustion, and cement factories. Uranium mining and processing is also a significant source of ^{226}Ra. The mean concentration of ^{226}Ra in coal is of the order of 1 Bq g^{-1} and soil surrounding coal-fired power plant. Radium has no biological function; its toxicity derives from its radioactivity. As an alpha-emitter (Figure 1), it is particularly damaging to tissue when inhaled or ingested. Of particular interest is the case where ^{235}U undergoes nuclear fission, when the nucleus takes up a neutron to become ^{236}U (${}^{235}_{92}U + {}^{1}_{0}n = {}^{236}_{92}U$), and due to its unstable nature, splits apart. This kind of decay, the transition of an excited nucleus to a lower energy state or to the ground state by the emission of γ -radiation (photons), is not considered a process of disintegration, but rather de-excitation (Lilley, 2001).

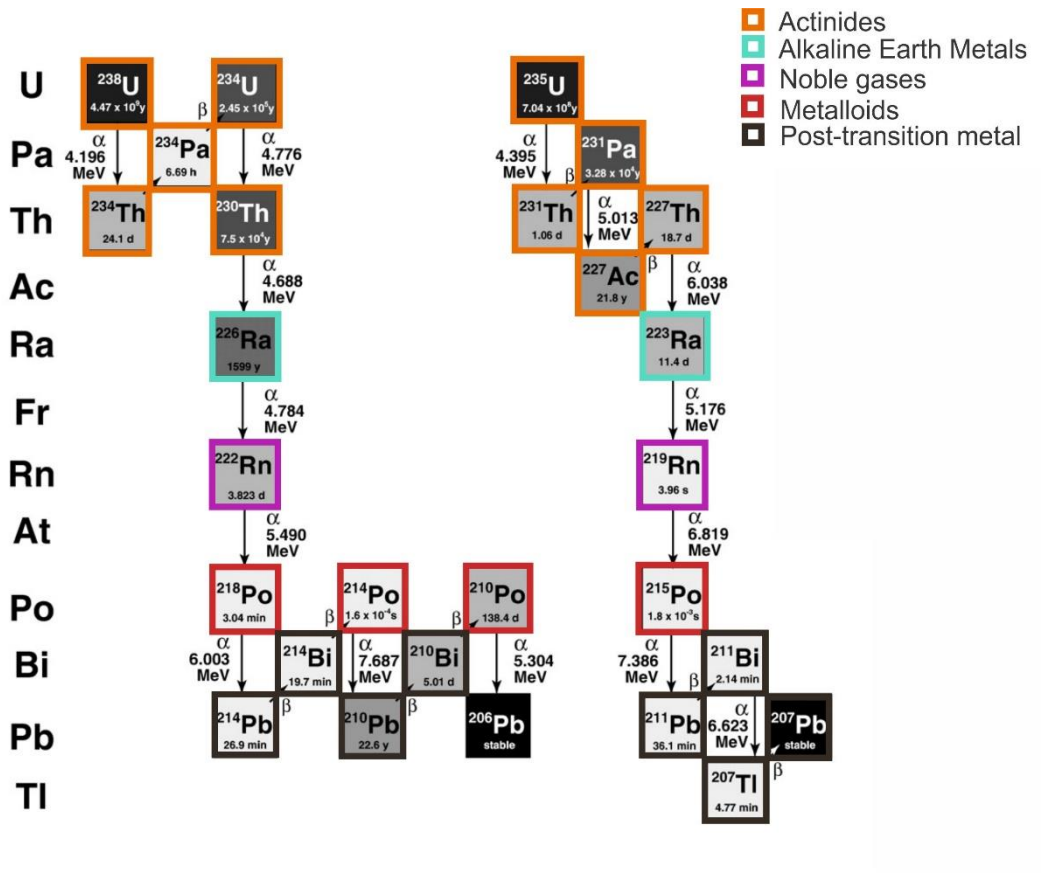

Figure 1. Schematic diagram of ^{238}U and ^{235}U decay series. The grayscale indicates half-life, with darker greys for longer half-lives (Bourdon et al., 2003).

Distribution in minerals, rocks: Due to its large ionic radius and high charge, uranium is not easily incorporated into the crystal structures of common rock-forming silicates (White, 2018). There are 2 major factors that influence the U content in the environment (*i*) detrital source mineralogy, and (*ii*) the redox chemistry of U, which is strongly influenced by the geochemical processes operating during the weathering of source rock and sediment transport within the depositional environment and during subsequent burial diagenesis. The geochemical particularities of elevated U concentrations are to be expected in metamorphic (sedimentary) rocks, and as ore deposits in sedimentary rocks rich in organic matter (Cinelli et al., 2019). Taken together, these facts mean that in general at a given oxidation state, the heavier actinides like U will be more easily incorporated in minerals than the lighter ones, like Th (Bourdon et al., 2003). Therefore, the main ore minerals for U are pitchblende (UO_2 and UO_3) and uraninite (UO_2 and UO_3); theoretically, these two contain up to 85% of uranium. However, the majority of U-bearing minerals contain U in only small or trace amounts (Singh, 2010). The median U concentration in the upper continental crust (UCC) is 2.7 mg kg^{-1} (Rudnick & Gao, 2004).

According to the FOREGS dataset, total U concentration (mg kg^{-1}) varies from <0.1 to 30.3 in subsoils and from 0.2 to 53.2 in topsoil, with a median of 2.0 and 2.0, respectively (Salminen et al., 2005). At the same time, elevated U concentrations in subsoil occur in relation with granitic rocks.

Uses of uranium: Due to its heavy weight U is used for inertial guidance devices, gyrocompasses, and as ballast in missile re-entry vehicles. Armour-piercing munitions and tank armour both use so-called depleted uranium (depleted ^{235}U). To create high-energy X-rays, pure U is also employed as an X-ray target. Enriched U metal has higher than natural abundance of ^{235}U and is as fuel for nuclear reactors (White, 2018). It should be noted that, the naturally occurring uranium isotopes (^{238}U(^{226}Ra)) have both been concentrated in certain environments which may be accessed by humans or have been uncovered during human activities such as manufacturing, mineral extraction, mining, and coal-production processing. Four primary sources of industrial activities can enhance certain elements of the environment, including soil, sediment and water, and the biosphere with U: (1) nuclear fuel cycle from U mining to water processing; (2) the military use of depleted U; (3) the production of coal, and (4) the agricultural use of phosphate fertilisers (Garnier et al., 2001).

Toxicity: U is a radiotoxic and a carcinogen element, and its harmfulness is principally considered to lie in its radioactivity and that of its decay products rather than in its chemistry. Three types of radiation to which humans and other life forms are exposed derive from U: firstly, external, essentially from U and its decay products present in rocks and soils; secondly, internal, from the ingestion of food and drinking water containing trace amounts of U and/or radium; and thirdly, the inhalation of dust particles containing ^{238}U decay products (Figure 1) like radon. Intake levels of 20-40 mg U can result in kidney damage and even failure (White, 2018). The long-term retention in the lungs of large quantities of inhaled insoluble U particles can lead to serious respiratory problems, as many seen on the Agency for Toxic Substances and Disease Registry toxicity lists (ASTDR, 2013).

2.2.2 Thorium (Th, ^{232}Th)

Thorium (Th) is a refractory, lithophile and an actinide series element with the atomic number 90, and an atomic weight of 232.038. The density of the pure metal form is 11.72 g/cm^3. When pure, thorium is a silvery-white metal that is air-stable and retains its lustre for several months. When contaminated with the oxide, thorium slowly tarnishes in air, becoming grey and finally black. The metal is incredibly ductile, very soft and rollable. Its purity determines its characteristics, and the most prevalent impurity is oxide, which makes the substance more

brittle (White, 2018). Thorium is electropositive, has only one oxidation state, and in solution it is present as Th^{4+}. However, the ionic radius of Th results in behaviour as a trace metal in solids which is quite different to that of Zr or Hf. Thorium metal can be dissolved easily in concentrated hydrochloric acid or in aqua regia (White, 2018). Under all environmental conditions Th displays low mobility, mainly due to the high stability of its insoluble oxide (ThO_2) and the strongly resistant nature of its ore minerals. Thorium cannot be oxidised to a stable cation equivalent to the highly mobile uranyl ion UO_2^{2+}. The soluble species $Th(SO_4)^{2+}$ may form pH < 3 under aerobic conditions. Any Th released into solution will be rapidly associated by clay minerals and hydrolysed to the hydrous oxide $Th(OH)_4$, which will be intimately associated with the clay mineral fraction (Salminen et al., 2005).

Isotope and decay series: Thorium has six naturally occurring isotopes, and of all known radioactive isotopes of Th, ^{232}Th has the longest half-life ($1.41*10^{10}$ years) and comprises 99.98 % of the total Th mass. It is estimated to be about three times more abundant than U in the Earth's crust (10.5 mg kg^{-1}; Rudnick & Gao, 2004).

Table 1. Thorium isotopes and their use in geosciences.

Isotope	Half-life	Decay	Parent	Application
^{234}Th	24.1 days	β	^{238}U	Elemental scavenging, particle/carbon fluxes in the oceans, particle mixing
^{232}Th	14.01 Gyr	β	Th	Trace element, Pb isotope
^{230}Th	75.584 (±110) year	β	^{234}U	Elemental scavenging, sediment dating, coral growth dating, magma chamber dynamics, melt transport
^{228}Th	1.912 (±0.002) year	β	^{228}Ac	Particle/carbon flux in the oceans
^{227}Th	18.72 days	β	^{227}Ac	Particle/carbon flux in the oceans

The decay chains of natural Th and U give rise to minute traces of ^{228}Th (half-life: 1.912 (± 0.002) year, ^{230}Th (half-life: 75.584 (±110) year); and ^{234}Th (half-life: 24.1 days), however the presence of these mass terms is negligible (Table 1; Figure 2). Thorium-232 decays to the stable Pb isotope ^{208}Pb (Figure 2).

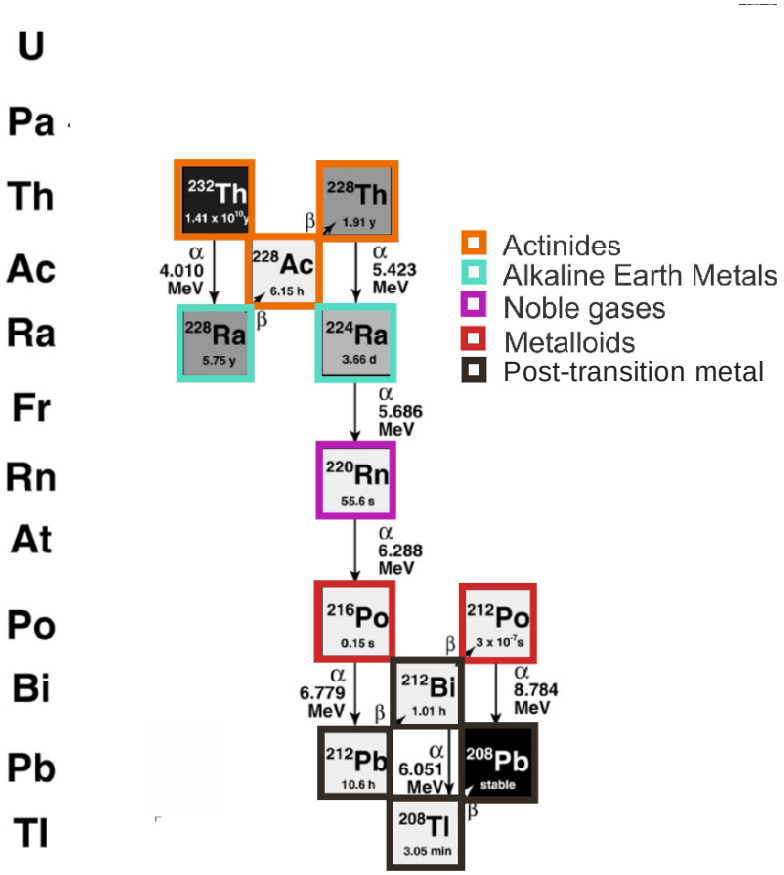

Figure 2. Schematic drawing of ^{232}Th decay series. The grayscale reflects the half-life, with darker greys for longer half-lives (Bourdon et al., 2003).

Distribution in minerals, rocks: Thorium is mainly present at minor to trace concentration levels (< 1 g/100 g) in minerals such as zircon and apatite, and it is a major component (> 1 g/100 g) in monazite ((Ce, La, Nd, Th), (PO_4)) and the rare minerals thorite ($ThSiO_4$) and thorianite (ThO_2). Because of its sensitivity to magmatic differentiation and concentration in the late stages of crystallisation, it is enriched in granitic rocks. Thorium is immobile and tends to be geochemically separated from mobile mineral fractions (e.g., U) during weathering and the alteration of primary minerals from igneous parent rocks.

Thus, Th concentrates in resistant detrital heavy minerals (e.g., zircons, monazite, apatite, etc.); or if released during weathering, it is strongly adsorbed by clay minerals and iron and manganese oxyhydroxides (Cinelli et al., 2019). The median concentration of Th at the UCC is 10.5 mg kg^{-1} (Rudnik & Gao, 2004). According to the FOREGS dataset the median Th content is 8.0 mg kg^{-1} in subsoil and 7.2 mg kg^{-1} in topsoil; the range varies from <0.1 to 71.7 mg kg^{-1} in subsoil and 0.3 to 75.9 mg kg^{-1} in topsoil. The average ratio of top/subsoil is 0.925. Th normally has a higher background in granite, gneiss and alkaline rock in northern Europe

as a result of climate or pH-determined paedogenic processes, particularly leaching (Salminen et al., 2005). Thus, Th sub- and topsoil are similar in Europe.

Uses of thorium: Th (and U) mining, milling and processing, phosphate rock processing and phosphate fertiliser production, and coal-fired power plant utilities and industrial boilers are the primary anthropogenic sources of thorium in the environment (ASTDR, 2017).

Toxicity: It has no biological function, but is rather chemo toxic, radiotoxic and a carcinogenic element. In the environment, Th behaves similarly to the REEs, substituting for Ca in bones and teeth. Based on the ASTDR (2017) report, children may be more susceptible to both the chemical and radiological effects of Th than adults. Long-term exposure to Th increases the chances of developing lung diseases, pancreatic and bone cancer (Salminen et al., 2005).

2.2.3 Potassium (K, ^{40}K)

Potassium (K) is an alkali metal (oxidation state: +1) with an atomic mass of 19 and atomic weight of 39.098. It is as a lithophile (and biophile) due to its large atomic and ionic radii and its affinity. Native K is a low-density (0.89 g/cm^3) metal that is malleable, ductile, and thermally and electrically conductive (White, 2018). Potassium is highly reactive under ambient atmospheric conditions.

Chemistry: Elemental K tarnishes rapidly in the presence of oxygen gas (O_2), and in the presence of liquid water (H_2O), K reacts aggressively to form potassium hydroxide (KOH) and flammable hydrogen gas (H_2), which exothermic chemical reaction releases significant heat in the form of a characteristic lilac flame (White, 2018). Potassium is highly soluble and occurs as the simple cation K^+ over the entire stability of field of natural water. It is mostly limited by three processes: (*i*) it is readily incorporated into clay mineral lattices because of its large size; (*ii*) it is absorbed more strongly than Na+ on the surfaces of clay minerals and organic matter; (*iii*) it is readily taken up by growing plants. Consequently, K concentrations exceeding a few tens of mg/l are unusual, except in water with a high dissolved solids content or water from hydrothermal systems (Salminen et al., 2005).

Isotope and decay series: Potassium has three natural isotopes, including two stable ones, namely ^{39}K (93.3 % of total), ^{41}K (6.7 % of total) and the long lived radioactive ^{40}K (1 248 million years; 0.0117 % of total), which decays to either ^{40}Ca (89.3 % = 1.311 MeV) by emitting a beta particle or to the gas ^{40}Ar (10.7 %) emitting a gamma-ray photon of energy 1.51 MeV after electron capture or positron emission. It is the 8th most abundant element in the Earth's crust. Because the average human body contains between 100 and 150 g of K, thousands of atoms of ^{40}K decay within our bodies each second, leading some communities to

consider K as a “natural” cause of genetic mutation in humans and other animals and plants (Cinelli et al., 2019).

Distribution in minerals, rocks: Potassium is a major element in many igneous and metamorphic rocks and in chemically precipitated sedimentary rocks. Igneous rocks display an abundance of main K silicate minerals, such as feldspars, micas and amphiboles. Potassium is, therefore, a major element in granites, granodiorites, rhyolites, and syenites (Cinelli et al., 2019). In the median UCC, (K_2O) is 2.8 m/m % (Rudnik & Gao, 2004). Based on the FOREGS dataset (Salminen et al., 2005), the median K_2O content (m/m %) is 2.02 in subsoil and 1.92 in topsoil, with a range between <0.01 and 6.0. The average ratio of topsoil to subsoil is 0.940. Elevated K_2O content is found over Alpine terrains, and in Greece and Bulgaria (Cinelli et al., 2019). Other enhanced K content may be related to sea spray, regional mineral dust, smoke from biomass burning (K^+), industrial emissions and in plant debris (Lazo et al., 2019).

Anthropogenic sources: The consumption of K in commercial industry is primarily determined by the use of agricultural fertilisers (approximately 85% of US potash sales), with significantly smaller quantities used to manufacture potassium hydroxide (KOH), potassium chloride (KCl), and potassium carbonate (K_2CO_3), which are used in several ways: as industrial water treatments, in soap manufacturing, in metal treatment and recycling, in fire extinguishers; in textiles and in food products. Also, many K-salts have medical and chemical applications. A high level of K^+ in soil water can, however, cause damage to germinating seedlings, inhibit the uptake of other minerals and reduce the quality of crops.

Toxicity: K is an essential element for all organisms. Its main role is as an electrolyte in the regulation of blood pressure, regulating intracellular fluids, solubilising proteins, operating nerve impulses, maintaining healthy blood pH levels, bone support and muscle contraction; K is also essential to the functioning of the nerves, kidneys and a host of other body processes. Potassium homeostasis is maintained by balancing consumption of K-containing foods/supplements along with the elimination of excess K through urine and to a lesser extent sweat. Kidney malfunction and/or the consumption of laxatives and diuretics, or the consumption of drinks such as alcohol, coffee, and other caffeinated drinks, can contribute to excessive losses and lead to a deficiency of K in the body, a condition known as hypokalaemia (White, 2018). Together with N and P, potassium is essential for the survival of plants. Its presence is of great importance for soil health, plant growth and animal nutrition. Its primary function in plants is in the maintenance of osmotic pressure and cell size, thereby influencing

photosynthesis and energy production. Potassium-40 appears at 219 in the Agency for Toxic Substances and Disease Registry toxicity lists (ASTDR, 2017).

2.2.4 Cesium (Cs, ^{137}Cs)

Cesium shows lithophile properties and is rare element of the naturally occurring alkali metals in terrestrial environments, with an atomic number of 55 and atomic weight of 132.905. Cesium is a reactive alkali metal.

Chemistry: Cesium is often very soluble in aqueous solutions and is almost always bound by electrostatic interactions to a variety of anions as Cs^{+1}. Cesium is water-soluble and can rapidly enter the biological cycles and accumulate in terrestrial ecosystems, behaving in a very similar way to potassium (K). It is known that Cs can be adsorbed both reversibly or irreversibly onto the clay minerals found in soils and sediments. Laboratory experiments on clay minerals showed that Cs has the most suitable hydrated ion size for adsorption on Frayed edge sites (FES). It can be adsorbed favourably because it has a relatively high charge density compared to other monovalent ions. Once Cs is dehydrated (based on the hydration energy), other cations can be hydrated (Lee et al., 2017). Cesium, with a large ionic radius similar to that of K+, tends to display geochemical behaviour similar to that of K+, and therefore in silicate rocks it tends to occur in greatest concentrations in K-rich minerals such as clay mineral (illite) and micas or feldspars (Salminen et al., 2005; White, 2018).

Isotope and decay series: There is one natural occurring stable isotope of the element, ^{133}Cs (100 % of total), while there are two synthetic radioisotopes (^{134}Cs and ^{137}Cs) produced by nuclear power plants, in accidents and also as fallout from nuclear weapons testing. However, there are 40 known radioactive isotopes of Cs, with atomic masses of 112 – 151. One of the many of these Cs isotopes, ^{137}Cs, is of special concern because it is a by-product of atomic energy production, with a half-life of 30.2 years and is characterized by high bioavailability. The nuclear fission of ^{235}U yields ^{137}Cs as a product emitting gamma-radiation (photons). This type of radiation is usually emitted in combination with beta or alpha decay occur first and it is followed gamma radiation (from excited daughter nuclei), following which nuclei are usually left on an intermediate energy level. The energy of the γ -rays emitted (not a particle with mass, but a high energy photon) is monoenergetic, characteristic of the parent isotope, and may range in energy from the keV range to the MeV range. Regarding the form of the decay scheme (Figure 3), ^{137}Cs decays to ^{137}Ba ($^{137}_{55}Cs \rightarrow {}^{137m}_{56}Ba + h\nu$ *(γ-ray photons)* (Figure 3) and its gamma emissions decay to decays to a stable state at 0.662 MeV. Two β^- decay channels are present, accounting for 94.7% of β^- decays, proceeding from ^{137}Cs to an excited state of ^{137}Ba^{m}

with a maximum electron energy of 0.514 MeV ($^{137}_{55}Cs \rightarrow {}^{137m}_{56}Ba + e^{\wedge} - + \bar{\nu}$ + Q (514 keV) (Figure 3). Accordingly, ^{137}Ba is generated in metastable state with a half-life of 2.55 min, it does, however become stable after the release of a photon in the form of γ radiation ($^{137}_{55}Cs \rightarrow {}^{137m}_{56}Ba + h\nu$ (662 keV).

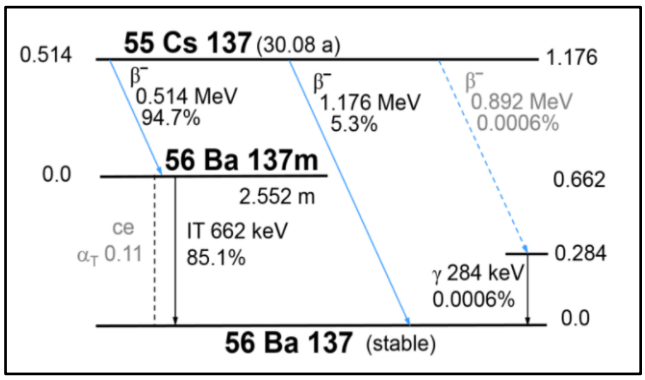

Figure 3. Cesium-137 decay scheme

The other 5.4% of β^- decay passes directly from ^{137}Cs to the ground state of ^{137}Ba with an electron energy of 1.176 MeV ($^{137}_{55}Cs \rightarrow {}^{137m}_{56}Ba + e^{\wedge} - + \bar{\nu}$ + Q (1176 keV)), (Figure 3). The general geochemical characteristics of ^{137}Cs is the same as the predominant, stable ^{133}Cs. Since Cs is strongly retained in the upper layer of mineral and organic soils and its vertical migration is limited (Ritchie & McHenry, 1990), the study of ^{137}Cs can be used as a tracer for resuspension, transport and deposition processes.

Distribution in minerals, rocks: Only one Cs-bearing mineral exists (pollucite: $H_4Cs_4Si_9O_{27}$), which contains max. 32 m/m % Cs_2O and has a number of commercial uses. Most Cs, however, is dispersed, and found in some common minerals, like micas and feldspars. The upper crustal abundance of Cs is of roughly 2.6 mg kg^{-1} (Rudnik & Gao, 2004).

Anthropogenic source: The main current use of non-radioactive Cs is in drilling fluids for the oil sector, along with its use in atomic clocks and other electrical devices (White, 2018). The Comprehensive Nuclear-Test-Ban Treaty Organization (CTBTO) introduced a list of 47 relevant[1] Cs fission products in 1999. Among those radioactive isotopes, ^{137}Cs has been used as a tracer in hydrologic research, in applications similar to those of ^{3}H (White, 2018). Both of these isotopes are produced largely by atomic bomb tests. With the initiation of nuclear testing in 1945, Cs isotopes were discharged into the atmosphere, where they are dispersed and

[1]In this content 'relevant' means that the nuclide would be produced in sufficient amounts and its half-life is long enough to give a reasonable chance of detection some days after the test (CTBTO, 1999)

deposited into environment returned to the Earth's surface as radioactive fallout (Figure 4) and where they can be exposed (a) externally to radiation from radioactive plumes, and (b) in internally as a result of inhaling radioactive material from the plumes (Figure 4). Therefore, later major nuclear accidents (Chernobyl 1986 and Fukushima 2011) have played the largest role in the distribution of ^{137}Cs into the ambient environment. The radiological importance of a given nuclide depends on the amount released during the accident, its radiation characteristics and how effectively it is transferred through the ambient environment to the public (De Corte et al., 1998).

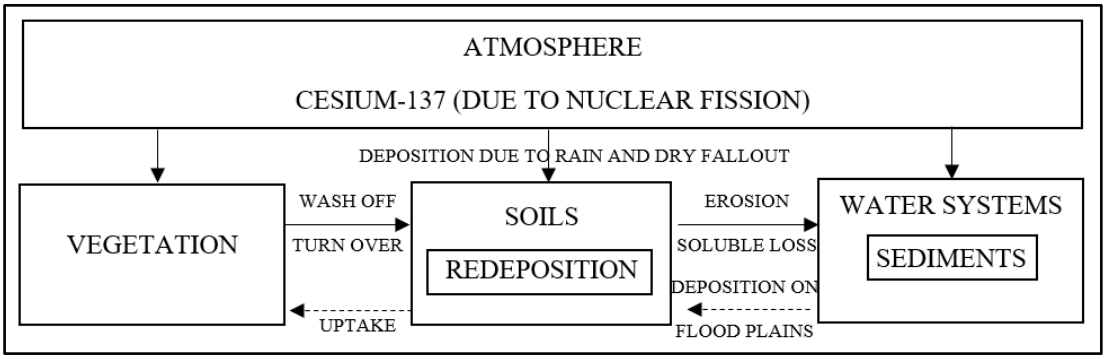

Figure 4. Environmental pathway of ^{137}Cs (Ritchie and McHenry, 1990)

The mining and processing of pollucite ore could also be a source of contamination. Coal ash from coal burning and municipal waste incineration may also be sources of ^{137}Cs (Kabata-Pendias, 2011).

Toxicity: Cs is not an essential element to plants and humans. Ingestion of any Cs compound is generally to be avoided; however, humans sufficiently exposed to enough stable (^{133}Cs) and radioactive cesium (^{134}Cs and ^{137}Cs) may experience health effects due to its gamma emission with a component. With respect to its biogeochemical properties, ^{137}Cs is readily soluble in water, and in solution, it can be efficiently taken up by plants and assimilated by animals because of its chemical similarity to the essential nutrient K (Ashraf et al., 2014). Over a time, small soil particles holding ^{137}Cs can move through the environment via wind and be re-suspended into airborne materials: in the case of sufficiently small particles, these could be inhaled and enter into the food chain and be ingested.

3. Materials and Methods

3.1 Studied urban areas

3.1.1 Salgótarján

Salgótarján (48.0853°N, 19.7868°E), the capital of the Nógrad county, was a major mining and industrial city, which played a significant economic role in Hungary in the 19th and 20th centuries. Its population today is about ~33000. The city is situated in the encircled by the Karancs and Medves Mountains (Figure 5A), at height above sea level varying between 220 and 500 m, with a total area of 103 km^2 (Figure 5B). This area belongs to the temperate continental climate zone, with variable weather conditions, and well-marked cold and warm seasons. The annual average temperature and precipitations are 8 - 9°C and 593 mm (Bihari et al., 2018). The rocks covering the study area are volcanic and sedimentary formations (siliciclastic sandstone), (Kercsmar et al., 2010). The Miocene Salgótarján brown coal is embedded in the sedimentary formation and was used as a local energy source. Brown forest soil is the dominant soil type (Figure 5B) (Kercsmár et al., 2010).

Salgótarján had existed as a village for centuries, and in the 1850s brown coal was discovered. The foundation and development of ironwork started in the mid-18th century when brown coal deposits were discovered in the settlements. As a result of the iron and steel works, glassworks, mining machine factory, stove factory, and ferroalloy factory located along the main roads, Salgótarján was considered a multi-industrial town. The town and its adjacent area were provided with energy from the coal-fired power plant (Figure 6A), which was fed with the local brown coal mines (Figure 5B).

Approx. 17 million metric tons of coal were extracted from the brown coal mining (Wirth et al., 2012). As a consequence (not of this alone, but also of the industry and related activity), Salgótarján and its environment were polluted by several sources, such as coal production, the local CFPP (called Vizválasztó*;* Figure 5B, 6B), iron/steel works, machine and glass factories. As a result, the residuals of coal combustion (e.g., coal ash) and industrial activities (steel and glass slags) were released into the environment without any regulation and (piled up, in some cases literally, in the town (for instance, the Kucsord Hill slag hill, or the Pintértelep coal ash cone as disposal site (Figure 6A), the Inászó former mine site), (Figure 5B). Currently, the kitchen stove industry is still active in the city.

3.1.2 Ózd

Ózd (48.2241°N, 20.2889°E) is located 40 km northeast of Salgótarján, at 150-200 m above sea level in Borsod-Abúj-Zemplén county, Hungary, with a total area of 92 km^2 and population ~33000 (Figure 5C). The main geological formations of the Ózd study area are Neogene sedimentary (sandstones, marl and brown coal) and acidic pyroclastic rocks (Kercsmár et al., 2010). Brown forest soil is dominant in this county. The prevailing wind direction is northerly. The region has an 8-9 $^{\circ}$C average annual temperature and 700-800 mm average annual precipitation (Bihari et al., 2018).

Ózd also played a significant role in the Hungarian iron and steel industry between 1835 and 1990, while coal mines had operated since the 18th century and produced coal for iron and steel works (Figure 5C). Currently, a new steel factory (Figure 5C) is in operation in the northeastern part of Ózd. The industrial production of iron and steel wastes (named smelter slag) have accumulated without any regulation in the whole city area and outskirts such as slag dumps (Figure 5C).

As a consequence of the collapse of the old communist system, from the latter half of the 1980s, industrial production started to decrease, the shutting down of coal mines and most of the traditional heavy industries (Wirth et al., 2012) dramatically changed the employment rate, standard of living, and demographics of the whole region. This economic and social shift resulted in remarkable changes in the landscape of cities, where the reconstruction of new public establishments and facilities (particularly schools and kindergartens) and open-air recreation areas (playgrounds and parks) started. However, the footprint of the significant and long-term (at least 170 years) heavy industrial activities (coal mining, heavy industry, and transportation) can be recognised even today in both settlements due to the presence of potential contamination sources (e.g., the derelict remains of former smelters, coal mines, coal-fired the power plant, slag heaps and coal ash cones, etc.), (Figure 5C).

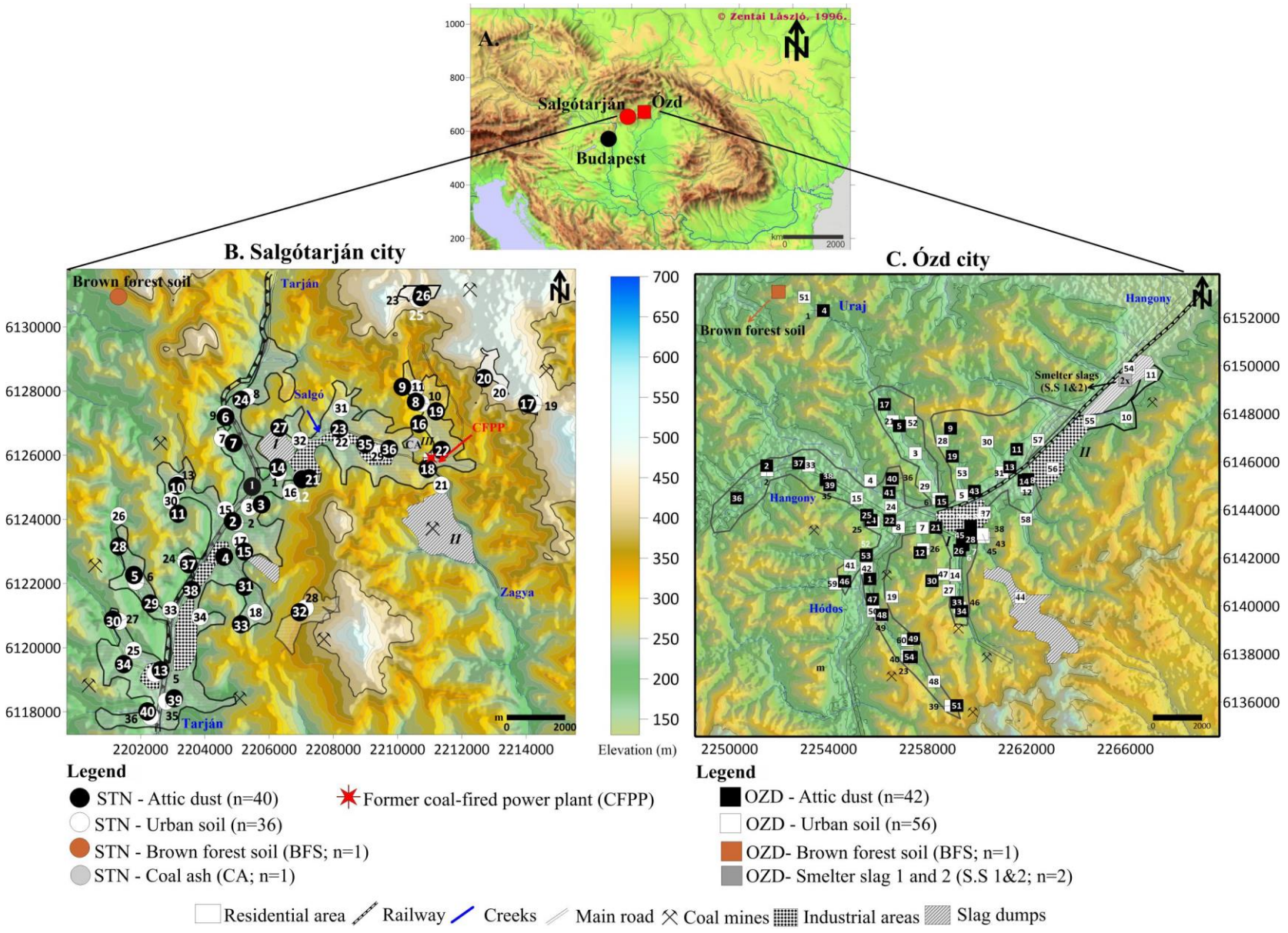
A.
© Zentai László, 1996.
Salgótarján
Ózd
Budapest
B. Salgótarján city
Brown forest soil
Tarján
Salgó
CFPP
Zagya
Tarján
C. Ózd city
Uraj
Hangony
Brown forest soil
Smelter slags (S.S 1&2)
Hangony
Hódos
Elevation (m)
Legend
STN - Attic dust (n=40)
STN - Urban soil (n=36)
STN - Brown forest soil (BFS; n=1)
STN - Coal ash (CA; n=1)
Former coal-fired power plant (CFPP)
Legend
OZD - Attic dust (n=42)
OZD - Urban soil (n=56)
OZD- Brown forest soil (BFS; n=1)
OZD- Smelter slag 1 and 2 (S.S 1&2; n=2)
Residential area
Railway
Creeks
Main road
Coal mines
Industrial areas
Slag dumps

Figure 5. A. Carpathian-Pannonian region, showing the geographical setting of the two cities studied (Salgátarján and Ózd). Color coding is as follows: brown - mountains (Carpathian Chain), green - plains (Pannonian Basin), blue - major rivers (Danube −1 and Tisza - 2). Studied urban areas. B. Salgórtarján study area: including attic dust, urban soil, brown forest soil sampling sites, residential areas, location of coal-fired power plant (Vizválasztó) and slag dumps (I- Kucsord slag hill; II- Inászó former brown coal mine; III- Pintértelep coal ash cone), CA - coal ash. C. Ózd study area: including attic dust, urban soil and brown forest soil sample, location of former steel works (I), present steel works (II), S.S 1 and 2 − smelter slags. In both cases, the topographic shaded relief model with elevation contour lines is overlaid. The residential area is marked by a contoured irregularly banded striped line. Names in blue names indicate local creeks (the Tarján, Salgó and Zagyva for Salgótarján; the Hangony and Hódos for Ózd). Map projections are in EPSG:3857, WGS 84 (Mercator system).

Figure 6. (A) Salgótarján coal ash cone at Pintértelep, (B) ruins of the former coal-fired power plant at Vizválasztó. The photos were taken by Áron Imre Bognár, 2018.

3.2 Sampling strategy of attic dust and urban soil samples

Sampling was designed to inspect 1*1 km^2 grid cells covering the Salgótarján and Ózd residential area, where representative targeted urban soil samples were selected based on the availability of desired site categories: kindergarten, playground, park, and ‘other’ (i.e., roadsides, cemeteries, soccer pitch and gardens) sites. In the case of attic dust, from each grid cell one attic dust sample was collected from the available buildings (e.g., a family house, blockhouse, and kindergarten). Urban soil samples were selected at distances not further than

500 m from the corresponding attic dust sampling sites. The sampling strategy is followed by international urban soil geochemical mapping by Demetriades et al., 2015.

A local coal ash sample (CA) was taken from an ash cone of the former CFPP in Salgótarján (Figure 5B), and smelter slag samples (SS 1 and 2) from the former and the recent smelter dumps in Ózd (Figure 5C). The local geochemical background samples, i.e., brown forest soils (Figure 5B and C), were taken from the nearby forest area, at considerable distance (~ 7 km) from all potential contamination sources (e.g., the former iron and steel works) in both cities. Sampling was carried out in 2016 for Salgótarján and in 2018 for Ózd.

3.2.1 Urban soil collection

Soil samples were collected in residential areas of Salgótarján and Ózd including samples from surrounding sites, like steel factories, coal mines, different smelter slag dumps, coal-fired power plant, and surrounding forests (Figure 5B-C). A 'zig-zag' sampling technique (Alloway, 2013) was used for urban soil based on the availability of desired sampling site categories, such as kindergarten (n = 9 and 15), playground (n =11 and 18), park (n = 6 and 4), and others (n = 10 and 19; i.e., roadside, cemeteries and gardens) from Salgótarján and Ózd, respectively (Table S. 1; S. 2). A total of 36 urban soil samples were collected from Salgótarján and 56 from Ózd (Figure 5; Table S. 1; S. 2). At each sampling site, 1-1.5 kg soil samples were gathered from a depth 0-15 cm using a steel spade and hand steel auger; these were then mixed thoroughly to obtain a bulk sample. All our selected sampling locations (Table S. 1; S. 2) are related to urban activities; therefore, the urban soil samples were considered as disturbed samples (Richard et al., 2019). Urban soil is also available in the prevailing shallow rooted grass vegetation cover in the urban environment studied. At sampling sites, each sampling point was selected at a point where the soil surface was covered by herbaceous vegetation and grass, away as far as possible from buildings, roads and trees in order to avoid local contamination effects (Figure 7). During the sampling, zip-lock plastic polyethylene bags (an effective means of transporting and storing a type of dust from any cross contamination) and powder-free nitrile protective gloves (contours of the hand which make easier in detail work; waterproof and chemical resistant) were used. At every 10^{th} sampling site, a duplicate sample was collected to allow the blind control of the sampling and analytical variability. All relevant information was recorded (photographs, GPS coordinates, land cover type, soil type, surrounding characteristics, such as local development history, landscape and land use).

Figure 7. Photographic documentation of urban soil sampling in a series of photographs: (1) Profile of urban soil, (2) Procedure of sampling and removing grass from the top (3) Profile of urban soil mixture with coal ash (4) Observation and documentation of the urban soil sample.

3.2.2 Attic dust collection

Our attic dust sampling guidance protocol was primarily followed by Völgyesi et al., 2014, in which paper other experiences and considerations (Cizdziel et al., 1998, 1999; Cizdziel & Hodge, 2000; Davis et al., 2005; Gosar et al., 2006) were compiled.

The sampling aimed to capture buildings (> 30 years) which had undergone only minimal renovation in their roof space. All attics were checked for disturbance by human activity and the samples were collected far from the attic entrance and at the best possible point in terms of minimising any potential effects of resident activities that might have disturbed them (Völgyesi et al., 2014a). The attic floor was not sampled, and organic materials, such as insects, or bird faeces, etc., were eliminated during the sampling. Two to twenty g of dust, composed of 3 to 5 sub-samples were taken primarily from wooden beams (Figure 8), depending on the specific conditions prevailing in any given attic. During the sampling, zip-lock plastic polyethylene

bags (an effective means of transporting and storing a type of dust safe from any cross contamination) and powder-free nitrile protective gloves (following the contours of the hand, making it easier for fine work; they are also waterproof and chemical resistant) (Figure 8). To avoid cross-contamination, fresh fine brushes and plastic gloves were used to collect each sample, including duplicate samples (Figure 8). Notably, in one building within the territory of the former iron and steel factory in Ózd we observed a two-layered attic dust accumulation, and here it was possible to collect a two dust samples, based on the different colors of the attic dust (Figure S. 1); an upper layer (OZD45ADUL) and a lower layer (OZD45ADLL) (Figure S. 1) (Tserendorj et al., 2022a). Approx. at every 10th sampling site, a duplicate sample was collected to permit the blind control of the sampling and analytical variability.

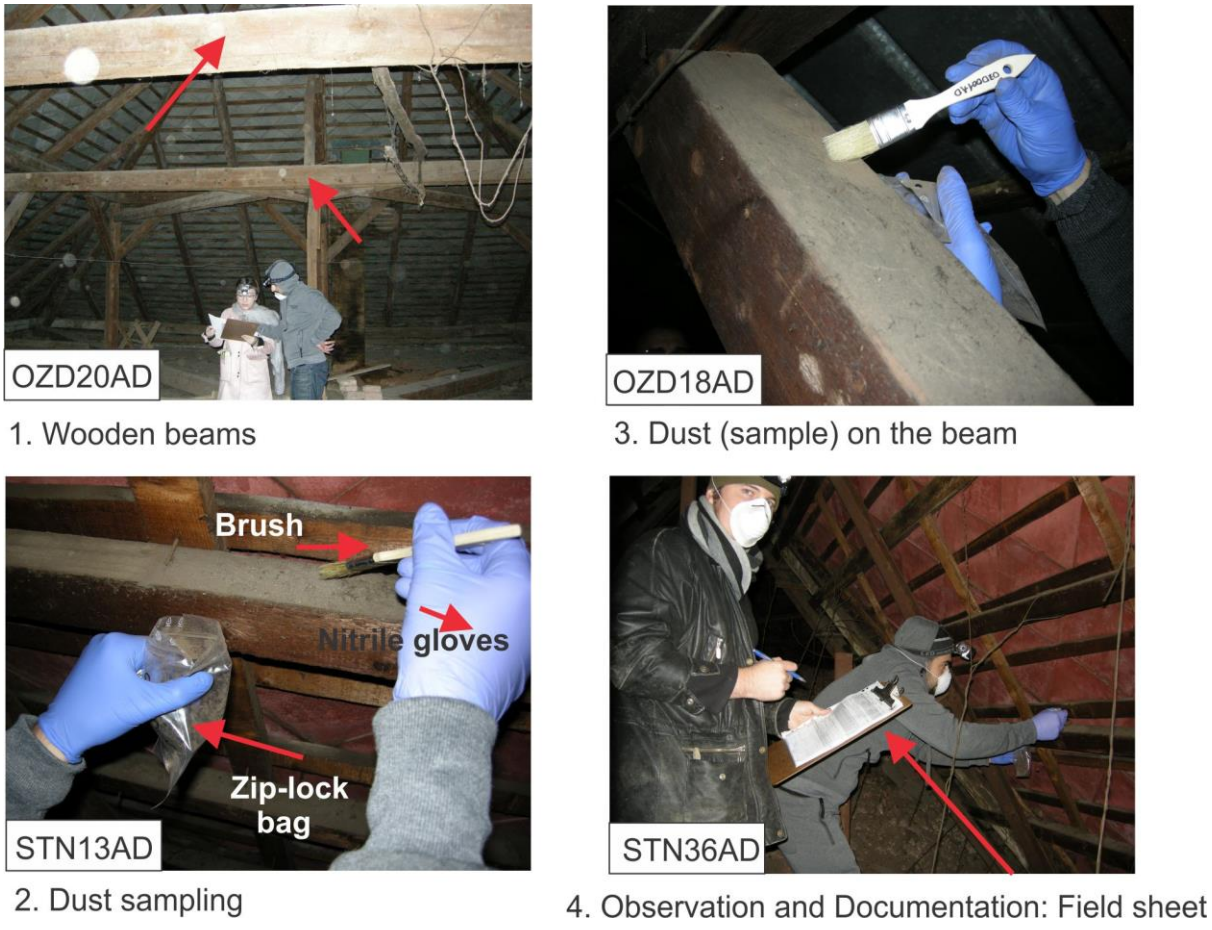

Figure 8. Photographic documentation of attic dust sampling: (1) Attic dust sampling at site, (2) Procedure of dust sampling, (3) Appearance of dust in situ on the wooden beam (4) Observation and documentation of the dust samples

During the sampling process, photographic documentation, geographic coordinates, and building characteristics such as the year of built and major reconstruction, roof material, function of the building (e.g., family house, church), construction material, slope of the ground below the building and elevation (construction height was added) were recorded (Table S. 1; S. 2). Residents were interviewed about the development and renovations history to ensure undisturbed samples. From Salgótarján a total of 40 attic samples was collected from family houses (n = 26), churches (n = 5), kindergartens (n = 3) and blockhouse (n = 2). The sampled buildings were built between 1890 and 1989 (Figure 5; Table S. 1; S. 2). From Ózd, 42 attic dust samples were collected from family houses (n = 26), from churches (n = 5), kindergarten (n = 4) and blockhouses (n = 7). These buildings were constructed between 1790 and 1971 (Table S. 1; S. 2)

3.2.3 Sample preparation

The urban soils were air-dried in the laboratory and passed through 2 mm sieves to obtain a representative portion. Following the procedure in Alakangas & Impola (2015), the coning and quartering homogenising method was applied to ensure that a given amount of a sample will represent the entire sample. The attic dust samples were sieved through a 0.125 mm mesh to remove residuals of insects, plants, faeces, wood, debris of construction material, etc. After, aliquots of homogenized subsamples were selected for further analysis. All these sample sieving and drying procedures were conducted at the Lithosphere Fluid Research laboratory of Eötvös Loránd University.

For elemental analysis, all attic dust and urban soil (including brown forest soil, coal ash and smelter slag) samples were dried at 60°C and sieved through a 0.180 mm mesh sieve. Additionally, the samples were pulverized by mild steel. The sample of coal ash was crushed, 70 % of which was sieved through a 2 mm mesh sieve before being pulverized and 85 % of this fraction sieved through a 0.075 mm mesh sieve. All pulverisation and crushing were performed at the Bureau Veritas Mineral Laboratories, Vancouver, Canada, for urban soil brown forest soil (BFS) and coal ash samples (CA) and smelter slags (SS 1 and 2).

For the gamma spectrometry analysis, attic dust samples were sieved through a < 0.125 mm mesh sieve to eliminate agglomerated organic materials (e.g., Cizdziel & Hodge, 2000; Ilacqua et al., 2003; Völgyesi et al., 2014a). Urban soil samples (including brown forest soil and coal ash) were sieved to < 2.0 mm, in line with studies undertaken on similar soils in Spain and Serbia, respectively (Charro et al., 2013a, b; Tanic et al., 2016). Sample preparations were done at the Lithosphere Fluid Research Laboratory (Eötvös Loránd University).

3.2.4 Particle size distribution (PSD)

All samples were analysed using a Horiba Partica 950-V2 LA Analyzer at the Laser Diffraction Particle Size Distribution Analyzer Laboratory at the Research and Instrument Core Facility of Faculty of Sciences, Eötvös Loránd University. This instrument is commonly employed for the determination of PSD, and the method incorporates the full Mie scattering theory (Horiba, 2016), which consists of high intensity and scattering monochromatic coherent light that treats the particles as a two-dimensional object and determines the particle-size as a function of the cross-sectional area (Konert & Vandenberghe, 1997). Consequently, wide measurement ranges, fast analysis, exceptional precision, and reliability have made laser diffraction the most popular technique in both industrial and scientific fields. According to the international USDA soil texture classification the following size fractions were considered: sand (2 - 0.05 mm), silt (0.05 - 0.002 mm) and clay (< 0.002 mm), (USDA, 2014). Nevertheless, based on experimental results by Konert & Vandenberghe (1997), a proposed grain size of 0.002 mm for the clay fraction by the sedimentation method corresponds to an actual grain size of 0.008 mm in laser diffraction analysis (Konert & Vandenberghe, 1997). In conformity with widely accepted standards (ISO 13320 and USP <429>), each attic dust and urban soil sample was measured 3 times, as reproducibility should meet specified guidelines (Horiba, 2016). Prior to the analysis, $Na_2P_2O_7$[2] liquid was applied in 24 hours before to disaggregate particles, which was further performed by applying to ultrasonic cleaner. From the results, instead of mean (*V* (intensity distribution), %) values median is more frequently. Since mean diameter is only appropriate for symmetric distribution (Horiba, 2016).

3.2.5 Inductively coupled plasma mass spectrometry (ICP-MS) measurements

In order to assess the extent, U, Th, Cs (mg kg^{-1}) and K (m/m %) were determined in 40 attic dust, 36 urban soils, 1 brown forest soil and 1 coal ash collected from Salgótarján; and from Ózd, 42 attic dust, 56 urban soil, 1 brown forest soil and 2 smelter slags samples were analyzed (Figure 5; Table S. 1; S. 2). Inductively coupled plasma mass spectrometry (ICP-MS) with a quadrupole as a single detector was conducted at the Bureau Veritas Mineral Laboratories, Vancouver, Canada. After homogenisation, ~ 1 g (in the case of attic dust) and 15 g (for urban soil) samples were digested in modified aqua regia (1:1:1 HNO_3: HCl: H_2O) at 95° C for 1 hours till soil solution completely digested (Reimann et al., 2009) in the Bureau Veritas Mineral Laboratories, Vancouver, Canada. Analytical quality was checked using certified reference

[2] sodium-pyrophosphate

materials STD DS11 for U, Th, Cs in mg kg^{-1} and for K in m/m % elemental contents. The analyzed (average) and expected elemental content for STD DS11 are 2.70 and 2.59 mg kg^{-1} for U (% recovery: 104.2), 7.60 and 7.65 mg kg^{-1} for Th (% recovery: 99.3), 2.72 and 2.88 mg kg^{-1} for Cs (% recovery: 94.4) as well as 0.40 and 0.40 m/m % for K (% recovery: 100), respectively.

3.2.6 Gamma spectrometry measurements

3.2.6.1 Attic dust γ-spectrometry measurement

Activity concentrations of the ^{226}Ra, ^{232}Th, ^{40}K and ^{137}Cs of the aliquot homogenised 1-2 g of attic dust samples were measured using Canberra GCW 6023 well-type HPGe detector (Figure 9A, B, C) Nuclear Security Department, Centre for Energy Research, Hungary. The shape of this detector allows the study of small amounts (low activity) of environmental samples because it combines low background with high detection efficiency due to the 4π solid angle, as well as shorter counting times (Barba-Lobo et al. 2021, Canberra, 2000; Laborie et al., 2000; Nafee et al., 2013). Based on Monte Carlo simulations, its applicable to place measurement samples both in the hole and on top of the endcap of a well-type HPGe detector (Unno et al., 2017), due to the fact that attic dust samples were placed into the detector hole, in this study. The active volume of the detector is 300 cm^3, the dimensions of the hole are 16 mm in diameter and 40 mm in depth (Figure 9A-B). The samples were put in closed cylindrical polyethylene plastic vials, while keeping the same sample heights (1.7 mm), while the mass was varied (mean 1.77 $\pm$ 0.48 gr) (Figure 9D). The relative efficiency of the detector is 62.8 %, with a full width at half-maximum (FWHM) of 1.39 keV at 122 keV (^{57}Co) and 2.13 keV at 1332 keV (^{60}Co), and a peak/Compton ratio of 63.3/1. The detector was placed in a low background-counting chamber with 30 cm thick pre-WWII iron shield and a 2 mm thick Cu layer to reduce the natural background interference (Figure 9A-C). Measurements were carried out at the Nuclear Security Department, Centre for Energy Research, Hungary. Full-energy peak efficiency (FEPE) for each selected energy was determined using Monte-Carlo simulations (Bognár, 2019), and also certified reference material, IAEA-447 (moss-soil) provided by the IAEA, was employed. This reference material contains natural radionuclides belonging to ^{238}U and ^{232}Th series.

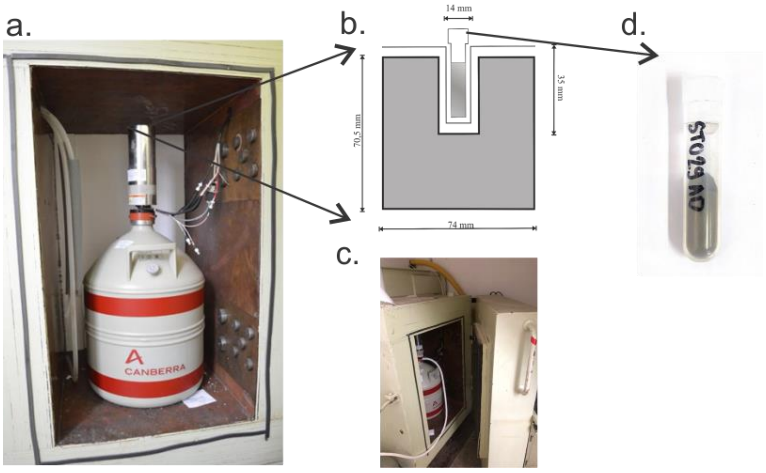

Figure 9. Ultra-low-background Canberra GCW 6023 well-type HPGe detector (Canberra, 2017). As installed at the laboratory of the Nuclear Security Department, Centre for Energy Research, Hungary; b. Schematic drawings of Well-type HPGe detectors fabricated hole; c. Figure of chamber with iron cube with a wall thickness of ~30 cm. d. Plastic vials (attic dust sample holder)

As shown in Figure 10 Monte-Carlo simulations (efficiency testing) were proposed to calculate detector efficiency using four different geometries of samples (9 mm-1 g; 13.5 mm- 1.5 g; 18 mm-2 g; 27 mm-3 g) and associated with all energies (keV). For each case, the detection efficiency may differ as a result of variation in the filling of the sample amounts. The same procedure was also followed with varying densities while keeping the filling height unchanged while mass was varied.

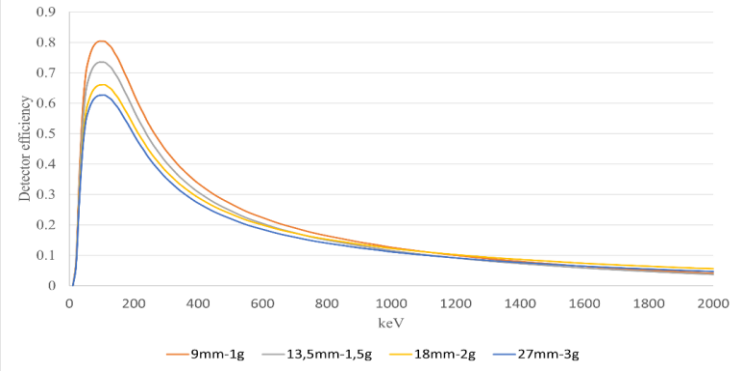

Figure 10. Monte-Carlo simulations with different sample heights and distance dependence of detector efficiency (Bognár, 2019)

3.2.6.2 Urban soil γ-spectrometry measurement

For urban soils, an average of 100 – 150 g homogenized samples (urban soil, brown forest soil and coal ash) were placed in a radon-leakage-free HDPE sample container (Kis et al., 2013). This special theoretically radon-leakage-free sample container made of HDPE was developed because this material has advantageous mechanical and radon permeability features (Kis et al., 2013), and so should, in theory, at least, be free of any leakage of radon. The inner diameter and height are 52 and 49.5 mm, respectively (Figure 11A). To reduce the absorption of low-energy photons, the wall thickness is 3.5 mm at the bottom, and 5 mm elsewhere. The container can be sealed using a threaded lid, which fastens a plug to the wall of the container. In order for radon and its daughter products to be kept in equilibrium, the container is air and watertight, sealed by means of a 2 mm thick Viton FPM 80 Standard fluorocarbon elastomer O-ring between the plug and the wall of the container (Kis et al., 2013), as shown in Figure 11B and the illustration drawings of the HDPE sample holder (Figure 11C).

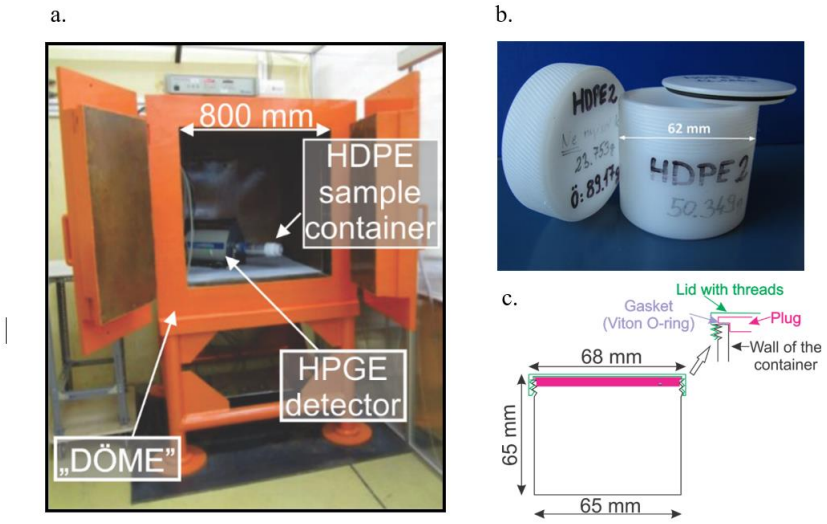

Figure 11 a. The low-background counting chamber, 'DÖME', with the HPGe detector and the HDPE sample container in a close sample-detector setup of the Nuclear Analysis and Radiography Laboratory (NARL) of the Centre for Energy Research. b. Sample container made of HDPE with the Viton O-ring, c. Schematic drawings of the HDPE sample holder (Kis et al., 2013)

All measurements were carried out in an n-type HPGe detector (Type: Canberra GR1319, with a relative efficiency of 13 %, energy resolution (FWHM) at 1.53 and 1.99 keV at 662 and 1332 keV, respectively, when the cylindrical detector is 46 mm in diameter and 41 mm in length) in

a low background-counting chamber DÖME[3] (from the Hungarian acronym of 'Extremely Heavy Measurement Instrument' (Figure 11) at the Nuclear Analysis and Radiography Laboratory, Centre for Energy Research, Hungary. This chamber is made of a 8 ton of pre-WW2 iron (in fact, from the wreckage of the bombed Elizabeth bridge in Budapest, 1945) to mitigate the background effect due to artificial radionuclides (e.g., from atomic bomb tests). It has internal dimensions of 800 × 800 × 800 mm (Figure 11). The 150 mm thick iron wall is covered inside with a graded shielding consisting of lead (5 mm) and copper (1.5 mm) layers. As a result of this passive shielding, the overall background within the chamber is about 1.39 cps over the energy range of 7-3.150 keV, which compares to 211 cps outside the chamber (a reduction factor of almost 152), (Kis et al., 2013).

All spectra were analysed using Fitzpeaks (Version 3.71) software. All samples were placed in the holder at least one month before measurement for them to reach secular equilibrium between ^{226}Ra and its progenies. Gamma spectrometry measurements were performed over different live times varying between 86400 to 604800 sec (1 – 7 days). Activity concentrations were determined for the following set of radionuclides (the selected gamma lines appear in brackets): ^{137}Cs (661.9 keV), ^{40}K (1460.8 keV), ^{232}Th (238.6 keV of ^{212}Pb; 583 keV of ^{208}Tl; 727 keV of ^{212}Bi and 911 keV of ^{228}Ac) and ^{226}Ra (295.2 and 351.9 keV of ^{214}Pb), the decay series of ^{238}U. To determine the background distribution in the environment around the detector, a count was conducted using an empty container using the same method and in the same geometry as the samples. The activity concentration of each radionuclide was calculated using the equation: $A = \frac{N_{net}}{I_\gamma \, \varepsilon \, m \, t}$ [Equation 1] here A is the activity concentration of a certain radioactive nuclide, N_{net} the net peak area count with the background subtracted; ε is the absolute efficiency of the detector; $I_{(\gamma)}$ the emission probability of a specific energy photopeak t is time for collecting the spectrum of the sample; and m is the weight (gr) of the sample. The result is given in units of Bq kg^{-1}. The background spectra were used to correct the net peak area of γ -rays of the measured isotopes. The degree of precision achieved in the analysis of field duplicates varied by less than 10 % as measured by the ratio of RMSE (root mean square error) average. All results of ^{137}Cs activity concentrations decay corrected into sampling date of August 2016 (sampling time). An accurate knowledge of the experimental set-up and its routine is important in the achievement of a high degree of precision and the quantification of the measurement uncertainty. In this case, the accuracy of the sample measurement will depend

[3]DÖME' from its Hungarian name 'Dögnehéz Mérőeszköz' meaning in English 'Extremely Heavy Measurement Instrument'

on knowledge of the sample composition, its homogeneity, and geometrical parameters, including those of the sample container, etc. When the uncertainty (error propagation) of final activity concentration (activity per unit mass) results are to be found, error propagation has to be implemented taking into account the uncertainty of factors included in it, namely, uncertainty of the net peak area and of the accuracy of calibration of the germanium detector which is added to the error propagation. It should be noted here that, as the (value was <0.001 %, the uncertainty in gamma intensity was neglected). Therefore, detailed practical information on γ -ray estimate error propagation can be found in the work by Knoll dedicated to this topic (Knoll, 2009).

3.3 Statistical analysis

3.3.1 Descriptive statistics

To obtain an overview of the data, descriptive statistics were used and presented on box and whiskers plots, where outlying values are determined according to inner-fence criteria (Tukey, 1977). Box and whiskers plots are basic tools for visualising more than one statistic of a parameter on one graph, making interpretation and comparison clearer. The general rule for this box is to show the interquartile range (IQR), which measures the innermost 50% of the total values (calculating the difference between the 3rd (Q3) and the 1st (Q1) quartiles of the data) and the black line in the box represents the median. Two upright (top and bottom) lines (the whiskers) represent the data within the 1.5 interquartile range, and extend from the ends of the box, usually to the 5th and 95th percentiles (Kovács et al., 2012). Observations lying beyond these extremes may be shown as filled dots (outliers) (Davis, 2002), for example, see Figure 16 and 18. The interquartile range must be multiplied by a constant to achieve conformance with the spread measure of the underlying data distribution. The value is 0.7413 for an underlying normal distribution. The spread-measure IQR of a normal distribution is calculated using the following formula: IQR = 0.7413 $\times$ (Q3 $-$ Q1) (Reimann et al., 2008). To achieve better interpretation and comparison between locations within one town, or between the cities, it is necessary in every possible case (U, Th, K and Cs [mg kg^{-1}] and activity (^{226}Ra, ^{232}Th, ^{40}K and ^{137}Cs, Bq kg^{-1}) concentrations to visualise the results on spatial maps of some type. In addition, the graphical representation of the data distribution can make it apparent if the distribution of the variables looks different. It may be preferable to characterise the data distribution by number of parameters in a table rather than looking through innumerable data distributions (Reimann et al., 2008). To do so, the following general statistical distribution measures were identified: the arithmetic mean, mode - highest probability occurrence, median

(MED), maximum (MAX), minimum (MIN), range (max - min), Interquartile range, (IQR), and standard deviation were used for the data set in this study. All analyses were carried out using SPSS and STATIGRAPHs software. The all-data set of each variable will be provided in general statistics summary tables (e.g., Table 2, 3, 4).

3.3.2 Quality Control (QC)

In an environmental science survey, the purpose of a repeated measurement is to check the representativeness of the given sample. The key concepts[4] are accuracy, precision and representativeness (Cinelli et al., 2019). In general, accuracy is essentially the absence of bias, while precision is the closeness of agreement between independent test results obtained under specified conditions (Reimann et al., 2008; Cinelli et al., 2019). During the collection of the samples, the analysis of field duplicates in both attic dust and urban soil sampling was carried out (frequently, 5- 10 percent). For every 10 samples, one duplicate sample was taken for both sampling collections and of field duplicates differed by less than 10% for elemental concentrations, and less than 20% for activity concentrations, respectively, as measured by the ratio of RMSE (Root mean square error) average:

$$RMSE = \sqrt{\frac{1}{N}\sum_{i=1}^{N} \quad (y_i - \hat{y}_i)2)} \qquad \text{(Equation 2)}$$

The insertion of analytical duplicates in experimental analyses (frequently, 10-20 %; Reimann et al., 2008) confirmed that the uncertainty remained in the 10% range in laboratory duplicates of both measurements (see Table S. 3).

3.3.3 Comparison of medians

Based on our findings, the median activity concentrations of measured radionuclides between attic dust and urban soil were assessed using the nonparametric Mann-Whitney (Wilcoxon) homogeneity test to compare for and significant differences (Mann & Whitney, 1947). The Wilcoxon test should always be used when the hypothesis of normality is not justified (e.g., Hollander & Wolfe, 1973). For an in-depth analysis and comparison of the attic dust and urban soil sample activity concentrations, the data was first tested for normal (Gaussian) distribution using the Shapiro-Wilk test since the sample number was rather low ($n < 50$) (Ghasemi & Zahediasl, 2012; Reimann et al., 2008), 95% of the data for normally distributed variables was expected to lie within its limits.

[4] Repeatability: same method, lab, person, and conditions (ideally).
Reproductivity: different methods, labs, and conditions.

3.3.4 Strength and direction of relationships between pairs of variables

The correlation coefficients indicate determine the strength and direction of an association between variables (Schober & Schwarte, 2018). Regarding non-normally distributed continuous data (distribution free), the Spearman rank method (Spearman, 1904) was employed to describe a monotonic relationship between two variables (Schober & Schwarte, 2018; Cinelli et al., 2019). Hypothesis tests are used to test the null hypothesis of no correlation, and confidence intervals provide a range of plausible values for an estimate. Also, correlations were checked by the visual inspection of scatter plots.

3.3.5 Regression analysis

Regression is a commonly employed statistical tool that determines the relationship between one independent variable and one or more dependent variables via mathematical functions. An ordinary least squares straight line equation, $y = a + bx$, where x is independent, y is dependent, a is an intercept and b is the regression coefficient (known as slope) is used (OLS; Goldberger, 1964; Freeman, 2018). The advantage of OLS is to fit the model and the overall validity values close to 1, which indicates an excellent fit. The f-statistic is computed to indicate whether the model has satisfactorily explained the degree of data variability. If the associated p-value exceeds 0.05, it is an indication that the model has failed to explain the data variability adequately (Reimann et al., 2008), this procedure was performed with the help of SPSS (25.0, SPSS Inc., Chicago, USA), to determine the significance of differences (at the $p \leq 0.01$ probability level, at the $p \leq 0.05$ probability level). In this way, the effect of predictors, namely the distance from (km) the CFPP as well as of the measured radionuclide activities was assessed using bivariate least squares regression analysis (Reimann et al., 2008) with the relationship regarded as significant at p <0.05.

Data outliers and extreme values are considered to be of special importance in regression analysis (Reimann et al., 2008). In accordance with this robust regression methods were applied to the data since least square methods are very sensitive to statistical outliers (Yu & Yao, 2017). Whereas the latter is capable of providing more reliable results by limiting the weight of outliers. From that base, some comparative simulations, robust MM (maximum likelihood method) estimates (least square approach) have the best performance from among a number of robust methods (Wilcox et al., 2012; Yu & Yao, 2017; Kalina et al., 2020). The estimation was employed when assessing the house ages vs. ^{137}Cs activity concentration using the 'rlm' function (robust linear models from the 'MASS' module in R), a free software for statistical

computing in environmental issues (see Figure 23). However, when exploring the altitude effect, OLS regression was sufficient, given to the lack of outliers.

3.3.6 Meteorological simulation

When radionuclides released from nuclear bomb tests and accidents enter the environment, they can be subjected in different processes, following different pathways, a point elucidated in section 2.1 and 2.2.4**.** Considering all of those, the meteorological aspect has been developed and has become a noteworthy methodology for the simulation of transport and the behaviour of radioactivity in the environment over extended distances. Following on in this direction, meteorological data evaluations were estimated based on the ERA[5] reanalysis records of the European Centre for medium-range weather forecasts (ECMWF), (Link 3). The time ranged from of January 1, 1979, to July 1, 2018. The data sets cover the NE part of Hungary (47.0˚N - 49.0˚N, 19.0˚E - 21.0˚E), with a spatial resolution of about 8 × 8 km (geographic grid 0.125˚ × 0.125˚) and a time resolution of 3 hours. All computations were performed using Jupyter in Python 3.7 with standard modules.

3.3.7 Geostatistical analysis

To obtain a representative interpolated map of attic dust, the measured radionuclide activity (^{226}Ra, ^{232}Th, ^{40}K and ^{137}Cs), a geostatistical analysis was conducted (Webster & Oliver, 2007). For each radionuclide, the basic function of geostatistics, the semivariogram, was calculated to describe the spatial autocorrelation structure of the radionuclides (^{226}Ra, ^{232}Th, ^{40}K and ^{137}Cs), and to obtain the weights necessary to be able to predict their values at unsampled locations using Kriging (Cressie, 1990; Hatvani et al., 2017; Tserendorj et al., 2022). Specifically, empirical semivariograms were calculated, onto which theoretical ones were fitted using least squares fitting with the Matheron algorithm (Matheron, 1965), Equation 3:

$$\gamma(h) = \frac{1}{2N(h)} \sum_{i=1}^{N(h)} [Z(x_i) - Z(x_{i+h})]^2 \qquad \text{[Eq. 3]}$$

where $\gamma(h)$ represents the semivariance, $N(h)$ indicates the number of sample point pairs with a distance h, $Z(x_i)$ indicates the measured value at observation site i, and $Z(x_{i+h})$ is the measured value at observation site $i+h$.

Next, theoretical semivariograms were fitted to the empirical ones using least squares fitting. Ordinary point kriging was used to obtain the interpolated maps (Cressie, 1990), and is

[5]ERA reanalysis is a global atmospheric reanalysis from 1979, continuously updated in real time.

considered one of the best interpolation algorithms in providing prediction for radionuclide fallout (e.g., Mabit & Bernard, 2007). One of the most important characteristics of the semivariogram is its spatial range within which the samples become uncorrelated (Chilés & Delfiner, 2012). In fact, the range obtained is usually attributed to environmental processes that act on the same scale (e.g., Hatvani et al., 2017, 2020). At shorter ranges, variables are assumed to have a physical relationship (e.g., Chilés & Delfiner, 2012; Hatvani et al., 2020). All reported ranges of coordinates in the study are planar distances in km (EPSG: 3857) and the fit statistics are reported along with the semivariograms and explained in Hatvani et al. (2017) and Tserendorj et al. (2022).

3.4 Radiological assessment of attic dust and urban soil

Possible health effect, due to the external exposure to natural gamma radiation, was estimated based on the obtained results for radionuclide activities of ^{226}Ra, ^{232}Th, ^{40}K and ^{137}Cs (Bq kg^{-1}) in the urban soil since it is considered that upper layer of urban soil contributes to the external gamma radiation. To assess the risk of population near the CFPP and slag dumps (Figure 5B, 6A-B), total absorbed gamma dose rate *(D)* (nGy h^{-1}) [Eq. 4] and the annual effective dose (*E)* (mSv y^{-1}) was calculated for the urban soil samples. However, the total absorbed gamma dose rate (*D*) calculation is for extended materials e.g., building materials, as an estimation it was calculated to the attic dusts and to the coal ash, too.

The total absorbed gamma dose rate *D* (nGy h^{-1}) in air at 1 m above ground level was estimated as given in the Eq. 4, provided by UNSCEAR 2008 Report (UNSCEAR, 2010). The equation was modified to include the contributions of artificial radionuclide ^{137}Cs. Dose coefficient of ^{137}Cs given value is 0.124 nGy h^{-1} according to Antovic et al. (2012). These factors are representative of the absorbed dose rates in air per unit activity per unit of sample mass.

$$\mathrm{D\ (nGy\ h^{-1})} = 0.462(^{226}\mathrm{Ra}) + 0.604(^{232}\mathrm{Th}) + 0.0417(^{40}\mathrm{K}) + 0.124(^{137}\mathrm{Cs}) \quad \text{[Eq. 4]}$$

The annual effective dose *E* (mSv y^{-1}) was calculated using a factor of 0.7 (Sv Gy^{-1}) to convert the absorbed dose in air *D* (nGy h^{-1}) to the effective dose rate for adults for environmental exposure to gamma rays, using an outdoor occupancy factor (fraction of time spent outdoor) of 0.2 and a time, 8760 (hy^{-1}) proposed by UNSCEAR (UNSCEAR, 2010). Accordingly, the annual effective dose (*E*) was calculated using Equation 5.

$$\mathrm{E\ (mSv\ y^{-1})} = \mathrm{D\ (nGy\ h^{-1})} * 8760\ (\mathrm{hy^{-1}}) * 0.2 * 0.7\ (\mathrm{Sv\ Gy^{-1}}) * 10^{-6} \quad \text{[Eq. 5]}$$

4. Results

4.1 Particle size distribution (PSD) in urban soil, attic dust, brown forest soil, coal ash and smelter slag samples

The analysis of particle size distribution (PSD) was performed using the laser diffraction method, as described in 3.2.4. The statistical characteristics of the PSD of attic dust and urban soils collected in both cities are summarised in Table 2.

Table 2. Summary statistics (minimum, maximum, standard deviation and median values) of median particle size distribution (µm) in attic dust and urban soil samples from Salgótarján and Ózd.

Samples	Min.	Max.	Standard deviation	Median
Salgótarján attic dust (*n*=40)	21.2	64.6	9.9	34.9
Salgótarján urban soil (*n*=36)	12.8	79.0	14.4	25.7
Brown forest soil (BFS) (*n*=1)				102.7
Coal ash (CA) (*n*=1)				116.8
Ózd attic dust (*n*=42)	18.7	74.5	12.6	39.0
Ózd urban soil (*n*=56)	10.5	186.2	30.7	21.9
Brown forest soil (BFS) (*n*=1)				10.3
Ózd upper layer (OZD45UL)				18.7
Ózd lower layer (OZD45LL)				40.5

In the urban soil samples (*n*=36) from Salgótarján, the median particle size was 25.7 µm, and ranged between 12.8 and 79.0 µm, with standard deviation of 14.4 µm (Table 2; Figure 12). In the local brown forest soil (STN BFS; *n*=1), the median was 102.7 µm, that is, much coarser than that of the attic dust and urban soil samples (Table 2; Figure 12), and comparable to coal ash (CA; *n*=1; 116.8 µm). In Ózd, the urban soil samples (*n*=56) were found to have a median particle size of 21.9 µm, and to range between 10.5 and 186.2 µm, with standard deviation of 30.7 µm (Table 2; Figure 12). In the local brown forest soil (OZD BFS; *n*=1), the median was 10.3 µm, relatively small in comparison to that of the Salgótarján BFS soil sample (Table 2; Figure 12). It is important to note that in smelter slag samples (slag 1 and 2), the PSD measurement was challenging due to the agglomeration of stony material in these samples from Ózd.

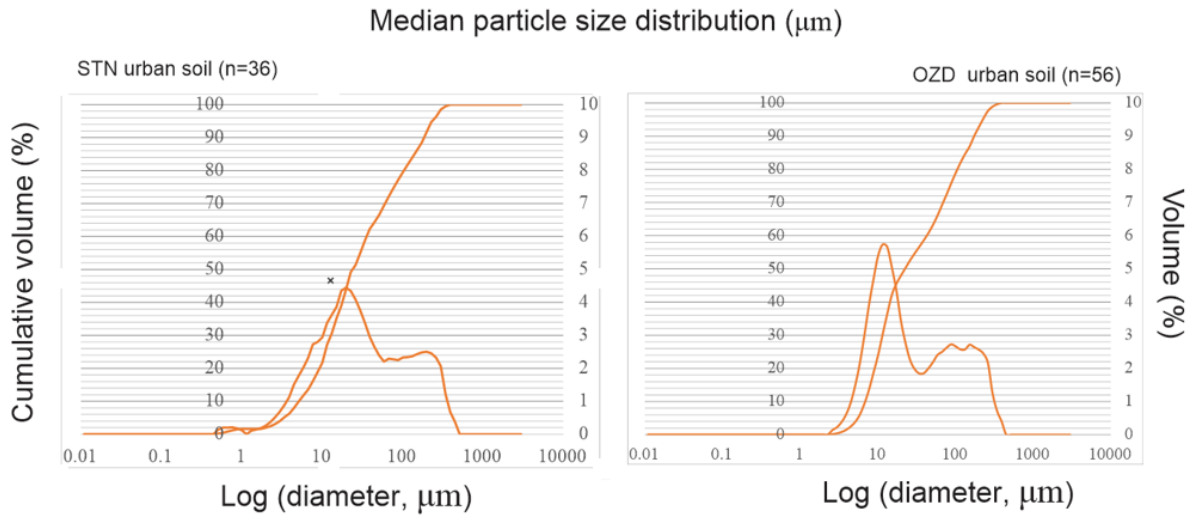

Figure 12. Median particle size distribution (µm) of urban soil from Salgótarján and Ózd, respectively.

Based on these soil texture results (Figure 13), it can be said that the Salgótarján urban soil samples have a clay fraction (based on V, %) representing between 4 and 40 % of the total, a silt fraction ranging between 40 and 72 %, and a sand fraction representing between 7 and 57 %; the following medians refer to the mass %: clay, 16 ± 7; silt, 52 ± 9; and sand, 31 ± 13. Almost 88 % (*n*=32) of the urban soil samples were found to belong to the loam and silt loam texture classifications (Figure 13). In brown forest soil (BFS) and coal ash (CA) samples, these contained, respectively and in order, fractions of sand (49 and 62 %), silt (40 and 27 %) and clay (11 and 11 %) with loam and sandy load soil textures (Figure 13). Data from the Ózd urban soil clay fractions ranged between 3 and 30 %, the silt fraction between 23 and 68 % and the sand fraction between 8 and 72 %, with following medians expressed as mass %: clay, 13 ± 6 silt, 51 ± 9 sand, 33 ± 13 (Figure 13). Loam and silt loam account for 90 % of the Ózd urban soil samples, and a similar tendency is seen in the Salgótarján urban soils. The Ózd brown forest soil (BFS) is characterised by a large clay fraction (35 %) compared to the other urban soil samples considered to be belong to the silty clay loam classification (Figure 13).

The descriptive statistics of particle size (*v*, %) reveals that 91 % of Salgótarján attic dust samples (*n*=40) display a clear bimodal distribution with distinctive peaks in the 0.5 – 2.0 µm and 8- 110 µm fractions (Figure 14). The dominant median PSD is 34.9 µm, the median ranges from 21.2 to 64.6 µm, with a median standard deviation of 9.9 (Figure 14). In Ózd, the particle size distribution of all attic dust samples (*n*=42) also displays a clear bimodal distribution

(~85 %, with distinct peaks in the 4 to 20 µm and 40 to 120 µm size fractions (Figure 14), which is coarser than those of Salgótarján attic dust particle size distribution (Figure 14).

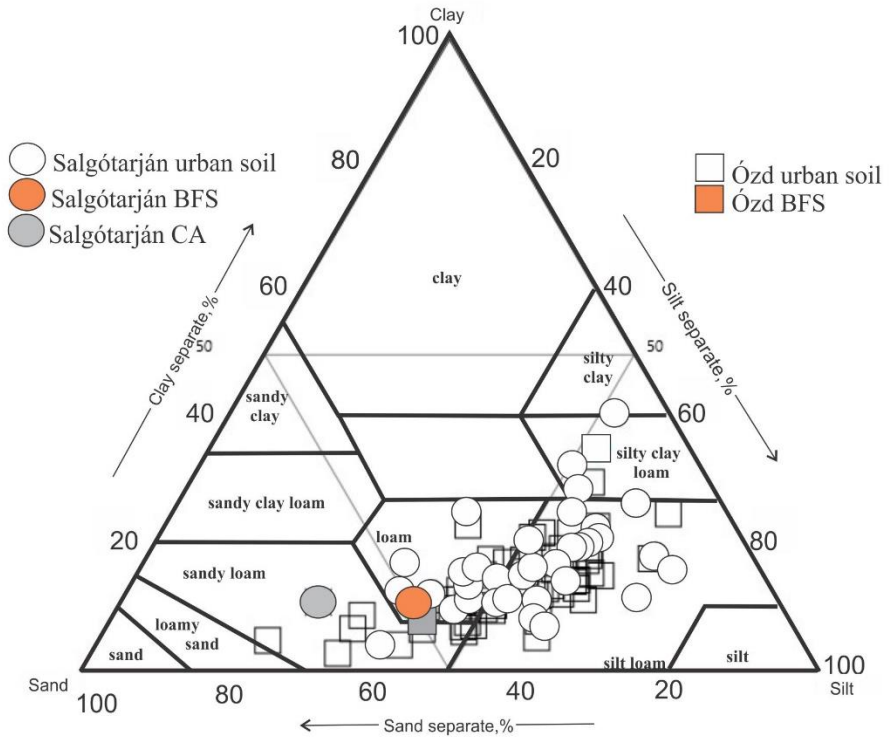

Figure 13. Triplot (according to USDA soil texture classification, USDA 2014) of urban soil grain size fractions (%), including urban soil, brown forest soil and coal ash samples from Salgótarján and urban soil and brown forest soil samples from Ózd.

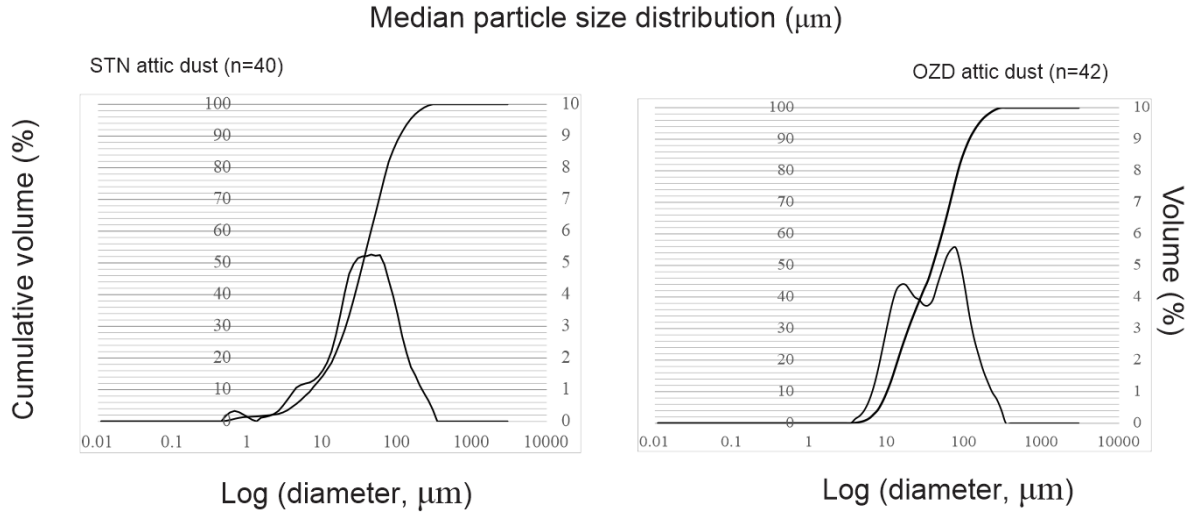

Figure 14. Median particle size distribution (µm) of Salgótarján and Ózd attic dust, respectively.

The median particle size distribution is 39.0 μm, with a range between 18.7 and 74.5 μm, with a median standard deviation of 12 (Table 2). Interestingly, the layered attic dust sample collected from Ózd has clearly distinct PSD distributions, comparing the upper (OZD45UL: 18.7 μm) and lower layers (OZD45LL: 40.5 μm) (Table 2).

Generally, the PSD of attic dust and urban soil yielded similarly bimodal results (Figure 12, 14) and the medians (μm) are broadly comparable between both cities (Table 2); however, only ranges (μm) differences are noticeable.

4.2 Elemental concentrations of U, Th, K and Cs in urban soil, attic dust, brown forest soil, coal ash and smelter slag samples

In Salgótarján urban soil (STNUS; *n*=36), U (mg kg^{-1}), Th (mg kg^{-1}) and K (m/m %) content range from 0.6 to 2.3 (mean 1.0), from 2.8 to 6.5 (mean 4.3) and from 0.1 to 0.4 (mean 0.3), respectively, which are higher than those of the local brown forest soil (BFS) (from 1.0 to 3.0 and 0.2, respectively, Figure 16A, B, C; Table 3); this is, however, lower than those of the Salgótarján attic dust samples (Figure 15, 16; Table 3). The only outlier value for U in urban soil samples (STN29US: 2.3 mg kg^{-1}; Figure 16) from a park in close vicinity to the two outlier attic dust samples (STN18AD-family house and STN35AD-family house; Figure 15, 16). This is also true for Cs content in urban soil, where STN29US (park; 1.7 mg kg^{-1}) represents one of the outlying values, together with STN09US (park: 1. 9 mg kg^{-1}) (Figure 16). The concentration of Cs in the local BFS sample is even more elevated (2.1 mg kg^{-1}) (Figure 16; Table 3) than those of the Salgótarján urban soil.

The urban soil spatial distribution maps show that patterns of U and Cs coincide on the same hotspots and on the decreasing tendency from east to southwest (Figure 15). Comparation between Salgótarján attic dust and urban soils in terms of U, Th, K and Cs spatial distribution reveals random patterns, whereas in the case of urban soil samples, a medium to low in relation to those of the attic dust samples (Figure 15). Concentrations of U, Th and Cs in coal ash (CA; *n*=1; 6.3, 12.8 and 2.7 mg kg^{-1}, respectively) give the highest values (Figure 16; Table 3). However, K content in coal ash is lower (0.5 m/m %) than the mean value in attic dust, and higher than that in urban soil values (Figure 16; Table 3).

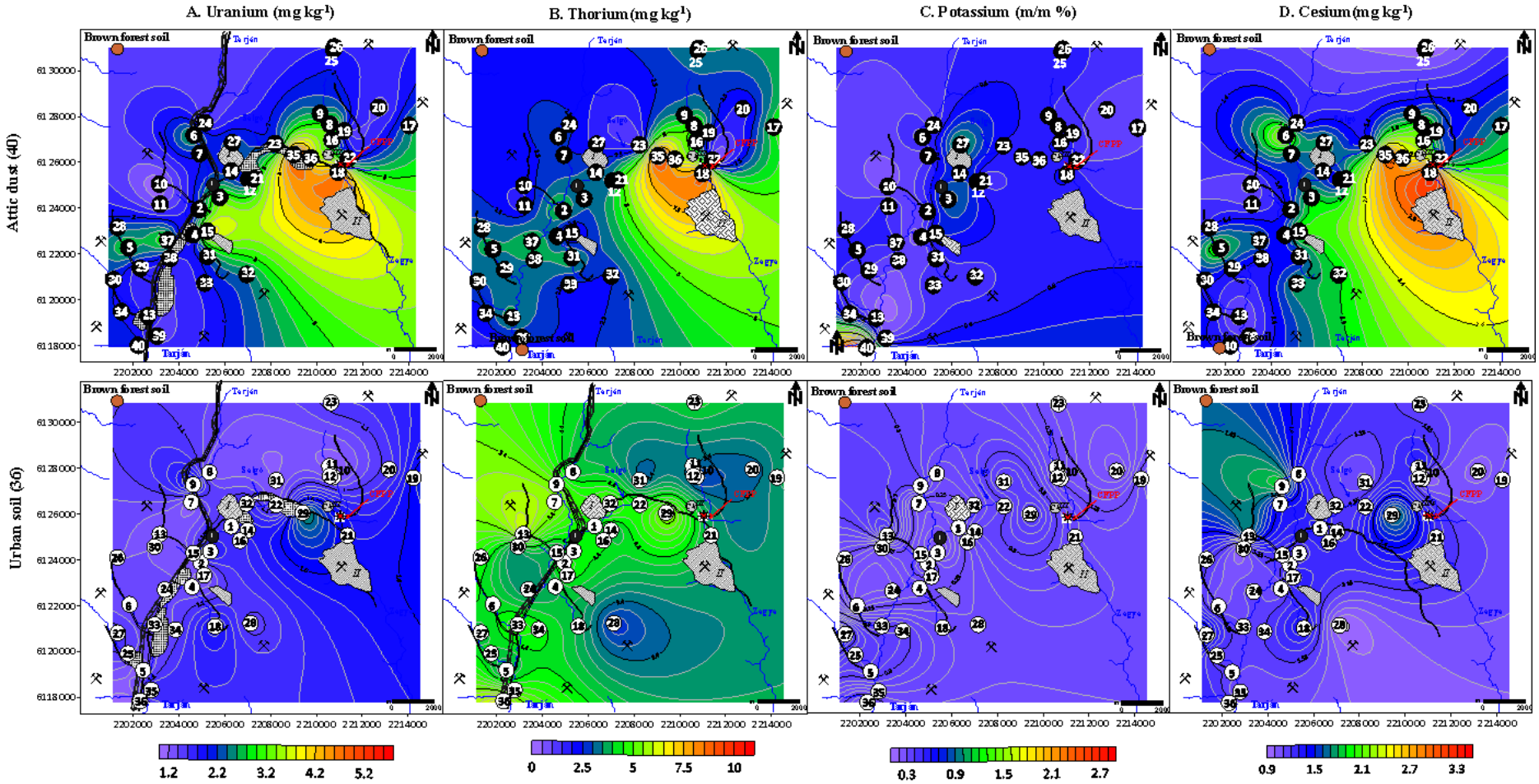

Figure 15. Spatial distribution maps of U, Th, K and Cs in attic dust (filled circle) and urban soil (open circle) in Salgótarján city showing sampling sites, locations of coal ash and local brown forest soil (Table S. 1); blue lines: creeks (map projection: EPSG:3857, WGS 84/Mercator projection)

In Salgótarján attic dust (STNAD samples; *n*=40), U (from 1.0 to 5.6; mean 2.3 mg kg^{-1}), K (from 0.2 to 2.7; mean 0.5 m/m %) and Cs (from 0.9 to 3.3; mean 1.6 mg kg^{-1}) concentrations are higher than those of the Salgótarján urban soil and brown forest soil samples (BFS: 1.0 for U; 0.2 for K and 2.1 for Cs, respectively) (Figure 16A, C, D; Table 3Table 3). In contrast, a lower mean value was obtained for Th in attic dust (3.3 mg kg^{-1}) than that of the urban soil mean value (4.3 mg kg^{-1}), with the exception of two outlier values (STN18AD-family house: 8.8 and STN35AD-family house: 10.5 mg kg^{-1}; Figure 16B; Table 3).

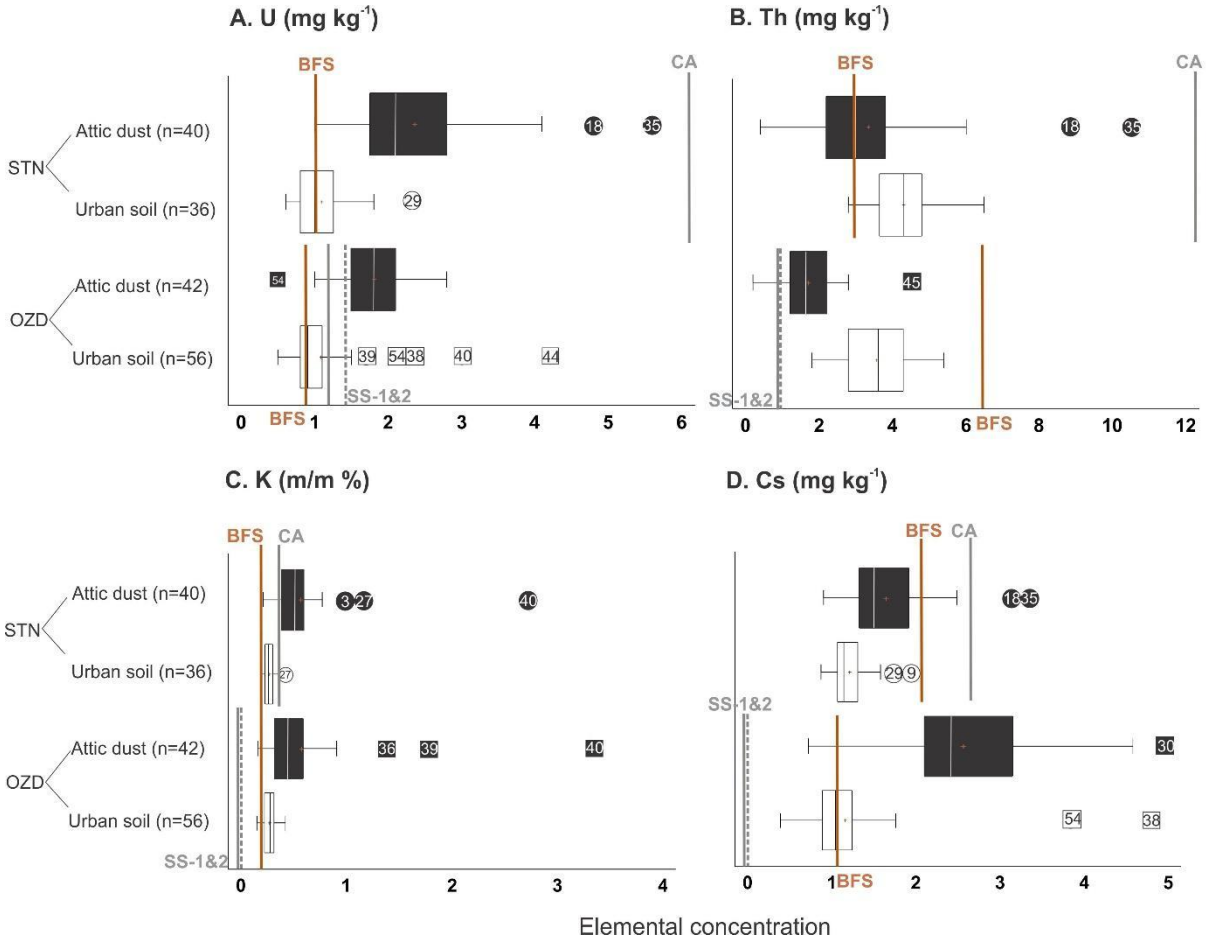

Figure 16. Box and whisker plot of the elemental concentration (for U, Th, Cs in mg kg^{-1} and for K in m/m %) in 40 attic dust and 36 urban soil samples from Salgótarján and 42 attic dust and 56 urban soil samples from Ózd. Local brown forest soil (BFS), and 1 coal ash (CA) from Salgótarján and 2 smelter slag samples (SS-1, SS-2) from Ózd, respectively, are indicated by vertical brown and grey lines, respectively**.** Median (fine vertical white lines for attic dust and fine vertical black line for urban soils) and mean values (small brown dots) are also indicated.

This is also true for U and Cs elemental concentrations in attic dust, where these two outlying values (STN18 and STN35) are observed (Figure 16A-D) on the eastern side of Salgótarján (Figure 15). For K, three outlier values in attic dust were obtained (Figure 16; Table 3C) in a family houses (1.0 m/m % for STN03; 1.2 m/m % for STN27; 2.7 m/m % for STN40AD; Figure 16A; Table 3) located along the roadside on the western side of the city (Figure 15). The spatial distributions of the attic dust data (Figure 15A, B, D) show that elevated U, Th and Cs concentrations in attic dusts are highly characteristic, particularly near the former coal-fired power plant, with only the exception of K distribution (Figure 15C, 16; Table 3).

In Ózd urban soil (OZDUS; *n*=56), five outlying U values were observed from playground (OZD39US: 1.7 mg kg^{-1}), one recent and two former industrial sites (roadside) (OZD54US: 2.1 and OZD44US: 4.2 mg kg^{-1} and OZD38US: 2.3 mg kg^{-1}), and park (OZD40US: 3.0 mg kg^{-1}) locations display higher values than those of local brown forest soil (BFS; 0.8 mg kg^{-1}) (Figure 16A, 17A). In contrast, Ózd urban soil samples yield substantially lower values than local brown forest soil (6.4 mg kg^{-1}) (Figure 16, 17B; Table 3). The Cs mean value in Ózd urban soil is comparable to that of the local brown forest sample. This, however, is still less than in the Cs mean attic dust sample (Figure 16D; Table 3). Since two outlying values were found in roadside samples (recent industrial site) (OZD54US: 3.8 mg kg^{-1}) and (OZD38US-former industry: 4.7 mg kg^{-1}) (Figure 16; Table 3D). The spatial distribution of data (Figure 17A, B, C, D) shows that Th content is highly enriched in urban soils in comparison to that found in attic dust (Figure 17B). In Ózd, two samples smelter slag (SS-1, SS-2) were investigated from a new industrial area, and in these, U (1.4 mg kg^{-1}; 1.2 mg kg^{-1}), Th (1.0 mg kg^{-1}; 0.9 mg kg^{-1}), K (0.01 mg kg^{-1} ; 0.01 mg kg^{-1}) and Cs (0.01 mg kg^{-1}; 0.01 mg kg^{-1}) levels were found to be lower than in the Ózd attic dust and outlying urban soil samples (Figure 16A, B, C, D; Table 3). Smelter slag samples 1 and 2 have lower U content than those of the Ózd attic dust (Table 3; Figure 16A). Despite this, OZD44US, located close to a former industrial site, had substantially higher U content than those in all the samples studied (Table 3; Figure 16A, 17). However, in the case of Th, K and Cs content, it seemed lower than in samples of attic dust and urban soil (Figure 16B, C, D). Additionally, the average values in the upper continental crust (UCC; Rudnik & Gao, 2004) and European top soils (ETS; Salminen et al., 2005) are elevated in comparison to those of the bulk compositions mean values of U, Th, K and Cs, respectively (Table 3). Uranium content of the two outlying attic dust samples (STN18AD-family house and STN35AD-family house) from Salgótarján are obviously

distinguishable (Figure 16A) by having values even higher than the reference values (UCC and ETS) indicating particular enrichment.

In Ózd attic dust (OZDAD; *n*=42), the values for U (from 0.5 to 2.8; mean: 1.8 mg kg^{-1}), K (from 0.2 to 3.3; mean:0.5 m/m %) and Cs (from 0.7 to 5.0; mean: 2.5 mg kg^{-1}) are above the average values of those in Ózd urban soil samples: 0.5 to 2.3, mean: 1.1 mg $kg^{-1;}$ 0.2 to 0.4, mean: 0.3 m/m %; and 0.4 to 4.8, mean: 1.2 mg kg^{-1}, respectively (Figure 16A, C, D; 17; Table 3). Lower and narrower range values were obtained for Th content (0.2 to 4.5; mean: 1.7 mg kg^{-1}) in Ózd attic dust than that of the urban soil samples (1.8 to 5.4; mean: 3.5 mg kg^{-1}) (Figure 16B). In terms of U content (Figure 16A), the lowest value (0.5 mg kg^{-1}) in OZD54AD attic dust, collected from a church, was even lower than all the other studied samples, including the Salgótarján (Figure 16A). The three outlier values for K content in Ózd attic dust, obtained from (OZD40AD-family house: 1.7 m/m %, OZD36AD-family house: 1.8 m/m %, and OZD39AD-family house: 2.8 m/m %; Figure 16C; Table 3) the western side of the city (Figure 5, 17C). one of which represents an outlying value (OZD40AD-family house) are even higher than the Salgótarján attic dust outlier (STN40AD-family house) (Figure 16C; 17C). Cesium content shows wider and higher ranges (from 0.7 to 5; mean: 2.5 mg kg^{-1}) than that of urban soil samples (from 0.4 to 4.8; mean: 1.2 mg kg^{-1}) (Figure 16D; Table 3). The spatial distribution maps of U, K and Cs values for Ózd attic dust show elevated content in attic dust samples compared to that of urban soil, particularly in the central part of city, and much more densely dominated by studied elements (Figure 17A, C, D; Figure 16A, C, D). On the contrary, in the entire northwestern and southeastern part of the city, urban soils contain uniformly higher amounts of Th compared to attic dust, whereas attic dust Th contents are relatively low (Figure 17B).

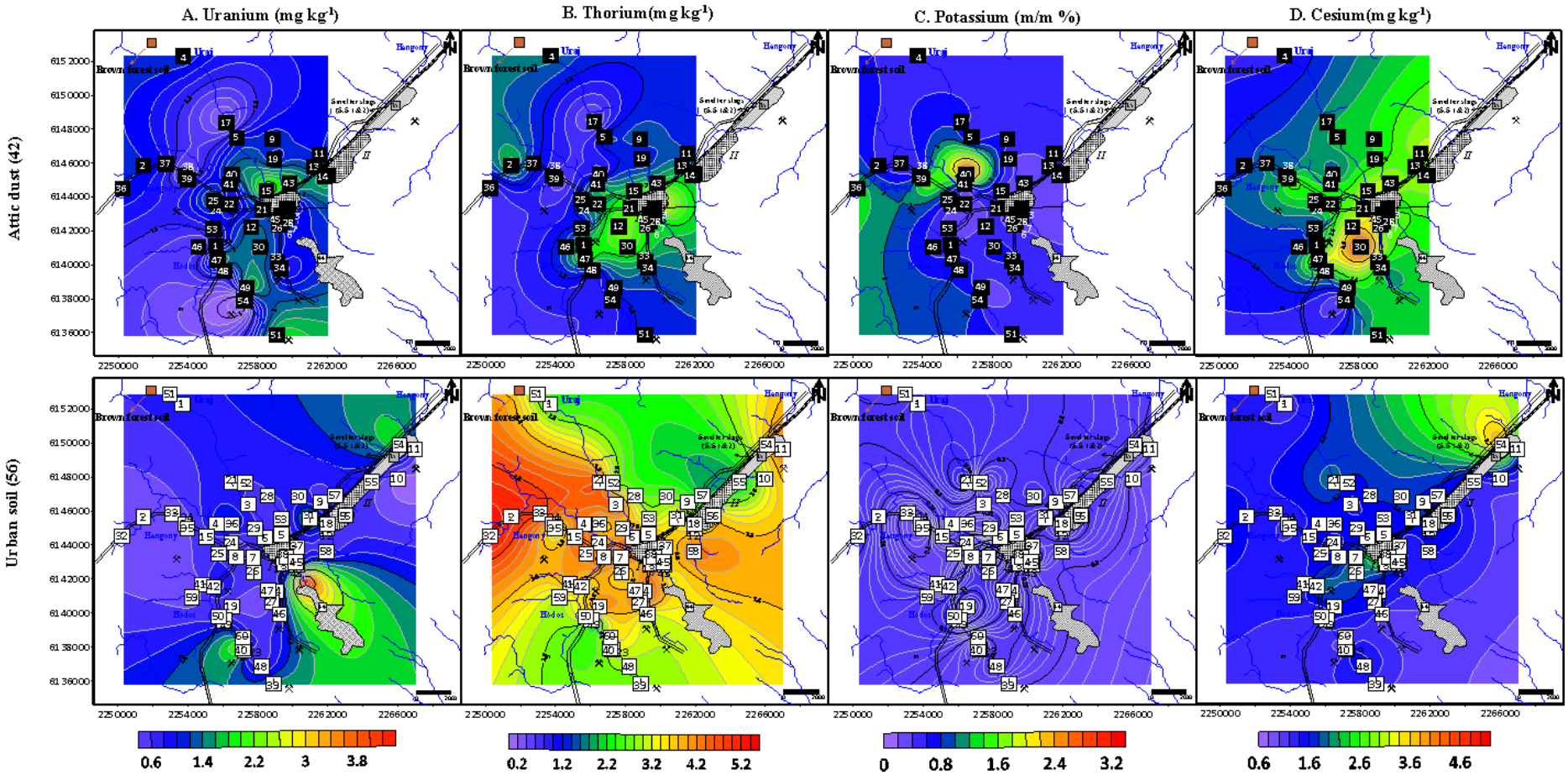

Figure 17. Ózd spatial distribution maps of U, Th, K and Cs in attic dust (filled square) and urban soil (open square), showing sampling sites, locations of smelter slag, and local brown forest soil (BFS) samples (Table S. 2). Blue lines: creeks (map projection: EPSG:3857, WGS 84/Mercator projection

Table 3. Summary statistics of elemental concentrations (mg kg^{-1}) in attic dust (n=40) and urban soil (n=36) from Salgótarján (STN) and attic dust (n=42) and urban soil (n=56) from Ózd (OZD).

		Samples	Min	Max	Standard deviation	Mean	Median	Inter quartile range	UCC	Topsoil (median) FOREGS	Brown forest soil	Coal ash/ Smelter slag
U mg kg^{-1}	STN	Attic dust	1.0	5.6	0.9	2.3	2.1	1.0	2.7	2.0	1.0	6.3*
		Urban soil	0.6	2.3	0.4	1.0	1.0	0.5				
	OZD	Attic dust	0.5	2.8	0.5	1.8	1.8	0.6			0.8	1.41**
		Urban soil	0.5	2.3	0.6	1.1	0.9	0.3				1.26***
Th mg kg^{-1}	STN	Attic dust	0.4	10.5	1.9	3.3	3.0	1.6	10.5	7.2	3.0	12.8*
		Urban soil	2.8	6.5	0.9	4.3	4.3	1.1				
	OZD	Attic dust	0.2	4.5	0.8	1.7	1.6	1.0			6.4	1.0**
		Urban soil	1.8	5.4	0.9	3.5	3.6	1.5				0.9***
K m/m %	STN	Attic dust	0.2	2.7	0.4	0.5	0.5	0.2	2.8	2.0	0.2	0.5*
		Urban soil	0.1	0.4	0.0	0.3	0.3	0.1				
	OZD	Attic dust	0.2	3.3	0.5	0.5	0.4	0.3			0.2	0.01**
		Urban soil	0.2	0.4	0.1	0.3	0.3	0.1				0.01***
Cs mg kg^{-1}	STN	Attic dust	0.9	3.3	0.5	1.6	1.5	0.6	4.9	3.7	2.1	1.1*
		Urban soil	0.9	2.0	0.2	1.2	1.1	0.2				
	OZD	Attic dust	0.7	5.0	0.8	2.5	2.4	1.0			2.7	0.01**
		Urban soil	0.4	4.8	0.7	1.2	1.0	0.4				0.01***

UCC - Upper continental crust (Rudnik & Gao, 2004)

European mean topsoil value published in FOREGS Geochemical Atlas of Europe (Salminen et al., 2005)

*Coal ash sample from Salgótarján; **Smelter slag–1 from Ózd; ***Smelter slag–2 from Ózd

4.3 Activity concentrations of ^{226}Ra, ^{232}Th, ^{40}K and ^{137}Cs in urban soil, attic dust, brown forest soil, coal ash

The activity concentration of three primordial (^{226}Ra, ^{232}Th, ^{40}K) and artificial (^{137}Cs) radionuclide was measured in a total of 36 attic dust samples from Salgótarján and 25 attic dust samples from Ózd, together 19 urban soil samples, one brown forest soil (BFS) and one coal ash (CA) sample from Salgótarján (detailed comprehensive information about sampling sites is also given in Table S. 1 and S. 2. The descriptive statistics of activity concentrations of primordial and artificial radionuclides analysed in this study are reported in Table 4**.**

In Salgótarján urban soils (in Bq kg^{-1})**,** ^{226}Ra varies from 15.0 ± 1.3 to 38.3 ± 1.4 (mean: 25.2 ± 1.6); ^{232}Th ranges from 18.9 ± 2.3 to 48.8 ± 3.6 (mean: 32.8 ± 3.2) and ^{40}K changes from 344.8 ± 9.2 to 447.8 ± 8.4 (mean: 386.4 ± 8.6) (Figure 18A, B, C; Table 4). The lowest activity concentration values for ^{226}Ra; ^{232}Th and ^{40}K were measured (14.1 ± 1.3, 16.7 ± 2.3 and 318.8 ± 9.0, respectively) in the brown forest soil sample, (Figure 18Figure 18A, B, C; Table 4). The results for the artificial ^{137}Cs radionuclide ranges from 0.7 ± 0.2 to 17.3 ± 0.4 (mean: 5.6 ± 0.4) (Figure 18D; Table 4). The highest value was observed in brown forest soil (BFS; 18.5 ± 0.6) (Figure 18) out of all the urban soil samples (Tables S. 1; S. 2).

In Salgótarján attic dust, ^{226}Ra varies from 12.0 ± 6.0 to 145.6 ± 8.3 (mean: 43.3 ± 4.6 Bq kg^{-1}), including two outlier samples (STN35AD-family house and STN18AD-family house), too (Figure 18A, B, C; Table 4). These values are higher than those of urban soil and brown forest soil samples (Figure 18). There was one sample, STN15AD-family house (Figure S. 2B and C), in which ^{226}Ra activity concentration was below the detection limit (0.9 Bq kg^{-1}). Note that this sample has the lowest ^{232}Th activity concentration as well (Tables S. 1; S. 2). The outlier values are at least five-times higher than all the values for urban soil and brown forest soil samples (Figure 18B; Table S. 1, S. 2, 4). However, ^{232}Th showed wider range (from 8.0 ± 2.6 to 94.3 ± 9.6 Bq kg^{-1}) and similar mean (34.0 ± 2.4) compared to urban soil (Figure 18B; Table 4), except the two outlier samples (STN35AD-family house and STN18AD-family house) mentioned above (Figure 18B). Elevated activity concentration of ^{40}K (from 309.2 ± 21.7 to 1382.3 ± 76.6; mean of 534.4 ± 39.1) and relatively higher ^{137}Cs values (from 5.5 ± 0.9 to 169.8 ± 2.9; mean of 88.5 ± 5.1) were measured in attic dust relative to those in urban soil and brown forest soil (Figure 18C-D; Table 4). One outlier, the ^{40}K activity concentration in attic dust, was observed at a family house (STN40AD; 1382.3 ± 76.6 Bq kg^{-1}; Figure 18C; Table 4). The majority of the roofs on the homes where samples were taken are tile (n = 19)

and slate (n = 13), with a few combinations of slate/tile roofs (n = 2) and metal roofs (n = 2), as characterized in Tables S. 1 and S. 2.

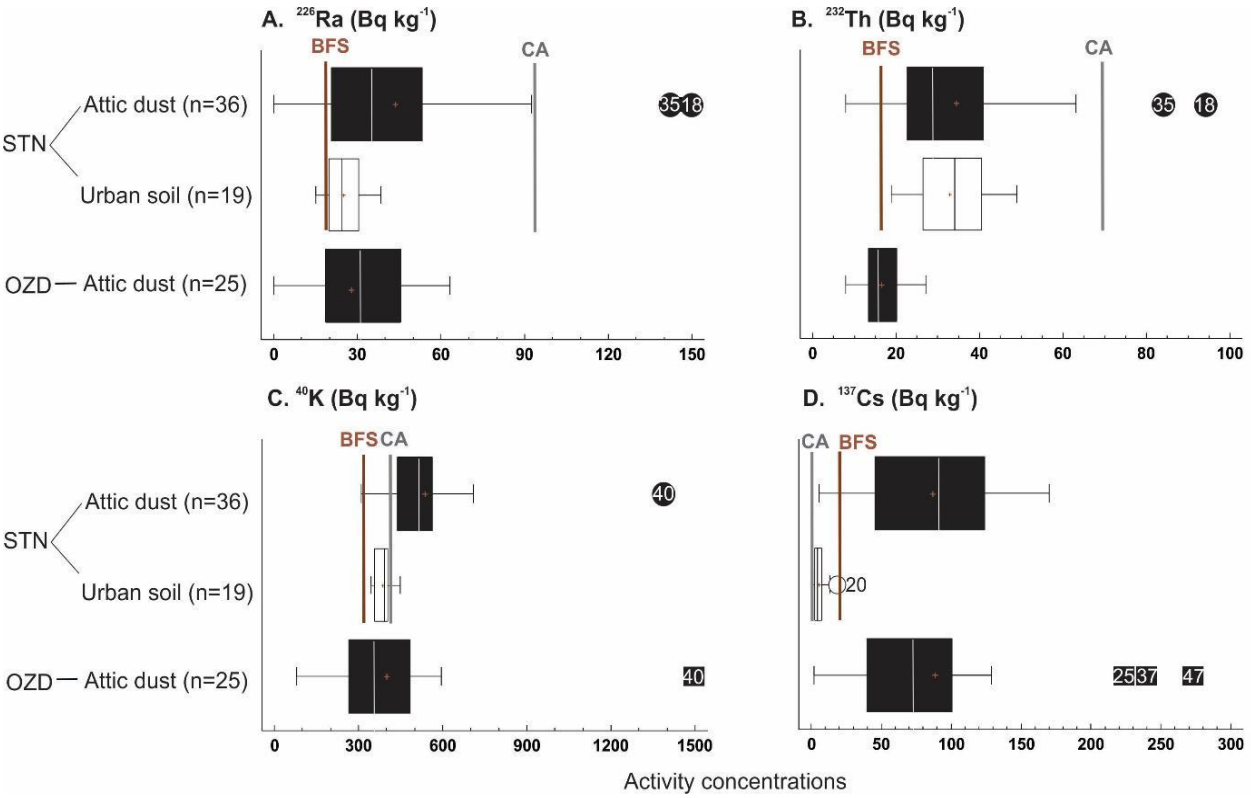

Figure 18. Box and whisker plot of the activity concentration (for ^{226}Ra, ^{232}Th, ^{40}K and ^{137}Cs bq kg^{-1}) in 36 attic dust and 19 urban soil samples from Salgótartján and 25 attic dust samples from Ózd. Samples of coal brown forest soil (BFS) and coal ash (CA) from Salgótarján are marked by vertical brown and black lines, respectively**.** Median (fine vertical white lines for attic dusts and fine vertical black line for urban soils) and mean values (small brown dot) are also indicated.

In Ózd attic dust, activity concentrations (Bq kg^{-1}) varied between 9.5 ± 2.8 to 63.3 ± 0.6, with a mean value of 35.7 ± 3.3 for ^{226}Ra; from 8.0 ± 6.2 to 27.1 ± 3.4, with mean of 16.6 ± 0.9 for ^{232}Th; from 80.5 ± 15.6 to 1493 ± 78, with mean of 399.8 ± 29.1 for ^{40}K and for ^{137}Cs its range was from 1.9 ± 1.0 to 272.9 ± 13.1, with a mean of 87.8 ± 4.5 (Figure 18A, B, C, D; Table 4). Three outlying values were found: OZD25AD-blockhouse 223.4 ± 6.5 Bq kg^{-1}, OZD37AD-family house 238.6 ± 11.5 Bq kg^{-1} and OZD47AD-family house 272.8 ± 13.0 from the southern and western parts of the urban area (Figure 18D; Table 4), will be discussed below.

It is clear that the levels of ^{137}C activity concentration in attic dust in the two studied cities (Salgótarján and Ózd) are comparable to one another despite their being considerably higher than those found in the urban soil of Salgótarján (Figure 18D; Table 4).

At the sampling site where two-layered attic dust was found (former iron and steel industry), the upper layer (OZD45ADUL) contains lower ^{137}Cs activity concentration, 1.9 $\pm$ 1.0 Bq kg^{-1} than the lower layer (OZD45ADLL), 16.0 $\pm$ 1.4 Bq kg^{-1} (Table S. 2; Figure S. 1). In Ózd, the majority of the attic roofs were tile (n = 16), followed by slate (n = 7) and metal (n = 3), Table S. 2.

Table 4. Summary statistics of activity concentrations (Bq kg^{-1}) of ^{226}Ra, ^{232}Th, ^{40}K and ^{137}Cs in attic dusts (*n*=36) and urban soils (*n*=19) from Salgótarján; and attic dust (*n*=25) from Ózd.

			Min	Max	Standard deviation	Mean	Median	Mann-Whitney (Wilcoxon) test[a]	Tests[b]
^{226}Ra	OZD	Attic dust	9.5 ± 2.7[c]	63.3 ± 0.9	18.3	35.7 ± 3.3	31.0	-	**0.57***
	STN	Attic dust	12.0 ± 6.0[c]	145.6 ± 8.3	33.8	43.3 ± 4.6	35.1	**0.03**	0.00
		Urban soil	15.0 ± 1.3	38.3 ± 1.4	6.8	25.2 ± 1.6	24.5		**0.47***
^{232}Th	OZD	Attic dust	8.0 ± 6.2	27.1 ± 3.4	4.9	16.6 ± 0.9	15.7	-	**0.64***
	STN	Attic dust	8.0 ± 2.6	94.3 ± 9.6	18.2	34.0 ± 2.4	28.9	0.52	0.00
		Urban soil	18.9 ± 2.3	48.8 ± 3.6	8.7	33.0 ± 3.2	34.0		**0.53***
^{40}K	OZD	Attic dust	80.5 ± 15.6	1493 ± 78	253.0	399.8 ± 29.1	354.4	-	0.00
	STN	Attic dust	309.2 ± 21.7	1382.3±76.6	169.6	534.4 ± 39.1	516.6	**0.00**	0.00
		Urban soil	344.8 ± 9.2	447.8 ± 8.4	28.4	386.4 ± 8.6	391.5		**0.98***
^{137}Cs	OZD	Attic dust	1.9 ± 1.0	272.9 ± 13.1	65.7	87.8 ± 4.5	73.0	-	0.00
	STN	Attic dust	5.5 ± 0.9	169.8 ± 8.8	47.9	88.5 ± 5.1	91	**0.00**	**0.18***
		Urban soil	0.7 ± 0.2	17.3 ± 0.4	4.5	6.0 ± 0.4	4.3		0.00

[a] Reject the null hypothesis for alpha >0.05, bolded values show that the medians area significantly different,

[b] *p* significance values are greater than >0.05, bolded data are normally distributed* Shapiro-Wilk normality tests

[c] Note that among the ^{226}Ra activity concentrations there were one sample from Salgótarján (STN15AD-blockhouse) and three samples from Ózd (OZDAD17-family house**;** OZD34AD-family house, OZD52AD-family house) below the detection limit of activity concentration Bqkg^{-1}

Salgótarján brown forest soil and coal ash samples are not included in this table

4.4 Results of calculated radiological assessment due to ^{226}Ra, ^{232}Th, ^{40}K and ^{137}Cs in Salgótarján attic dust and urban soil

As it was pointed out first by Eisenbud & Petrow (1964), the natural radioactivity contained in coal could result in high quantities of radioactive substances being released into the ambient environment, more even than during the safe operation of nuclear power plants. Therefore, CFPPs are the source of certain amount of additional ^{226}Ra, and ^{232}Th and their decay products finding their way into the soil, sediment and water as well as dust around CFPPs and their slag dumps (UNSCEAR, 2010). Gamma radiation from these radionuclides represents the main external source of irradiation to the environment and human body (UNSCEAR, 2010).

To assess the risk of Salgótarján population living or working near the former CFPP (Figure 5B and its slag dump Figure 6A), the total absorbed gamma dose rate (D) [Eq. 4] and the annual effective dose (E) [Eq. 5], were calculated for the urban soils and attic dust samples.

Examining the results that the minimum, maximum, standard deviation, mean and median are about 32.3, 64.3, 47.5, 46.7 and 9.05 nGy h^{-1} for urban soil (*n*=19), respectively and about 22.1, 155.5, 73.8, 67.6 and 30.2 nGy h^{-1} for attic dust (*n*=36), respectively, for absorbed gamma dose rates (D) (Table 5).

In Salgótarján, the annual effective dose rate (E) is 0.04, 0.08, 0.06, 0.06 and 0.01 mSv y^{-1} for urban soil (*n*=19), respectively (Table 5).The brown forest soil sample displays one of the lowest values (D: 32.3 nGy h^{-1} and E: 0.04 mSv y^{-1}) among the urban soils, whereas coal ash (D: 101.4 nGy h^{-1} and E: 0.12 mSv y^{-1}) behaves in a way similar to attic dust results (Table 5).

Table 5. Calculated absorbed gamma dose rate, D (nGy h^{-1}) and annual effective dose, E (mSvy^{-1}) for an attic dust and urban soil samples from Salgótarján

Types of samples			Min	Max	Standard deviation	Mean	Median
Urban soil (*n*=19)	D	[nGy h^{-1}]	32.3	64.3	9.0	47.5	46.7
	E	[mSv y^{-1}]	0.04	0.08	0.01	0.06	0.06
Attic dust (*n*=36)	D	[nGy h^{-1}]	22.1	155.5	30.2	73.8	67.6

5. Discussion

5.1 Uranium, Th, K and Cs in urban soil, attic dust, brown forest soil, coal ash and smelter slag samples in Salgótarján and Ózd

The U-Th-K triplot graphically depicts the ratios of these three elements in studied different media (Figure 19). Variations of U and Th concentration (mg kg^{-1}) as well as of K (m/m %) in the U-Th-K triplot, measured in all samples studied from Salgótarján and Ózd (Figure 19A-B) show an intimate link between Th and U content, creating a closed cluster along the Th - U side, with a gradual decrease in Th relative to U for all urban soils and for the majority of attic dusts (Figure 19C). However, it is seen that urban soils (from both cities) are richer in Th and poorer in U than the attic dusts (from both) (Figure 19C). Both local brown forest soil samples fell into within the range of the urban soil samples (Figure 19A, B, C). It is characteristic of the Salgótarján attic dust samples that they are richer in U and Th than those in Ózd, with extremely high U and Th content (around 5 and 10 mg kg^{-1}, respectively) in samples STN18AD-family house and STN35AD-family house, collected in the immediate vicinity of the Salgótarján coal-fired power plant (CFPP) (Figure 5B, 15, 16A-B; 19A). These particular attic dust samples have an also distinct group with coal ash sample (Figure 16A and 19A) and represent a reasonable proxy for the characteristics found in the in coal ash signature (U: 6.3 mg kg^{-1} and Th: 12.8 mg kg^{-1}; Tables S. 1) from the Salgótarján CFPP (Figure 5B, 6B). Interestingly, uranium enrichment in one urban soil sample (STN29US-park; 2.3 mg kg^{-1}; Figure 15A, 16A, 19A) from Salgótarján must have been derived from continuous U-Th supply from local coal ash cone over the course of decades, since this sampling sites are ~1100 m from the coal ash cone (Figure 5B; 6A-B; 15 and 16A-B), which is the clear candidate for the local pollution source in Salgótarján.

In contrast, the two Salgótarján urban soils with the highest Th content (STN13US-kindergarten: 6.2 mg kg^{-1} and STN36US-other (cemetery): 6.5 mg kg^{-1}; Figure 5B, 15B, 16B; 19A) also display the lowest U content (Figure 16A-B; 19A), a fact revealing the geochemical nature of U during chemical weathering in an oxidative environment. Under such circumstances U^{+6} is highly soluble in aqueous system and can be leached out from soil (Salminen et al., 2005). Conversely, Th (as Th^{+4}) remains immobile in resistant heavy minerals (e.g., zircon) present in soil (Salminen et al., 2005) or is adsorbed on the surface of clay minerals and organic substances (Cinelli et al., 2019). This alteration mechanism is an important factor in the U-Th distribution in Salgótarján and Ózd urban soils, and is responsible for the low relative abundance of U.

In addition, in terms of U content, Ózd urban soils almost totally match Salgótarján urban soils (Figure 19C); there are, however, five outliers among the Ózd urban soils (OZD38-other (roadside at the former industry), OZD39-playground, OZD40-park, OZD44-other (roadside at the former industry) and OZD54-other (roadside at the recent industry) (Figure 5C, 17A; Table S. 2), since the majority of these sampling sites are close to former industry district and its slag dumps (e.g., OZD44-other (roadside) (see Ózd sampling sites; Figure 5C; Table S. 2). This then provides an explanation for the significant input of contaminants from local industries on soils, as suggested by Abbaszade et al. 2022. Considering variations in the presence of the U-Th-K triplot in Ózd urban soil and attic dust samples (Figure 19B), it is highly likely that Ózd urban soil samples have two principal components: geogenic Ózd brown forest soil (BFS) and anthropogenic smelter slag.

It is an unexpected result that the two geogenic local brown forest samples (Salgótarján and Ózd) significantly differ in Th content (Figure 19A-B). Ózd brown forest soil has a Th content more than twice as high as that of Salgótarján brown forest soil, this latter being notable for being one of the highest in case (Figure 16B; 19C; Table 3). This discrepancy can be explained by the local geological differences (i.e., besides the similar sedimentary formations, in Salgótarján two kinds of volcanic rocks commonly occur which are not present in Ózd (Kercsmár et al., 2010).

Only the OZD45AD-blockhouse (former iron and steel factory) sample displays a Th concentration higher than 4 mg kg^{-1}, while the OZD54AD-church sample has an extremely low U content (0.5 mg kg^{-1}) (Figure 5C; 16A-B, 19B). Moreover, the upper layer of the one layered sample (OZD45ADUL; Figure S. 1; Table S. 2) had the greatest Th level among the samples of attic dust from Ózd (Figure 19B). The average values of the upper continental crust (UCC; Rudnik & Gao, 2004) and European topsoil (ETS; Salminen et al., 2005) overlap and reveal the degree of variability in K-content in the urban soils and attic dust studied in both cities (Table 3; Figure 19C). The majority of these samples have low, insignificant K-content ranged from 0.19 to 0.42 m/m % in urban soil, from 0.21 to 2.72 m/m % in attic dust in Salgótarján, and 0.15 to 0.42 m/m % in urban soil; 0.16 to 3.34 m/m % in attic dust in Ózd (Table 3; Figure 15C, 16C). However, from four attic dust samples from Salgótarján (STN15-blockhouse, STN22-family house, STN27-family house (outlier), STN40-family house (outlier), and six attic dust from Ózd (OZD17-family house, OZD36-family house (outlier), ÓZD39-family house (outlier), OZD40-family house (outlier), OZD48-family house, OZD54-church) form a distinct pattern in triplot (Figures 5B-C; 16; 19A, B, C; Table 3, S. 1 and S. 2). These are clearly

distinguishable due to their particular composition., namely, their elevated K content (Figure 16C). In particular, attic dust sample STN40-family house from Salgótarján has significantly elevated K-content (Figure 16C; 19A-B) even compared to the UCC (Rudnik & Gao, 2004) and European top soil (ETS; Salminen et al., 2005; Table 3). One likely reason for this seems to be that the residents stored potassium-based fertiliser in their attic space which could increase K levels. Attic dust sample STN27-family house has the second highest K content (1.15 m/m %), while having the lowest Th/U ratio (0.75; Figure 16C, 19A; Table S. 1). A similarly low Th/U ratio is characteristic of attic dust sample STN03-family house, collected from around one of the slag dumps, the Kucsord slag hill (0.88; Figure 16, 19; Table S. 1). In case, attic dust samples STN15-blockhouse and STN22-family house yield figures of 0.73 m/m % and 0.39 m/m %, and the lowest Th/U ratio (0.32; 0.20, respectively; Table S. 1; Figure S. 2), as well as an elevated U content (4.1 and 2.0 mg kg^{-1}, respectively; Table S. 1); taken together, these data strongly modify the U-Th relation observed in attic dust (Figure 19A-C).

Attic dust STN15-blockhouse is an unusual attic dust sample derived from a two-storeyed attic area whose roof was renovated (i.e., the tiles were replaced) in 2006 (Figure S. 1; Table S. 1). Thus, the accumulation time for attic dust was only around 12 years in this changes environment, a period during which the majority of the industrial factories were already shut down. Consequently, this sampling site provided one of the smallest amounts of dust collected in Salgótarján (~3 g), and this is a sample with a highly elevated U-content of unknown provenance (Table S. 1). It should be noted, however, that metal timber structure was present (Table S. 1) in the attic, which is rarely used in the studied cities (Figure S. 2).

Moreover, Ózd attic dust samples display a higher variability in their K-content than those from Salgótarján (Figure 16C; 19B-C). Three attic dust samples (OZD36-family house:1.3 m/m %; OZD39-family house: 1.8 m/m % and OZD40-family house: 3.3 m/m %) are highly enriched in K content and form a distinct group (Figure 16C; 19B). These sampling sites are located in the western and northern parts of the city (Figure 5C; 15C, 17C), areas where smallholder agricultural activity is characteristic, and which lie more than 4 km from the former and recent industrial areas (Figure 5C, 17C), and the use of K fertiliser represents a common soil treatment. It is true that all these attic dust sampling sites are located near agricultural areas (Figure 5C) where any surface soil dust may easily be transported locally by wind. It should be stated, however, that the role of soils and anthropogenic activities in atmospheric K fluxes remains unclear and is a subject requiring further research (Quennehen et al., 2012).

In terms of distinguished samples (Figure 19C), attic dust samples OZD54AD-church (U: 0.5 mg kg^{-1}; Th-0.9 mg kg^{-1} and K: 0.91 m/m %) OZD48AD-family house (U: 1.5 mg kg^{-1}; Th: 0.8 mg kg^{-1}; K: 0.73 m/m %) and OZD17AD-family house (U: 1 mg kg^{-1}; Th: 0.2 mg kg^{-1}; K: 0.75 m/m %) from Ózd, are a good example of natural origin, which corresponding to furthest sites from the industrial zone (Figure 5C, 17, 19B).

Study of the chemical composition of soils around CFPPs had already been published in Bangladesh (Habib et al., 2019; Figure 19C), with the authors reporting 4-9 times higher U- and 5-7 times higher Th- content in their soil samples than in those found in the Salgótarján and Ózd urban soil and attic dust samples, respectively (Figure 19A, B, C). Significant differences in U and Th content, between Salgótarján and the Bangladesh urban soils can be explained by chemical differences in the coal ash components present in urban soils from both areas.

The Cs concentration found in the Ózd attic dust samples (median: 2.1 mg kg^{-1}) is higher than those of the Salgótarján attic dust (median: 1.5 mg kg^{-1}) and urban soil (median: 1.1 mg kg^{-1}), whereas the brown forest soil (2.1 mg kg^{-1}) and coal ash (2.7 mg kg^{-1}) values are lower than the UCC and FOREGS values (Table 3; Figure 15D, 16D, 17D); 4.9 mg kg^{-1} Rudnik and Gao, 2004; 3.7 mg kg^{-1} Salminen et al., 2005). This may well relate to their different origins, which will be discussed later.

The highest concentrations of U (6.3 mg kg^{-1}) and Th (12.8 mg kg^{-1}) occur in the coal ash sample in Salgótarján (Figure 19 A-B; Table S. 1), supporting that by-products from the CFPP are indeed significant sources of U and Th enrichment in the studied samples, similarly to studies published from other countries (e.g. Lauer et al, 2015 and Llorens et al, 2001). It should, however, be noted that the only coal ash sample examined was that single one in Salgótarján (Figure 5B; 19); this, in turn, has lower U and Th content than those from coal ash samples from Poland (Silesia: 20.7 and 13.6 mg kg^{-1} and Lublin: 17.2 and 18.2 mg kg^{-1}, respectively; Parzentny & Róg, 2019), Spain (22.9 and 22.1 mg kg^{-1}, respectively; Llorens et al., 2001), Turkey (34 and 22 mg kg^{-1}, respectively; Finkelman, 1993); China (< 51.9 and < 50 mg kg^{-1}, respectively; Dai et al., 2014) and Bangladesh (26.6 and 65.1 mg kg^{-1}; Habib et al., 2019), respectively. These data on coal ash samples indicate the impact of differences in local geology, including the age of coal mined and used, in the physical (particularly meteorological) conditions, and in the operational technology of power plants and repository methods for by-products.

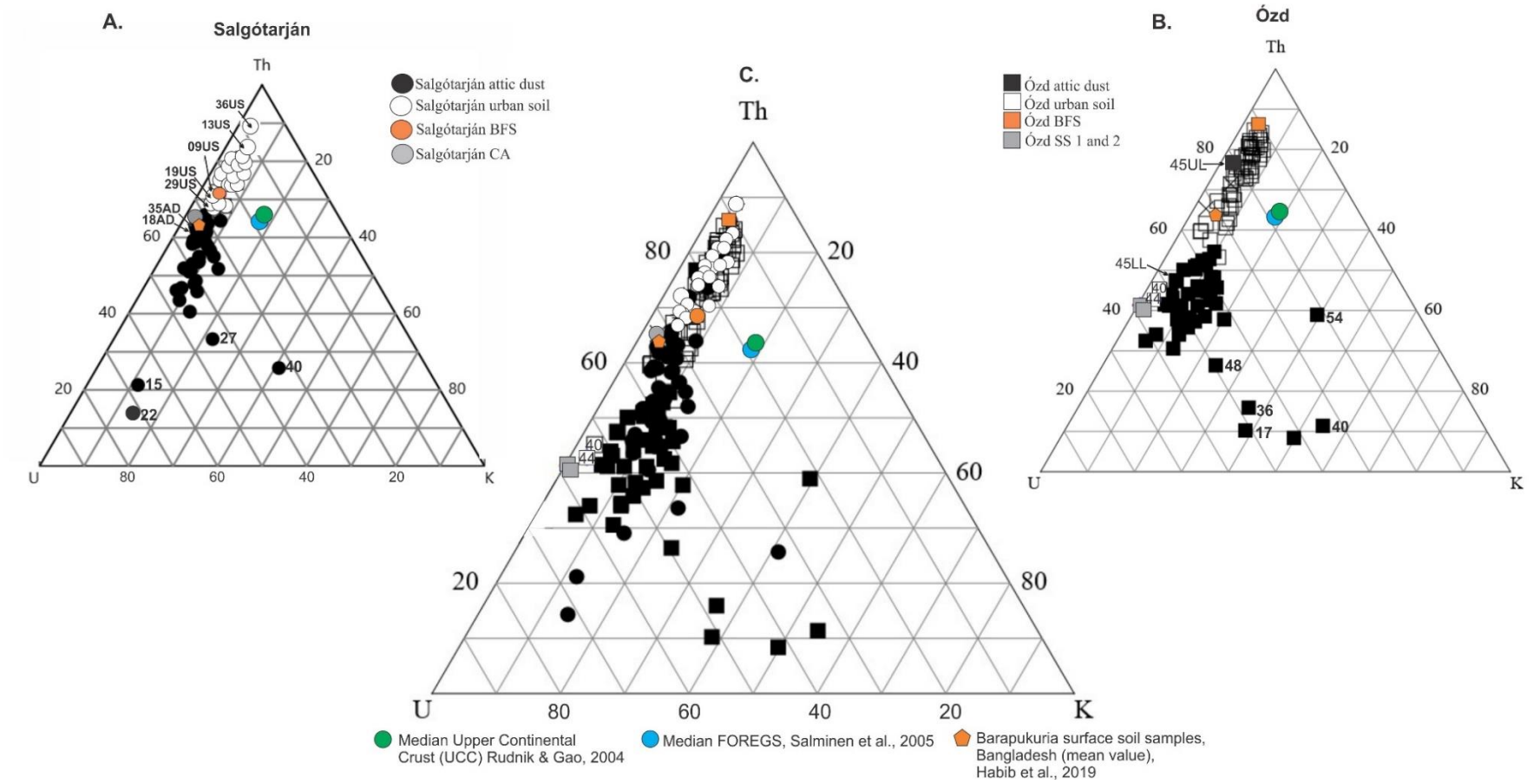

Figure 19. Variation of U-Th-K content (A) in Salgótarján urban soil (white circle), attic dust (black circle), brown forest soil (BFS) (orange circle), coal ash (CA) (grey circle) and (B) in Ózd urban soil (white square), attic dust (black square), brown forest soil (BFS) (orange square), smelter slag (SS-1, -2) (grey square), and (C) compilation of all studied samples in comparison with median of upper continental curst (green circle) (Rudnick and Gao, 2004), median of FOREGS (blue circle) (Salminen et al., 2005) and mean of Barapukuria (Bangladesh) surface soil (Habib et al., 2019).

5.2 Radium-226, ^{232}Th, ^{40}K and ^{137}Cs in urban soil, attic dust, brown forest soil and coal ash samples Salgótarján and Ózd

5.2.1 Urban soil from Salgótarján

All of the studied urban soil samples exhibit higher ^{226}Ra, ^{232}Th and ^{40}K concentrations than the one of brown forest soils (BFS) (14.1 ± 1.3, 15.7 ± 2.3 and 318.8 ± 9.0, respectively), whereas all of them contain lower ^{137}Cs concentrations than the BFS sample (18.4 ± 0.6) (Table 4; Figure 18A, B, C, D). Therefore, the local brown forest soil is indeed considered as a significant natural geogenic contribution to the studied urban soil samples.

Three urban soil samples, namely STN29US-playground, STN09US-park and STN21US-other (roadside) (Figure 5B), exhibit the highest ^{226}Ra (38.3 ± 1.4, 36.2 ± 1.5 and 33.7 ± 1.4, respectively) and ^{232}Th (46.0 ± 2.6, 48.8 ± 3.6 and 34.0 ± 3.9 Bq kg^{-1}, respectively) activity concentrations among the urban soils (Figure 20A; Table S. 1). Urban soil STN09 (which also exhibits an elevated elemental Th concentration (Figure 20A; Table S. 1) is close to one of the largest slag dumps in the city called Kucsord Hill (Figure 5B), which must be considered the leading candidate for the supply of Th to urban soils. Moreover, STN21US - other and STN29US - playground are closest to the CFPP, suggesting again the coal ash has a significant contribution to the studied urban soils, discussed later.

The ^{226}Ra-^{232}Th-^{40}K triplot graphically depicts the ratios of these three radionuclides in different media (in the studied urban soil, brown forest soil, attic dust and coal ash) (Fig. 20A, B, C). The activity concentrations (Bq kg^{-1}) were normalized to 100. For the purpose of a comparison, the same activity concentration values of surface soils and attic dust in the vicinity of other CFPP are also indicated in the plot. (Note that coal ash and attic dust are compared following). The activity concentrations of urban soils in Salgótarján fall within the mean values from China (Dai et al., 2007), Greece (Papaefthymiou et al., 2013), Poland (Bem et al., 2002), Serbia (Tanic et al., 2016), Spain (Charro et al., 2013a) and Turkey (Cevik et al., 2008) (Figure 20C). Note that the brown forest soil and mean values of soils worldwide (not only in the vicinity of CFPPs) also fall within those measured in Salgótarján (UNSCEAR, 2010) (Figure 20C).

The mean value of surface soil samples in the vicinity of CFPP in India is richer in ^{232}Th (Mishra, 2004), moreover, in Bangladesh (Habib et al., 2019) and Malaysia (Amin et al., 2013) are richer in ^{232}Th and ^{226}Ra, whereas in Brazil (Flues et al., 2002) and Ajka (Hungary) (Papp et al., 2002) much higher concentrations of ^{226}Ra are found compared to urban soils in Salgótarján (Figure 20C; Table 6). In Ajka, certain disturbed surface soils have activity concentrations as high as 1256 Bq kg^{-1} (Papp et al., 2002). It was reported that the Cretaceous

brown coal from Ajka contains approximately 94-152 mg kg^{-1} U concentration (Szabó, 1992), whereas Miocene brown coal from Salgótarján contains only 1 mg kg^{-1} U (Salazar – Yanez et al., 2021), shedding light on the differences in the local geology (age of coal) and coalification process, which increase the U concentration and as a result the ^{226}Ra activity concentration in its by-product, namely coal ash (Tables 6 and S. 1).

In fact, all the mean ^{226}Ra activity concentrations of soils compared in the vicinity of CFPPs, such as in Ajka (Hungary), Serbia, Spain, Turkey, China, India, Brazil, Greece, Malaysia and Bangladesh, are higher than those in Salgótarján, except in Poland (Table 6). Furthermore, the ^{232}Th activity concentration is only lower in Poland, whereas it is almost the same in Ajka (Hungary), Brazil, Greece, Serbia and Turkey but higher in Bangladesh, China, India, Malaysia and Spain (Table 6).

Potassium-40 activity concentrations are lower in Poland, Brazil and Malaysia, the same in Ajka (Hungary), Greece, India and Turkey, whereas higher in China, Serbia and Spain (Table 6). The ^{137}Cs activity concentration is only lower in Poland and higher in all the other referred countries (Table 6). Overall, urban soils from Salgótarján contain lower values of ^{226}Ra, ^{232}Th, ^{40}K and ^{137}Cs when compared to soils in the vicinity of other CFPPs and those worldwide.

5.2.2 Attic dust from Salgótarján and Ózd

Due to the absence of a worldwide long-lived natural radioactivity database for attic dust, our data were compared to the Salgótarján urban soils and coal ash, the attic dust samples from two other Hungarian industrial cities, namely Ózd and Ajka, and the surface soil samples in the vicinity of the CFPP in Ajka as well as those in other countries (Figure 20C, Table 6).

It can be seen from the boxplots that the ranges of ^{226}Ra, ^{232}Th, ^{40}K and ^{137}Cs activity concentrations of the attic dust samples are wider than for the urban soil ones (Figure 18; Table 6). Therefore, the activity concentrations of these radionuclides are more variable in attic dust samples than in urban soil ones. However, the ^{226}Ra, ^{232}Th and ^{40}K values contain outliers unlike the urban soil ones. The activity concentrations of ^{226}Ra, ^{40}K and ^{137}Cs in the attic dust samples are statistically significantly higher than in the urban soil ones in Salgótarján when comparing their medians (Figure 18; Table 4, 6). However, no statistically significant difference was observed in their ^{232}Th activity concentrations (Figure 18; Table 4, 6).

Rather distinct patterns were observable in variations of the ^{226}Ra-^{232}Th-^{40}K triplot between Salgótarján and Ózd attic dust (Figure 20C). Notably, the majority of Salgótarján attic dust has higher activity concentrations than those of attic dust collected from Ózd (Figure 20C; Table 4, 6). In Salgótarján attic dust, activity concentrations of ^{226}Ra vary from below the detection

limit (0.9 Bq kg^{-1}) up to 145.6 ± 8.3 Bq kg^{-1}, including the two outlier samples (STN35AD-family house and STN18AD-family house) (Figure 18A, 20A). The maximum activity concentration of Ózd attic dust samples are up to 63.3 ± 0.9 Bq kg^{-1}, which is a reason of the highly chemical characteristics of coal ash and smelter slag signatures as already stated (Figure 18, 20; Table 4, 6; Salazar-Yanez et al., 2021; Abbaszade et al., 2022). Broad elevated ranges of ^{232}Th activity concentration with partial overlap are seen in attic dust (from 8.0 ± 2.6 to 94.3 ± 9.6 Bq kg^{-1}) and urban soil samples (34.0 ± 2.4 Bq kg^{-1}; Table 4, 6) from Salgótarján, with the exception of the two outlier attic dust (STN35AD - family house and STN18AD-family house) (Figure 18, 20). However, the relatively low ^{232}Th activity concentration of Ózd attic dust samples (8.0 ± 6.2 to 27.1 ± 3.4 Bq kg^{-1}) indicates the possibility of low enrichment. Furthermore, ^{232}Th mobility was inhibited by the incorporation of Th^{4+} in insoluble heavy minerals (like zircon), followed by adsorption on clays and/or organics (Barnett et al., 2000), as stated earlier.

The two outlier Salgótarján attic dust samples (STN18AD-family house and STN35AD-family house) in terms of ^{226}Ra and ^{232}Th activity concentration form a distinct subgroup with the Salgótarján coal ash sample (Figure 18, 20) supporting our previous statement. This supports the conjecture that coal ash is an endmember in the studied samples under consideration here, indicating their contamination levels. Furthermore, attic dust samples STN17AD-family house (91.6 ± 6.4 and 61.0 ± 9.6 Bq kg^{-1}) and STN32AD-family house (91.6 ± 6.4 and 42.8 ± 12.4 Bq kg^{-1}) (Figure 5; Table S. 1) also have elevated activity concentrations, ^{226}Ra and ^{232}Th (Figure 20; Table S. 1), which are located in southeastern hilly part from local CFPP (Figure 5). The prevalent wind direction is from the northwest which is capable of transporting particles to the south from the nearby CFPP as well as from the coal ash cone, potential slag dumps e.g., Inászó slag dump and Kucsurd Hill (Figure 5B; 15 A-B). It is assumed that the local weather conditions can changes capable of changing the pathway of airborne dust materials, e.g., because of the presence of the valley stretching from the west to the east, which can also alter the direction of the wind and rain (Tserendorj et al., 2022a).

The radium-226 activity concentration in attic dust sample STN15AD-blockhouse from Salgótarján (Figure 5; S. 2), falls below the detection limit, and its ^{232}Th value is the lowest (Table S. 1; Figure S. 2, 20A). These strikingly low values of activity concentration (Table S. 1) are in accordance with the previous conclusions concerning the elemental concentration of Th (and U) (Table S. 1; Figure S. 1).

In addition, a distinct subgroup may be distinguished, composed of attic dust collected from Ózd (OZD17AD-family house, OZD34AD-family house, OZD40AD-family house, OZD52AD-family house and OZD54AD-church), this subgroup displays a significantly depleted level of ^{226}Ra activity concentration (3.3; <dl; 9.5 and 2.6 Bq kg^{-1}, respectively), (Figure 20B; Table S. 2). Low U content in the attic dust samples listed above can be assumed in terms of a sequence of natural processes, the rainwater (with lower pH) logging on the surface soil, washing the soluble U-oxyanion-complex [UO^{-}_{2}] from one place to another, a process that fractionates the Ra in the loosely bound surface soil (Abedin & Khan, 2022).

Outlier ^{40}K activity concentration in attic dust was measured at a family house (STN40AD: 1382.3 ± 76.6 Bq kg^{-1}; Figure 18, 20A; Table 6) close to this sampling site, a location that was responsible for the urban soil sample (STN36US-other, cemetery) bearing the highest amount of K. This is most probably due to the high K content (2.7 m/m %; Figure 16, 18, 20) supporting the assumption of Tanić et al. 2016, as previously discussed. This agreement between the studies highlights the common chemical features in these environmentally coupled samples (Figure 20) in Salgótarján. In accordance with, attic dust sample OZD40AD-family house collected from Ózd, displayed elevated ^{40}K activity concentration (1493.7 ± 78 Bq kg^{-1}; Figure 18, 20), a figure that can be characterized as a high K content (3.3 m/m %; Figure 18D, 20), possibly to a significant input of K from the surrounding agricultural area (Figure 5). However, the lowest ^{40}K activity concentration (OZD52AD-family house; 80.5 Bq kg^{-1}; Figure 20B; Table S. 2) and its K concentration also one of the lowest one (0.17 m/m %; Table S. 2). which is unusual feature compared to the majority of attic dust samples in Ózd (Figure 20B). This cannot be explained easily, some unknown mechanism (s) resulting in the lowest ^{40}K content as well as ^{226}Ra (< dl; Table S. 2) and ^{232}Th (8.1 Bq kg^{-1}) activity concentrations (Table S. 2).

Attic dust samples from other Hungarian industrialized city, namely Ajka, show different ^{226}Ra activity concentrations than those recorded in Salgótarján and Ózd. In Ózd, the values ranged between 9.5 ± 2.7 and 63.3 ± 0.9 with a mean of 35.7 ± 3.3 Bq kg^{-1} which are lower than those in attic dust from Salgótarján (Figure 20; Table 6), suggesting a different pollution source in Ózd, e.g. smelter slag (Salazar-Yanez et al., 2021) because of the former steel and iron works. On the other hand, in Ajka, these values ranged from 64.2 ± 5.0 to 587.7 ± 5.6 with a mean of 318.9 ± 53.7 Bq kg^{-1} (Tserendorj et al., 2022b), which are much higher than those from attic dust samples in Salgótarján and Ózd (Figure 20; Table 6). This must have been caused by the unusually high uranium concentration in the Ajka brown coal (Szabó, 1992) and the fact that

coal was combusted in Salgótarján for a shorter period from 1891 to 1973 than in Ajka from 1872 to 1995 (Papp et al., 2002; Wirth et al., 2012).

The mean values of atmospherically derived artificial ^{137}Cs activity concentrations in Salgótarján and Ózd attic dusts are ~15- and ~19 times higher (Tserendorj et al., 2022a) than that of Salgótarján urban soil samples (Figure 19D; Table 4) and higher than those reported in the literature about (surface) soils around CFPPs (Table 6; e.g., Bem et al., 2002; Charro et al., 2013). This indicates that attic dust is effective at recording ^{137}Cs, since it represents the long-term dynamic accumulation of material that may well have lain undisturbed for decades in closed space (Cizdziel et al., 2000; Tserendorj et al., 2022a). In contrast, in urban soils from open environments, such as park, kindergarten, playground, etc., the dispersion of particles to which ^{137}Cs had become attached probably took place because they migrated deeper than 15 cm into the upper soil or were washed away by natural processes (dissolution in water and precipitation), (Ritchie and McHenry, 1990).

In summary, the studied radionuclides exhibit much higher concentrations (except for ^{232}Th) and also a higher degree of variability in the attic dust than in the urban soils in the study area. By comparing ^{226}Ra and ^{232}Th activity concentrations in the attic dust from the two industrial areas, different pollution sources revealed that their activity concentrations in the attic dust depend on those in the local pollution sources. Regarding the ^{137}Cs activity concentration in attic dust versus that in urban soil, it is clear that attic dust can accumulate pollutants better than urban soil, therefore, attic dust would be a useful material for studies on pollution.

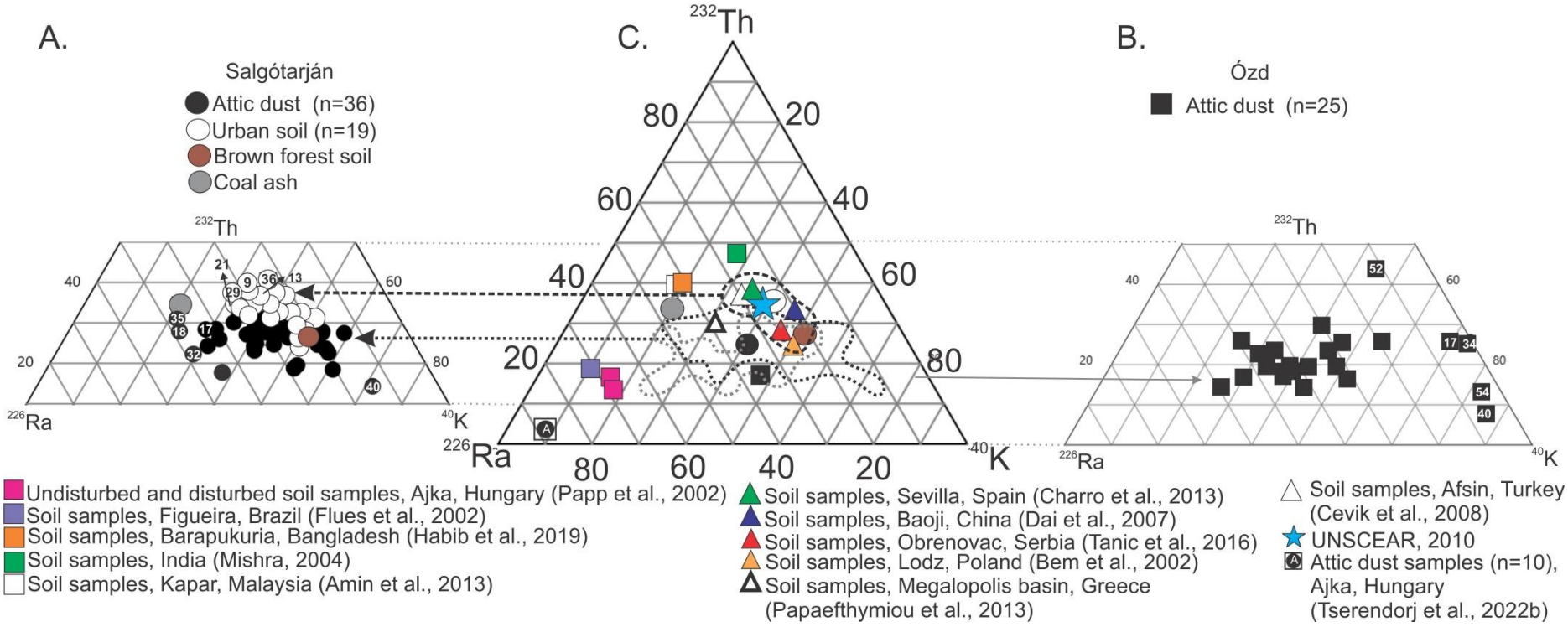

Figure 20. Variation of ^{226}Ra-^{232}Th-^{40}K activity concentration (Bq kg^{-1}) (A) in Salgótarján urban soil (white circle), attic dust (black circle), brown forest soil (BFS) (orange circle), coal ash (CA) (grey circle) and (B) in Ózd attic dust (black square), (C) compilation of all studied samples in comparison with mean surface soils of adjacent areas of coal-fired power plants from different countries (Table 6). Note: ^{40}K values divided by 10 for better comparison visibility.

Table 6. Comparison of the activity concentrations (Bq kg^{-1}) of ^{226}Ra, ^{232}Th, ^{40}K and ^{137}Cs in urban soils and attic dusts of Salgótarján and attic dust of Ózd, as well as surface soils of adjacent areas of coal-fired power plants from different countries. Median values for soil samples from all over the Earth (not just around CFPPs) are also shown (UNSCEAR, 2000).

Locality	**Type of samples**	**Activity concentrations (Bq kg^{-1}) mean (min-max)**				**References**
		^{226}Ra	**^{232}Th**	**^{40}K**	**^{137}Cs**	
Salgótarján city, Hungary	Attic dust n=36 (undisturbed)	43 (12*[1]-145)	34 (8 - 94)	534 (309 - 1382)	88 (5 -169)	This study
Salgótarján city, Hungary	Urban soil n=19 (disturbed, 0-15cm)	25 (15 - 38)	33 (18 - 48)	386 (344 - 447)	6 (0.7 - 17)	This study
Ózd, Hungary	Attic dust n=25 (undisturbed)	31 (2*[1] - 62)	16 (8 - 26)	400 (80 - 1493)	88 (2 - 272)	This study
Ajka, Hungary	Attic dust n=10 (undisturbed)	318 (64 - 587)	21 (15 - 31)	442 (190 - 1976)	85 (32 – 114)	Tserendorj et al., 2022b
Afsin, Turkey	Soil samples*, n=21 (0-15 cm)	33 (7-78)	36 (26-49)	379 (304-744)	--	Cevik et al.,2008
Ajka, Hungary	Soil samples*, n=38 (undisturbed,0-20 cm)	129 (15-883)	27 (12-43)	337 (146-596)	20 (3*[2] -150)	Papp et al., 2002
Ajka, Hungary	Soil samples*, n=47 (disturbed, 0-20 cm)	136 (21- 1256)	25 (15-41)	329 (176-567)	17 (2-69)	Papp et al., 2002
All over the country, India	Surface soil samples* n= >30	37 (14-155)	69 (18 - 155)	396 (11-706)	--	Mishra, 2004
Baoji, China	Soil samples*, n=24 (0-25 cm)	32 (23-40)	50 (38-66)	720 (498-858)	--	Dai et al., 2007
Barapukuria, Bangladesh	Soil samples*, n=24 (0-10 cm)	103 (51-77)	103 (71-126)	494 (210-763)	--	Habib et al., 2019
Figueira, Brazil	Soil samples*, n=52 (0-25 cm)	151 (12-282)	39 (18-55)	233 (88-299)	--	Flues et al., 2002
Kapar, Malaysia	Surface soil samples*, n=14 (0-5 cm)	63 (31 - 152)	50 (20-74)	288 (194-358)	--	Amin et al., 2013
Lodz, Poland	Soil samples*, n=29 (undisturbed; 0-30 cm)	16 (7-21)	15 (9-20)	310 (221-434)	5 (1-15)	Bem et al., 2002
Megalopolis basin, Greece	Surface soil samples*, n=14 (0-5 cm)	45 (21-125)	32 (24-40)	337 (234-412)	80 (7-314)	Papaefthymiou et al., 2013
Obrenovac, Serbia	Soil samples*, n=30 (disturbed, 0-10 cm)	32 (19-49)	33 (14-55)	598 (372-833)	--	Tanić et al., 2016
Sevilla, Spain	Surface soil samples*, n=67 (undisturbed; 0-5 cm)	38 (13-67)	43 (15-68)	445 (97-790)	29 (3*[2]-209)	Charro et al., 2013
Mean value of the World soil	Soils	35 (17-60)	45 (11-64)	412 (140-850)	--	UNSCEAR, 2010

*Authors named their samples which partially cover of the depth of urban soil samples. *[1] the number of samples are below the detection limit

5.2.3 Coal ash from Salgótarján

Salgótarján coal ash sample from the Pintértelep coal ash cone (Figure 5B, 6A) has higher ^{226}Ra (91.1±1.7 Bg kg^{-1}) and ^{232}Th (69.5 ± 3.3 Bg kg^{-1}) activity concentrations than all the other samples studied (i.e., higher than urban soil, brown forest soil and attic dust samples), with the exception of the two outlier attic dust samples: STN18AD-family house and STN35AD-family house (^{226}Ra: 145.6 ± 8.3 and 143.5 ± 8.1, ^{232}Th: 83.9 ± 8.0 and 94.3 ± 9.6 Bg kg^{-1}, respectively (Figure 18A-B; Table 6). Activity concentration of ^{40}K in coal ash sample is much lower than the majority of attic dust (414.8 ±8.9 Bq kg^{-1}), and activity concentration of ^{137}Cs which represents the lowest value among all studied samples (0.09 ± 0.4 ; Figure 18, 20D; Table 4). Salgótarján coal ash has slightly lower activity concentrations than those of average Hungarian data (*n*=75) on coal ash (^{226}Ra: 110, ^{232}Th: 114 and ^{40}K: 435 Bq kg^{-1} Trevisi et al., 2018) and even lower than those from other European countries (Germany, Poland, Czechia, Romania and Slovakia). However, the variations in activity concentrations are remarkably similar to those of the above-mentioned countries (Table 7). In addition, the two outlier attic dust samples (STN18-family house and STN35-family house) are in high degree of agreement with average coal ash values of the Central European countries (Table 7 ; Trevisi et al., 2018).

Table 7. Average activity concentration (Bq kg $^{-1}$) of ^{226}Ra, ^{232}Th and ^{40}K of coal ash samples from some European countries (Trevisi et al., 2018), and of coal ash (CA) from Salgótarján. For comparison values for the three outlier attic dust samples (STN18AD and STN35AD) are also shown.

Countries	Number of samples	^{226}Ra	^{232}Th	^{40}K
Salgótarján (this study)	1	91	69	414
STN18AD (this study)	1	145	83	708
STN35AD (this study)	1	143	94	649
Slovenia	2	250	37	383
Germany	30	164	94	517
Hungary	75	110	114	435
Slovakia	226	123	76	769
Romania	179	219	116	595
Czech Republic	1378	146	86	669
Poland	1941	200	118	798

Accordingly, these two attic dust samples can be taken as representative, in environmental geochemical features, of the original coal ash compared to that observed at the Pintértelep coal ash cone (Figure 5, 6B, 18; Table 7). The diminished activity concentrations in the Salgótarján coal ash can be explained by its long exposure time (the CFPP started operating in 1912; Wirth et al., 2012) and strong chemical (rain) and physical (wind) weathering processes acting at the Pintértelep coal ash cone (Figure 6A) as reported by Szabó et al. (2007) and Abbaszade et al. (2022).

5.2.4 Relationships among radionuclides of different origin

Prior to any hypothesis test in the comparison of Salgótarján attic dust and urban soil samples, the radionuclides were tested for degree of normality (Shapiro & Wilk, 1965; Reimann et al., 2008) (Table 8) in order to obtain an in-depth analysis for further statistical treatment. The dataset of radionuclides in attic dust turns out to be non-normally distributed (^{226}Ra: $p < 0.00$, ^{232}Th: $p < 0.00$ and ^{40}K: $p < 0.00$; Table 4, 8), except ^{137}Cs activity levels ($p = 0.18$; Table 8). In contrast, all datasets of urban soil samples are normally distributed (^{226}Ra: $p < 0.47$, ^{232}Th: $p < 0.53$ and ^{40}K: $p < 0.98$; Table 8), with the exception of ^{137}Cs ($p < 0.00$; Table 8). Given their non-normal sample distribution, a nonparametric test (Schober et al., 2018) was used to ensure the uniform and reproducible handling of the activity concentrations. The relationship of ^{232}Th with ^{226}Ra, and ^{232}Th with ^{40}K in attic dusts ($r = 0.75$, $p < 0.01$; $r = 0.4$, $p = 0.04$, respectively; Table 8) and those in urban soils ($r = 0.92$, $p < 0.01$; $r = 0.33$, $p = 0.05$, respectively; Table 8) were significantly and positively correlated (Table 8).

Table 8. Spearman correlation coefficients for the studied radionuclides (^{226}Ra, ^{232}Th, ^{40}K and ^{137}Cs) in attic dust and urban soil samples from Salgótarján, significant associations are bolded (p-values shown in parenthesis)

	Attic dust (n=36)			Urban soil (n=19)		
	^{226}Ra	^{232}Th	^{40}K	^{226}Ra	^{232}Th	^{40}K
^{232}Th	**0.92 (0.00) ****	1		**0.75 (0.00) ****	1	
^{40}K	0.30 (0.08)	**0.33 (0.05) ***	1	0.00 (0.99)	**0.4 (0.04) ***	1
^{137}Cs	0.04 (0.78)	- 0.02 (0.90)	0.30 (0.08)	0.12 (0.61)	0.31 (0.18)	0.33 (0.16)

** Significance level at <0.05; ** significance level at <0.01*

This indicates that the geological source of these natural radionuclides was common as pointed out by Navas et al. (2011) and Tanic et al. (2016), which in this case is the long-term use of

local Miocene brown coal (Kercsmár et al., 2010), 82 years of combustion at the local CFPP to be precise. The absence of any correlation between ^{226}Ra and ^{40}K reflects the differences in the origin and mobilization of both natural radionuclides (Navas et al., 2011). No correlation was observed between ^{226}Ra, ^{232}Th, ^{40}K and ^{137}Cs as a consequence of the Chernobyl NPP accident, which released ^{137}Cs into the environment (De Cort et al., 1998).

5.2.5 Relationship between radionuclides in attic dust and urban soil as a function of distance from a coal-fired power plant

Among the radionuclides studied, the decreasing activity concentrations of ^{226}Ra in Salgótarján attic dust and urban soil samples demonstrates a significant correlation with increasing distance from the CFPP (attic dust: r = -0.4, p < 0.01; urban soil: r = -0.4, p = 0.05; Figure 21A). Interestingly, a similar correlation is observed for the U content of attic dust as a function of distance from the CFPP (r = -0.5, p < 0.01) (Figure S. 3). Such a correlation is also true for ^{232}Th in attic dust (r = 0.4, p < 0.01), and indeed visible in the much steeper slope than that in urban soil (r = 0.04, p < 0.8; Figure 21B). No correlation was observed between the other radionuclides and elemental concentrations as the distance from the CFPP varied.

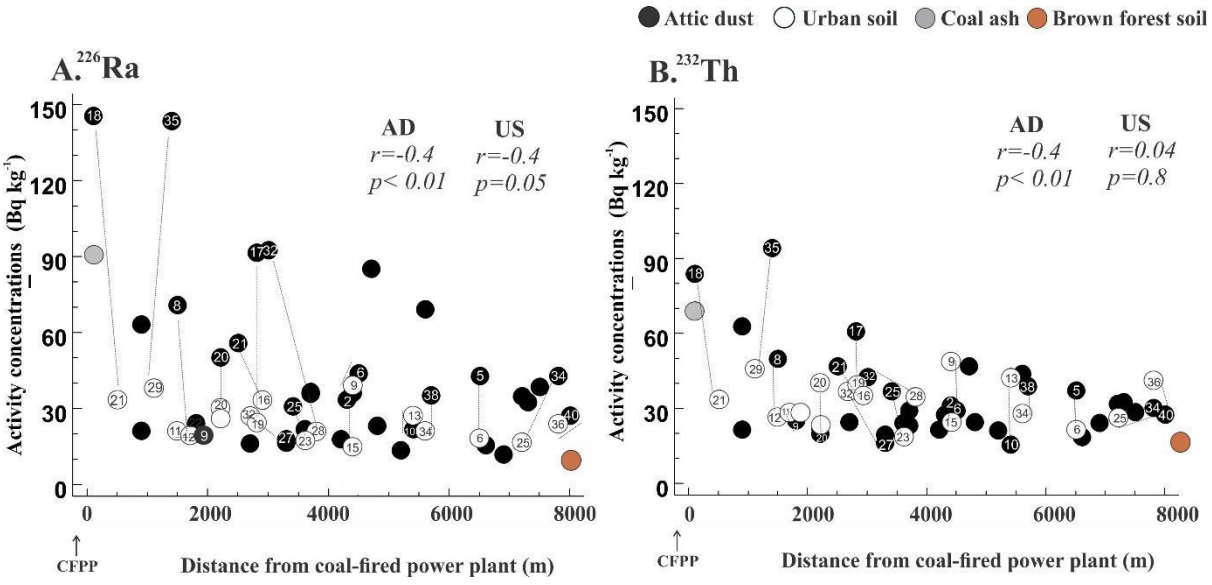

Figure 21. Relationship between distance of sampling site from coal-fired power plant (CFPP) and activity concentrations of studied radionuclides (A: ^{226}Ra and B: ^{232}Th) in Salgótarján urban soils and attic dusts. Note that sample STN15AD-blockhouse is excluded.

Furthermore, the lowest activity concentration of ^{226}Ra and ^{232}Th was measured in the brown forest soil (Figure 18A-B; 20; 21A-B), the sampling site farthest from the CFPP (8100 m) (Figure 21A-B). This supports the assumption that brown forest soil is a strong natural geogenic

component of all the samples studied, as discussed previously. On the other hand, the two outlier attic dust samples (STN18AD-family house and STN35AD-family house), located <1400 m from the CFPP, showed the highest activity concentrations of ^{226}Ra and ^{232}Th (Figure 21A-B). This is why these attic dust samples can be considered proxies for unweathered coal ash as argued above. Their corresponding urban soil samples (STN21-roadside and STN29-park) also had correspondingly slightly elevated activity concentrations of ^{226}Ra and ^{232}Th (Figure 21A-B). Thus, the question is raised of whether the attic dust-urban soil pairs (Figure 21A, B) shed light on any relationship between the two environmental sample types. The ratio of attic dust/urban soil in ^{226}Ra and ^{232}Th, respectively, in the 17 sample couples (Figure 22) shows a strong relationship (r =0.73; p = <0.01; Figure 22). As < 76 % (n=13) of attic dust samples have higher ^{226}Ra activity concentrations than those of ^{232}Th (Table S. 1). These couples (n=13) show the highest potential influence of the by-products of the CFPP (namely, coal ash) (Figure 21A-B; Table S. 1) and may also be a reflection of the undisturbed nature of the attic area. There are two low ratios (0.7/0.4 for STN27AD-family house/STN32US-park and 08/0.4 for STN10AD-family house/STN13US-kindergarten; Figure 22) associated with couples showing higher activity concentrations of ^{232}Th in urban soils than in corresponding attic dust samples (Table S1). These sampling sites are located further than 2700 m to the west from the CFPP. The ages of these houses are widely different (78 and 38 years; Table S. 1), and at least the older one would have been expected to have an elevated ^{226}Ra content, but the roof-space is not perfectly insulated, which means deposited particles might be transported or reaccumulation process occurred.

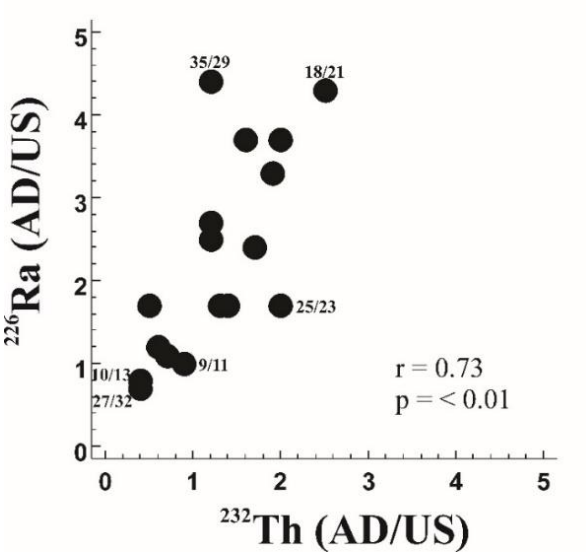

Figure 22. Relationship between Salgótarján attic dust and urban soil ratios of ^{226}Ra and ^{232}Th activity concentrations in attic dust-urban soil couples (n=17).

The other two attic dust-urban soil couples (STN09AD-family house, STN11US-park and STN25AD-church/STN23US-playground) map showing highly similar ratios of attic dust and urban soil in terms of ^{226}Ra and ^{232}Th activity concentrations, and are situated at to north of the CFPP at a distance of <4500 m (Figure 21A-B; 22 and Table S. 1). Furthermore, it is a clear indication that the chemical and physical properties of attic dust had been preserved for decades in undisturbed form rather than in the disturbed urban soil (Figure 16, 18, 19, 21). In contrast, physical mechanisms of soil redistribution (deposition) and leaching/sorption processes in soil layers were the driving force of the dispersion of such radionuclides as ^{226}Ra and ^{232}Th (Navas et al., 2011). As a result, the attic dust dataset was the only one capable of providing sufficient data for a map of the spatial distribution of ^{226}Ra, ^{232}Th and ^{40}K activity concentrations.

5.3 Impact of ^{137}Cs elevated in attic dusts collected from Salgótarján and Ózd

The ^{137}Cs activity concentrations (Bq kg^{-1}) found in Salgótarján and Ózd attic dusts are compared with two studies in the USA (Cizdziel et al., 1998, Ilacqua et al., 2003; Table 9). Unfortunately, there is no more data published about ^{137}Cs in attic dust. The arithmetic average of ^{137}Cs activity levels in attic dust (STN 88.5 $\pm$ 5.1 Bq kg^{-1} and OZD 87.8 $\pm$ 4.5 Bq kg^{-1}) is comparable to previous findings in Dover and New Jersey (Cizdziel et al., 1998) with an arithmetic mean of 42 $\pm$ 28 Bq kg^{-1}. The arithmetic mean values are (within the margin of errors) the same as at the Nevada test sites (NTS), including areas in Utah (Ilacqua et al., 2003), 75 $\pm$ 53 Bq kg^{-1}. However, in Europe, the total ^{137}Cs activity from the Chernobyl accident was estimated at around 85 PBq, whereas the global mean fallout was considerably lower, at around 20 PBq (De Cort et al., 1998). These data clearly suggest that most of ^{137}Cs contribution to Europe originated from the Chernobyl accident. Since there is a global scarcity of ^{137}Cs activity concentrations measured in attic dust samples, the present results are also compared to soil samples from Hungary and the surrounding countries (Table 9). The studied soils from central Hungary (Szabó et al., 2012) and northern part of Nógrád and Borsod-Abaúj-Zemplén counties Hungary (Szerbin et al., 1999) have lower ^{137}Cs activities (0 - 61.1 Bqkg^{-1}; 1 - 47 and 2 - 60 Bq kg^{-1}, respectively) than the attic dust (Table 9). A possible explanation for this is that the uppermost layer of various soils may be disturbed by anthropogenic activities (building and road construction, or even, conversely, the greening of the urban environment, potentially with soil replacement, etc.), or again by natural physical and chemical weathering processes. Thus, soil cannot preserve the past atmospheric ^{137}Cs pollution anywhere near as efficiently as attic dust.

Comparing the attic dust ^{137}Cs results herein with those of soils from other European countries, such as Spain (Navas et al., 2011), Macedonia (Dimovska et al., 2011), Greece (Vosniakos, 2012), Lithuania (Luksiené et al., 2015), Serbia (Milenkovic et al., 2015; Vukas et al., 2018), and Montenegro (Antovic et al., 2012), higher average values were recorded (Table 9). However, the study of soils in Austria and Romania elevated ^{137}Cs activity (over >200 kBq m^2 and from 6.6 - 2316.1 Bq kg^{-1}, respectively) (Bossew et al., 2001; Begy et al., 2017) than the Hungarian attic dusts, indicating a positive correlation with high annual rainfall in mountainous areas (i.e., Alps, Carpathians, Dinarides), as suggested by Begy et al. (2017). Although records of ^{137}Cs activity concentration in urban areas, particularly in attic dust, are globally highly scarce, it may be assumed that ^{137}Cs records in attic dust might support an approximate estimate of atmospheric deposition. It is of great interest that the report of the ^{137}Cs measurement of urban puddle sediment from Ekaterinburg (Ural region, Russia) with mean ^{137}Cs of 80 Bq kg^{-1} (Seleznev et al., 2010). The authors of this latter study proved that puddle sediment apparently traps the total accumulation of ^{137}Cs activity (Table 9). This average ^{137}Cs activity value is consistent with the estimated ^{137}Cs averages presented here from Salgótarján (88.5 $\pm$ 5.1 Bq kg^{-1}) and Ózd (87.8 $\pm$ 4.5 Bq kg^{-1}) urban areas (Table 9). This further suggests a long-term accumulation of ^{137}Cs in attic dust. The layered attic dust sample (OZD45AD-blockhouse, which is former iron-steel factory) from Ózd shows higher ^{137}Cs activities in lower layer (OZD45AD_LL; 16.0 $\pm$ 1.4 Bq kg^{-1}) than in the upper layer (OZD45AD_UL; 1.9 $\pm$ 1.0 Bq kg^{-1}) (Table S. 2; Figure S. 1). The sampled building was the repair hall of the former steel factory for more than a century, and this activity is assumed to provide the bottom layer. Later, the space was used as a small horsebox iron factory over a period of ~25 years. This activity also produced and released dust to form the upper layer, which displays a lower degree of variability in heavy metalloids than the lower layer (Salazar-Yanez et al., 2021). This observation might indicate the tendency of heavy metalloids to decrease concentrations of ^{137}Cs, a view supported by Outola et al, (2003) reporting on findings in a Finnish heavy metal industrial area.

Table 9. Comparison of ^{137}Cs activity concentration (Bq kg^{-1}) in different environmental samples (attic dust, urban soil, sediment and moss) of different countries deposited after Chernobyl nuclear power plant accident.

Country	Type of samples (Particle size, mm)	^{137}Cs activity concentration (Bq kg^{-1}) average (range)	References
Attic dust samples			
1. Salgótarján, Hungary	Attic dust n=36 (undisturbed); < 0.125 mm	88.5 ± 5.1 Bq kg^{-1} (5.5 - 169.9 Bq kg^{-1})	Present study
2. Ózd, Hungary	Attic dust n=25 (undisturbed); < 0.125 mm	87.8 ± 4.5 Bq kg^{-1} (16.0 - 272.9 Bq kg^{-1})	Present study
3. Nevada and Utah, USA	Attic dust n= 14 (undisturbed); < 2.36 mm	42 ± 28 Bq kg^{-1} (6 - 105 Bq kg^{-1})	Cizdziel et al. (1998)
4. New Jersey, USA	Attic dust n= 201 (undisturbed); NA	75 ± 53 Bq kg^{-1} (14-286 Bq kg^{-1})	Ilacqua et al. (2003)
Soil samples			
5. Pest County, Central Hungary	Soil samples, n=45 (0-30 cm, undisturbed); < 2 mm	9.5 Bq kg^{-1} (0-61.1 Bq kg^{-1})	Szabó et al. (2012)
6. All Hungarian counties across the whole country	Soil samples, n=19 (0-20 cm, disturbed, uncultivated); < 1.25 mm	1 - 47 Bq kg^{-1} (Nógrád county); 2-60 Bq kg^{-1} (Borsod-Abúj-Zemplén county)	Szerbin et al. (1999)
Across other countries and cities	**Soil and sediments samples**		
7. Austria	Soil samples n=2115 (measurements); NA	18.7 kBq/m^2 (>200 kBq/m^2)	Bossew et al. (2001)
8. Montenegro	Soil samples n=24 (0-5; 5-10; 10-15 cm, uncultivated); < 2 mm	65.3 Bq kg^{-1} (1.82 – 413 Bq kg^{-1}) 46 Bq kg^{-1} (1.9-141 Bq kg^{-1}) 36 Bq kg^{-1} (2-112 Bq kg^{-1})	Antovic et al. (2012)
9. Belgrade, Serbia	Urban soils n=22 (0-20 cm); < 2 mm	17 (0.7 – 35 Bq kg^{-1})	Vukašinović et al. (2018)
10. Kragujevac, Serbia	Soil samples n=30 (0-10 cm, undisturbed); < 2 mm	40.2 Bq kg^{-1} (0.5-90.5 Bq kg^{-1})	Milenkovic et al. (2015)
11. Kavadarci, Macedonia	Urban soil samples n=45 (0-5 cm); < 2 mm	41.5 Bq kg^{-1} (4 – 220 Bq kg^{-1})	Dimovska et al. (2011)
12. Lithuanian soil	Open meadow soil n =24 (0-10 cm, undisturbed); < 0.2 mm	5.04 Bq kg^{-1} (2 – 16.6 Bq kg^{-1})	Lukienė et al. (2015)
13. Transylvania region (Transylvanian Plateau and the Western Plain and Hills)	Soil samples (undisturbed) n=153 (0-20 cm); < 0.1 mm	177.3 Bq kg^{-1}(6.6 – 2316.1 Bq kg^{-1})	Begy et al. (2017)
14. Catchment in the Pyrenees, Spain	Soil samples (0-20 cm); < 2 mm	30.9 Bq kg^{-1} (4.4 – 64.7 Bq kg^{-1})	Navas et al. (2011)
15. All over Greece	Soil samples, n=780 (0-5 cm, undisturbed); < 2 mm	23.1 - 51.1 Bq kg^{-1}	Vosniakos (2012)
16. Ekaterinburg, Ural region, Russia	Puddle sediment (upper 0-5 cm); NA	80 Bq kg^{-1} (0-540 Bq kg^{-1});	Seleznev et al. (2010)

5.3.1 Relationship between age of house and ^{137}Cs activity concentrations in attic dust from Salgótarján and Ozd

Activity concentrations of ^{137}Cs in all attic dust samples from Salgótarján and Ózd seem to decrease gradually with increase in the age of the buildings (Figure 23). The regression (MM-estimator, Kalina et al., 2020) between ^{137}Cs and age of buildings is statistically significant is indeed robust: $r^2 = 0.05$, $p = 0.02$. In houses built after 1950 (the beginning of widespread nuclear testing), approx. 50 % of total attic dust samples have both a wide range (from 272.8 $\pm$ 13.0 to 5.5 $\pm$ 0.9 Bq kg $^{-1}$) and high ^{137}Cs average activity concentrations (108 Bq kg^{-1}), whereas attic dust collected in houses constructed before 1950 displays a narrower range (from 169.8 $\pm$ 8.8 to 1.9 $\pm$ 1.0 Bq kg^{-1}) and lower average activity concentration (71.9 Bq kg $^{-1}$; Figure 23 and Tables S. 1; S. 2). A study in New Jersey (Ilacqua et al., 2003) found elevated mean ^{137}Cs activity concentrations in older houses built 1955-1965, compared with more recent construction, as illustrated in Figure 23. The finding of the present research, that higher ^{137}Cs activities are to be found in houses built after 1950, is consistent with the results of Ilacqua et al. (2003) (Figure 23). However, the pattern of the three outlier samples with the highest ^{137}Cs values from Ózd (OZD47AD-family house OZD37AD-family house and OZD25AD-blockhouse; Figure 18D) shows a clear trend in the opposite direction: most elevated values derive from younger buildings (Figure 23). This cannot be easily explained: one or more unknown mechanisms resulting in ^{137}Cs enrichment seems to be operating - either that, or it may be that absolutely perfect isolation is responsible in attic area.

The remaining ~50% of total attic dust samples collected from houses built before 1950 shows a slightly decreasing tendency in activity concentration with increasing age of the houses (Figure 23; Table S. 1, S. 2). This trend indicates that ^{137}Cs activity concentration drops back to background values, to zero, if there is no additional source to overprint it. However, the elevated ^{137}Cs levels from four Salgótarján houses (STN17AD-family house, STN25AD-church, STN32AD-family house and STN34AD-family house) are noticeably higher than this general tendency would suggest. This variability in the data could be explained by one or more further accumulation processes. Of those four sampling sites, three (STN17AD-family house STN25AD-church, STN32AD-family house) are situated at the highest elevation in the study area (>410 m; Figure 5B; Table S. 1), and therefore it is probable that local topography is playing a significant role in accumulation. On the other hand, all of the other cases where average values fall below 59.2 Bq kg^{-1} in residential houses can be explained by the regular cleaning of attic areas in those houses, or the complete renovation of those houses, or an almost

airtight isolation. Cesium-137 activity in houses built before ~1950 may be assumed to have a long-term initial deposition in both settlements, a factor which will be readdressed in the geostatistical analysis. Therefore, even the well-constructed attic area can accumulate redistributed airborne particles (incl. ^{137}Cs) deriving from houses, which are uninhabited or in a derelict or ruined state, not to mention from gardens and streets, parks, playgrounds, etc. (Giardina et al, 2019). The efficiency of this process can be increased, for instance, by increasing elevation and wind speed as discussed herein, or, for instance, in cases of increasing building heights (Giardina et al., 2019). Consequently, it is obvious that even with the use of a strict sampling protocol (e.g., Völgyesi et al., 2014), it is not possible to avoid collection of particles and grains from construction materials, including entrance, chimney, wall, roof, etc.

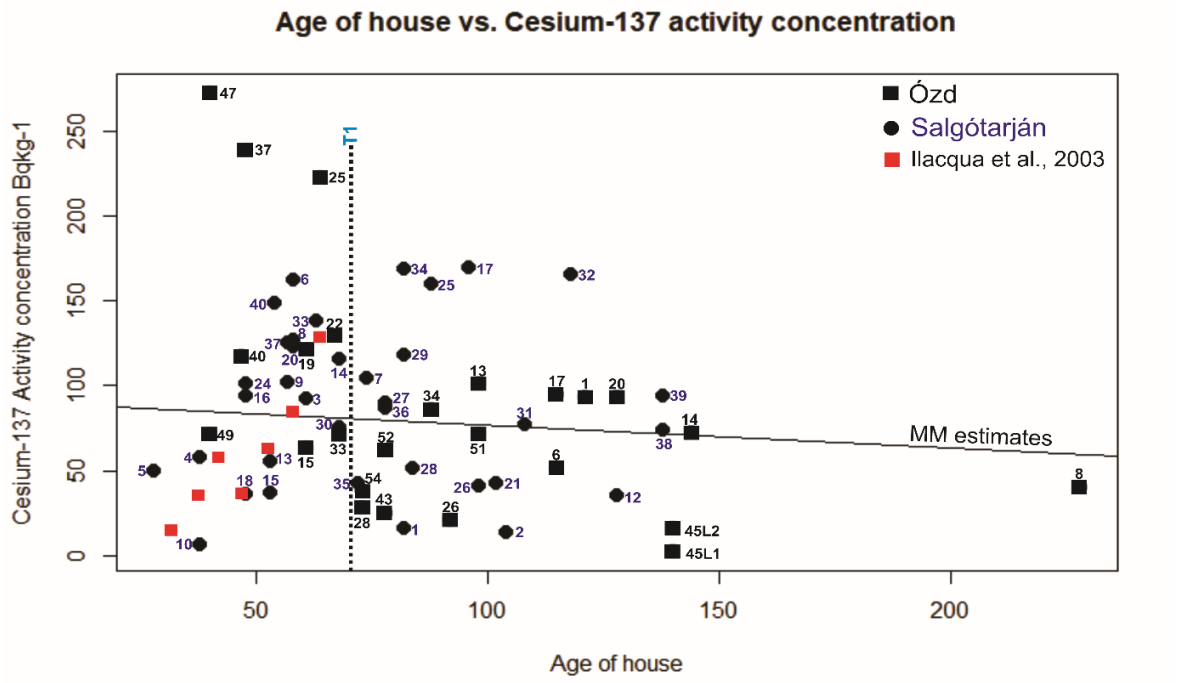

Figure 23. Robust relationship (MM estimates) between ^{137}Cs activity concentration of labelled attic dusts and age of houses in Salgótarján and Ózd (Table S. 1; S. 2). Vertical dotted and solid lines define marks (T1 = 1950). The red square displays ^{137}Cs activity concentration in attic dust from Dover, New Jersey (Ilacqua et al., 2003).

The two-layered attic dust sampling site (OZD45AD-repair hall of the former iron and steel factory, as discussed above) was built long before 1950 and also displays very low ^{137}Cs activity in the lower layer (OZD45LL-former iron and steel factory, 16.0 $\pm$ 1.4 Bq kg^{-1}; Table S. 2; Figure S. 1). The upper dust layer seems to have accumulated during the past ~25 years, and it also exhibits the lowest level of activity (OZD45UL- recently it is a Horse box factory;

1.9 ± 1.0 Bq kg[1]). It cannot be excluded that the upper layer at its lower boundary contains a certain quantity of material derived from the older lower layer by reaccumulation, thus comprising a source of ^{137}Cs that was not directly derived from the local environment, as discussed above.

The potential background value of ^{137}Cs activity concentration may be considered to be zero for all sampled buildings since ^{137}Cs emissions into the ambient environment started in 1945 via atomic bomb tests. Before 1945, in the absence of nuclear weapons and nuclear power, there could not be any no source of anthropogenic ^{137}Cs to be detected or tested for, at least to our best knowledge. In 1986, another significant ^{137}Cs emission happened, Chernobyl NPP accident, and the latest known NPP accident, producing detectable amount of ^{137}Cs released into the environment was at Fukushima in 2011 (e.g., Masson et al., 2016). Considering the half-life of Cs ($T_{1/2}$=30.17 years), the ^{137}Cs accumulation from atomic bomb tests had been present for twice the length of its half-life, thus reducing its activity concentration by up to 75%, by the time of the dates of the sampling of the data used herein (2016 and 2018). However, this decrease must have been overprinted by the Chernobyl NPP accident, which would result in an increase in the accumulation (and activity concentration). Then again, by the time of the 2016 (Salgótarján), 2018 (Ózd) sampling, ^{137}Cs fallout from the Chernobyl accident had again been through an entire half-life, and so be reduced by 50%. It also should be noted that the influence of the Fukushima accident is negligible (Masson et al., 2011). This means that if there is no unknown source to create a new ^{137}Cs accumulation to level up activity concentrations (and, naturally, we hope it will not happen), the activity concentration will once again be equal to the background value, here designated as “zero”.

5.3.2 Dust deposition processes in studied region

Dry and wet deposition processes are important pathways for the accumulation of radioactive pollutants on the surface (De Cort et al., 1998). To get a hint of the importance of meteorological conditions, surface wind direction (S), wind speed (m s^{-1}) and precipitation records (mm) from the ERA reanalysis from 1979 to 2017 were evaluated (Figure 24). The prevailing wind direction was remained a constant North to south throughout the Salgótarján and Ózd study areas over the last 4 decades based on meteorological data, while wind speed did not exceed 2.6 m s^{-1} in Salgótarján and 2.5 m s^{-1} in Ózd urban areas (Today the regular wind direction is NW, as stated already). However, within the area analysed (at a spatial resolution of 0.125*0.125 $^{\circ}$) including both settlements, wind speed varied between 0.002 and 14.77 m s^{-1} (Figure 24).

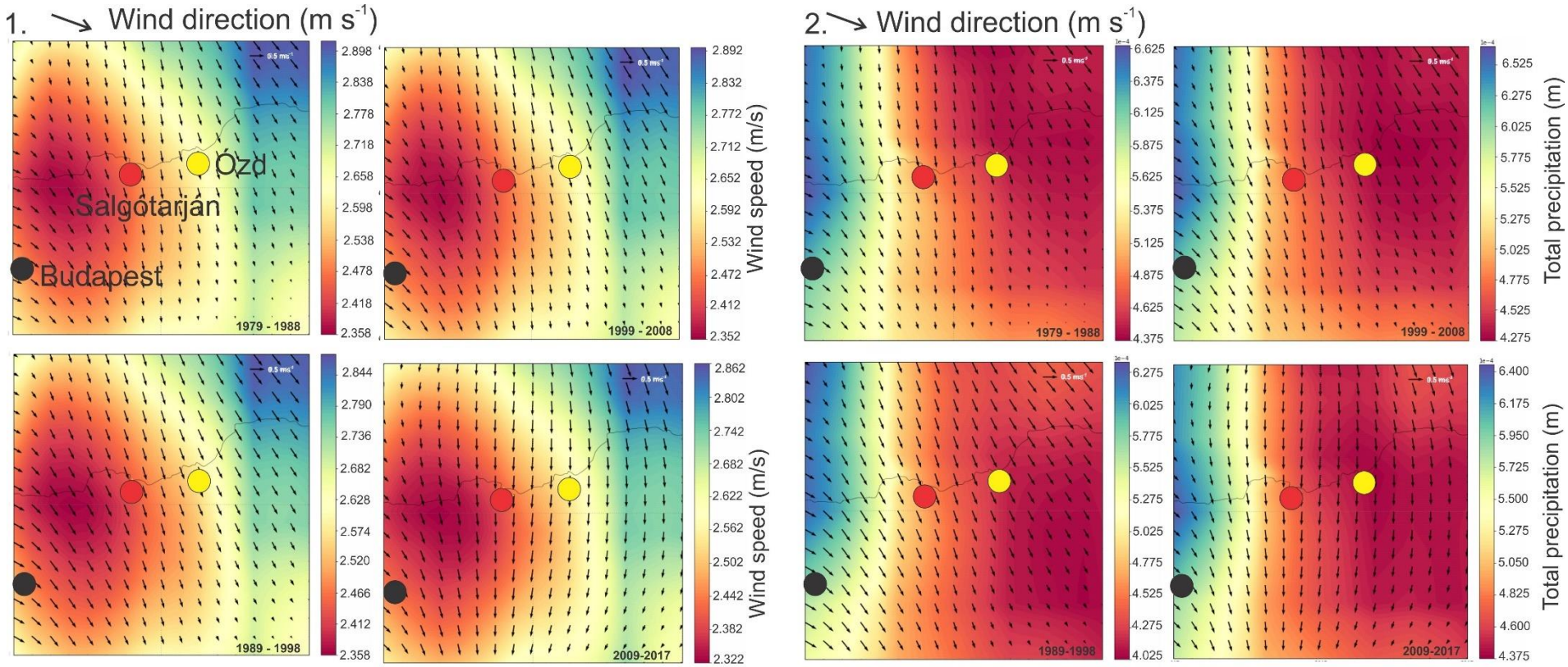

Figure 24. Meteorological data evaluation of the last 4 decades in Salgótarján and Ózd urban areas with median wind speed (unit: m/s), total precipitation (unit: m/1000) versus wind direction (↑). The yellow circle denotes the study area of Ózd, the red, Salgótarján, and the black, Budapest (data from the ERA5 reanalysis compiled and maintained by the European Centre for Medium-Range Weather Forecasts (ECMWF) with a spatial resolution of 0.125° × 0.125° and a time resolution of 3 hours.

After the Chernobyl accident (1986), ^{137}Cs contaminated particles were distributed non-uniformly, and their dispersal was determined primarily by wind and precipitation. A major part of the initial emission was dispersed at relatively high altitudes (Brandt et al., 2002), and the initial transport of the radioactive species was directed towards the north-west, up towards Sweden and Finland. In the following few days, the contamination was distributed over most of Europe, with major exposures in southern, eastern and central Europe (De Cort et al., 1998). The analyses presented here (Figure 25A-B) illustrate that over a two-day interval (26-28 April), the surface wind direction was from south to north and veered northeasterly, while no precipitation occurred. However, April 29-30 (Figure 25A-B), the wind direction changed from east to west; meanwhile, precipitation appeared. It is clearly demonstrable that the Ózd urban environment received its first rainfall following the accident in the course of this day (Figure 25A-B). Since wet deposition is known to be an important pathway for the fallout of radioactive plum (e.g., De Cort et al., (1998); Masson et al., (2011), the earlier precipitation might explain the appearance of higher ^{137}Cs activity concentrations in Ózd than in Salgótarján (Table S. 1; S. 2). The consequence of this for the present study is in agreement with one of the conclusions of a comprehensive European study by De Cort et al. (1998), in which high level concentrations were found to be correlated with wet deposition. From the day of May 1, higher level (1.5 km above ground) wind direction shifted to south-westerly in the Central-Eastern European region (De Cort et al., 1998).

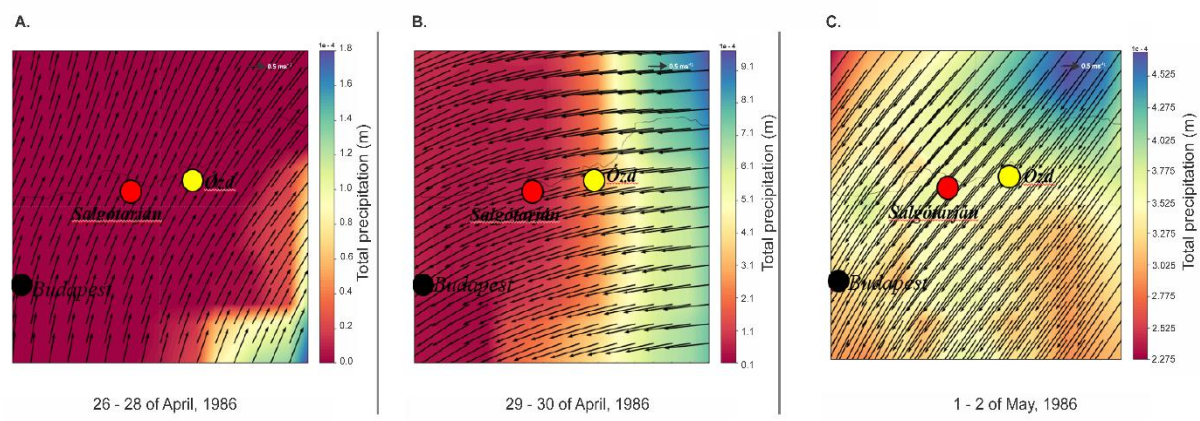

Figure 25. Seven days interval total precipitation (m) versus wind direction (↑), from April 26, 1986, 12:00 (CET) in selected region. Total precipitation and wind direction of time in intervals A. 26 – 28 April,1986; B. 29 – 30 April 1986; C. 1 – 2 May 1986.

This is also compatible with the results herein, which also are indicative of increased wind speed (Figure 25C; 26C). Atmospheric deposition of pollutants onto rough surfaces, such as the urban environment, depends on various factors like elevation, local variability of topography, local slope, season, building heights and configuration, etc. The latter can enhance the speed of wind in wind-tunnel effects between buildings (Buccolieri & Sandberg, 2008). Furthermore, the quasi-laminar sublayer can be affected by local features, triggering turbulence or increasing its intensity (Giardina et al., 2019). Obvious differences in dust deposition are observed between the two urban areas studied (Figure 25A, 26B). In the notably hilly region of Salgótarján (up to ~700 m; Figure 5B), the pattern of dust redistribution may easily be different from Ózd, where the elevation is only up to ~200 m (Figure 5C).

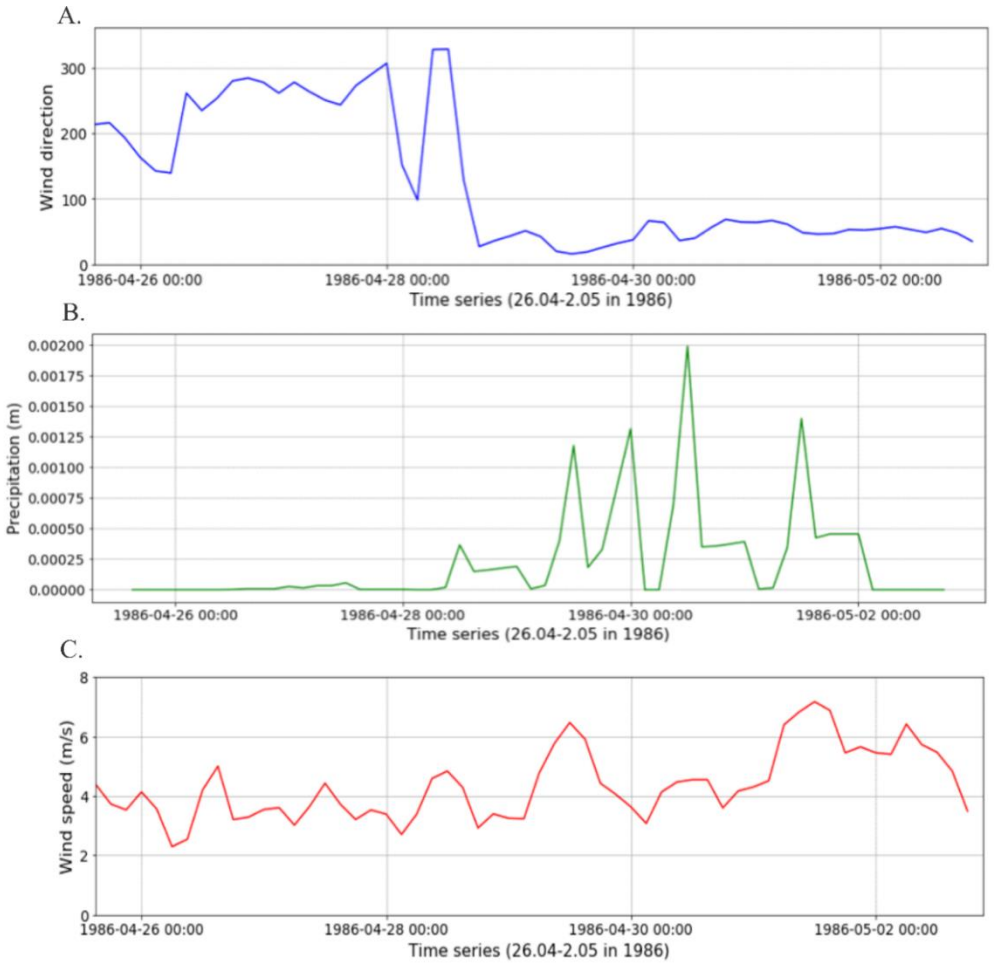

Figure 26. Meteorological data during the Chernobyl accident period (26 April 1986 to 2 May) at the Salgótarján and Ózd study areas. A. Wind direction (blue); B. precipitation (unit: m/1000; green); C. wind speed (unit: m/s; red) are shown.

In addition, different landscapes reflect the unequal deposition of ^{137}Cs in attic dust. The dry deposition process is recognized as an important pathway among the various removal processes of radioactive pollutants in the atmosphere (Giardina et al., 2019) over time.

5.3.3 Slope exposure as a factor of in ^{137}Cs distribution in attic dust from Salgótarján and Ózd

Slope exposure can be a significant factor in studying surface contamination or deposition, depending on the movement of air masses (e.g., Begy et al., 2017). Considering this factor, the attic dust sampling sites here were classified according to 8 cardinal compass directions (North, North-East, East, South-East, South, South-West, West and North-West), and the slope exposure of each sampling point was determined in keeping with terrain modelling (Moore et al., 1991). One can observe an increasing tendency from north (38.6 Bq kg^{-1}) to west (120.9 Bq kg^{-1}) for mean activity levels of these classes of samples (Figure 27), using the whole data set. The largest average ^{137}Cs levels (120.9 Bq kg^{-1}) are observed on W slope exposure, including 13 samples (4 from Ózd and 9 from Salgótarján; Figure 27). Notably, the three Ózd outlier values (Figure 27) are located on this slope. In agreement with the present results, Szerbin et al. (1999) also found that W and S sloping parts of Hungary received the highest ^{137}Cs concentrations after the Chernobyl accident.

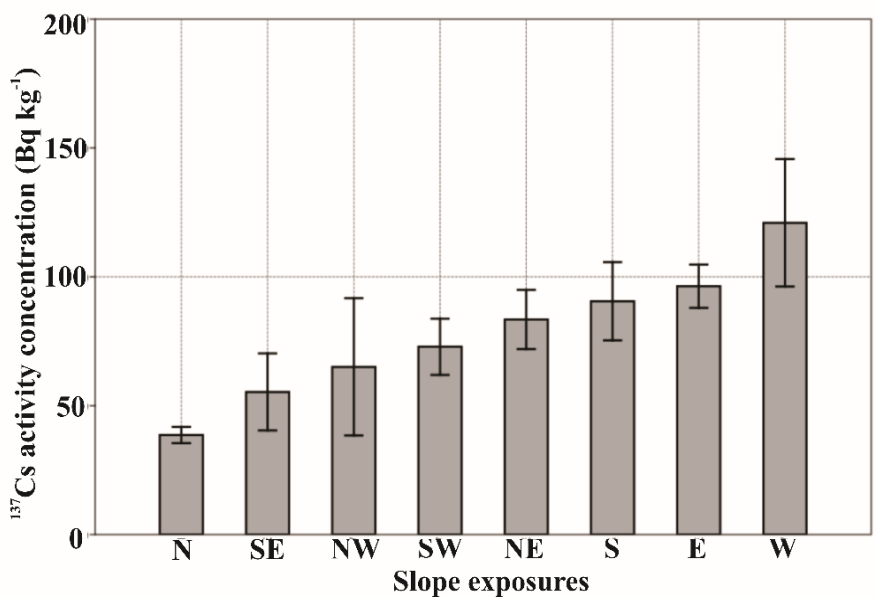

Figure 27. Bar chart of slope exposures of attic dust sampling points (total number of samples *n*=61; 36 from Salgótarján and 25 from Ózd). Error bar illustrates standard deviations.

Furthermore, it has also been mentioned by Bossew et al. (2001) that in SE Austria the W facing slopes of Hungary turned out to be a strong fallout zone, in which the slope was a significant factor in the volume of deposition. Since dust started to accumulate when a house was built on any of the slope sites, it could remain undisturbed, but would nonetheless have been open to influence by inertial and turbulence impact phenomena as well as human activity.

5.4 Relationship between ICP-MS and gamma spectrometric measurements in attic dust and urban soil samples results

It is necessary to evaluate data accuracy and precision since we applied two different measurement techniques in our studied environmental samples (basically attic dust and urban soil urban soil). The majority of the data points show good agreement between their elemental and activity concentrations in attic dust and urban soil samples (Figure 16, 18) as previously already discussed. Therefore, comparison between two analytical techniques (ICP-MS and HPGe γ-spectrometer) showed in good agreement between U (mg kg^{-1}) and Th (mg kg^{-1}) versus ^{226}Ra (Bq kg^{-1}) and ^{232}Th (Bq kg^{-1}) series, with values of 0.9 and 0.8 for urban soil (including brown forest soil and coal ash) and 0.6 and 0.8 for attic dust, respectively (Figure 28A-B). These indicate an approximate one-to-one correspondence between the two techniques. There is a good agreement for the total K (m/m, %) and ^{40}K (Bq kg^{-1}) values (r=0.7) for attic dust, however it is not true for urban soil, including brown forest soil and coal ash sample (Figure 28A-B). Since K is a major chemical component of soil, occurring particularly clay minerals and K-feldspar. Thus, in most environmental conditions, released as K+ from minerals through chemical weathering (rain) and readily taken up by plants (Cinelli, 2019). It is obvious that negative correlation of Cs vs. ^{137}Cs is observed between urban soil and attic dust samples with values of r=-0.06 and r=-0.05, respectively (Figure. 28A-B). Extremely low ^{137}Cs activity concentration found from coal ash sample (0.09 Bq kg^{-1}; Figure. 28A) since cesium in coal ash is easily mobilized into water as Cs+ and can spread through the aqueous environment (Namiki et al., 2014). It means that coal ash is an altered material due to its exterior depositions in urban are (Szabó et al., 2007), as already stated.

To summarize, our investigation produced highly acceptable results on elemental and activity concentrations in undisturbed attic dust samples by different measurement techniques.

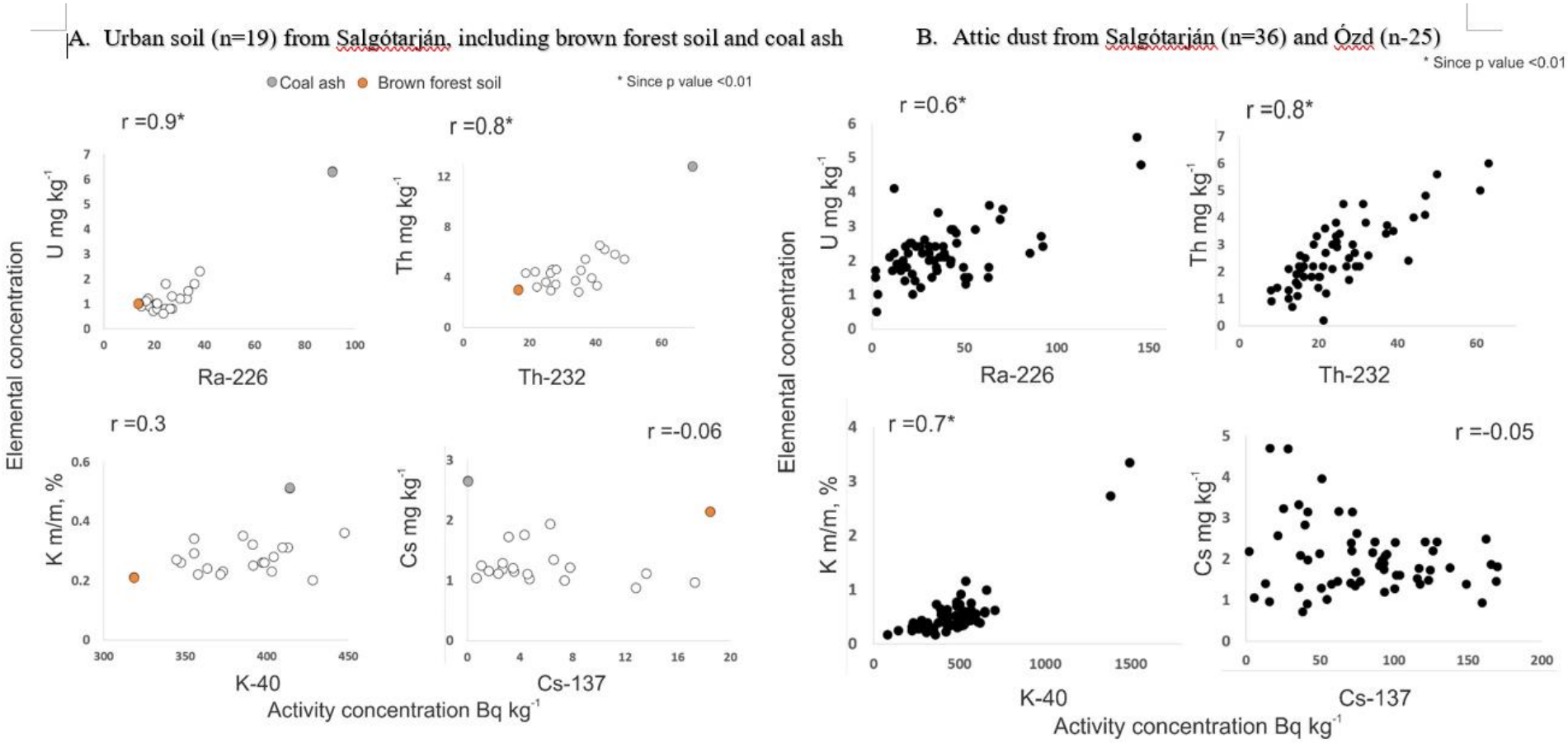

Figure 28. Correlation between the measurement by ICP-MS and gamma spectrometry. A. Urban soil samples (n=19) from Salgótarján (including brown forest soil and coal ash since same techniques was used for these samples, too); B. Attic dust samples from Salgótarján (*n*=36) and Ózd (*n*=25)

5.5 Isoscapes of radionuclides studied in Salgótarján attic dust (n=36)

Spatial maps, showing contours for identical radioactivity levels the studied radionuclides, were calculated according to the Matheron algorithm (Matheron, 1965), which provides a meaningful spatial autocorrelation structure (e.g., Chiles & Delfiner, 2012) for a study area, including areas where no data were available.

5.5.1 Isoscapes of ^{226}Ra and ^{232}Th in Salgótarján attic dust

The results for ^{226}Ra and ^{232}Th activity concentrations fitted models (r^2= 0.4 and 0.5, respectively) suitable for the application of kriging (Cressie, 1990), with the aim of obtaining interpolated activity concentrations maps (Figure 29A-B).

For ^{226}Ra, the parameters of the spherical semivariogram models fitted were C_0 = 325; C_0 + C = 1287; a_e = 5.5 km; r^2 = 0.4; RSS = 924360. For ^{232}Th, the parameters of the spherical semivariogram were C_0 = 109; C_0 + C = 398; a_e = 5.9 km; r^2 = 0.5; RSS = 70705; The bin width was uniformly 630 m, with a maximum lag distance of 6.3 km (Figure S. 4A and B) for ^{226}Ra and ^{232}Th. The unusual STN15AD-blokhouse sample (Table S. 1; Figure S. 2) is excluded due to its unsatisfactorily high degree of variance compared to neighbouring sites as pointed out above (Figure 29A-B). Maps drawn for ^{226}Ra and ^{232}Th are highly similar to each other throughout the area studied (Figure 29A-B). From the CFPP along lines I, II, III and IV (i.e., along the cardinal directions from S to NE) the same tendency in activity concentration of ^{226}Ra and ^{232}Th is seen (Figure 29C). In other words, an increasing influence of coal ash on the attic dust samples under consideration is observable as a function of decreasing distance from the CFPP (Figure 29A-B). The observations herein support the findings of other studies, which also noted that elevated radionuclide (^{226}Ra and ^{232}Th) activity concentrations in soils are generally confined to within a radius of ~3000 m from coal-fired power plants, a figure found in studies in Spain, China, Brazil, and Serbia (Charro et al., 2013a, b; Dai et al., 2007; Flues et al., 2002; Tanic et al., 2016).

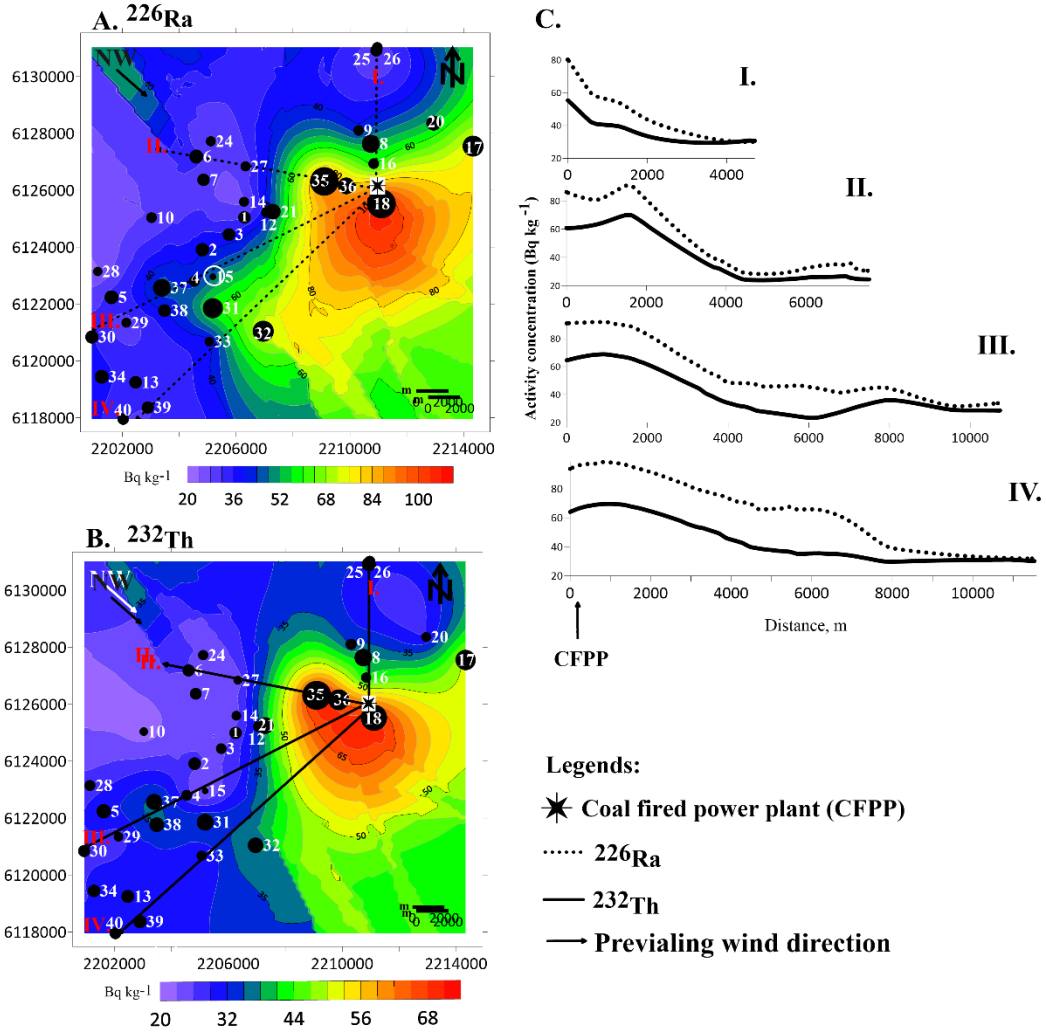

Figure 29. Spatial distribution of ^{226}Ra (A) and ^{232}Th (B) in attic dust obtained through application of the ordinary kriging method. The black circles are proportional to activity concentrations of ^{226}Ra (A) and ^{232}Th (B). Black dashed lines in sections from I to IV show the decreasing trend (C) of activity concentrations of ^{226}Ra (A) and ^{232}Th (B) from the surrounding sites of coal fired power plant. Projection is EPSG: 3857; WGS 84/Mercator projection (m).

5.5.2 Isoscapes of ^{40}K in Salgótarján attic dust

In addition to the above procedures, inverse distance weighting (Yu & Wong, 2008) was carried out to obtain an interpolated map of ^{40}K (Figure 30A-B), due to its similar activity concentration values to those of the data in the study area. For ^{40}K, the parameters are C_0 = 430; C_0 + C = 8040; ae = 8.9 km; r^2 = 0.3; RSS = 1.23E+0.7, with maximum lag distance of 8.9 km (Figure S. 4C). Therefore, it was unsuitable for the application of kriging (Hatvani et al., 2020). In the case of the latter, inverse distance weighting was performed to obtain an interpolated map of ^{40}K (Figure 30).

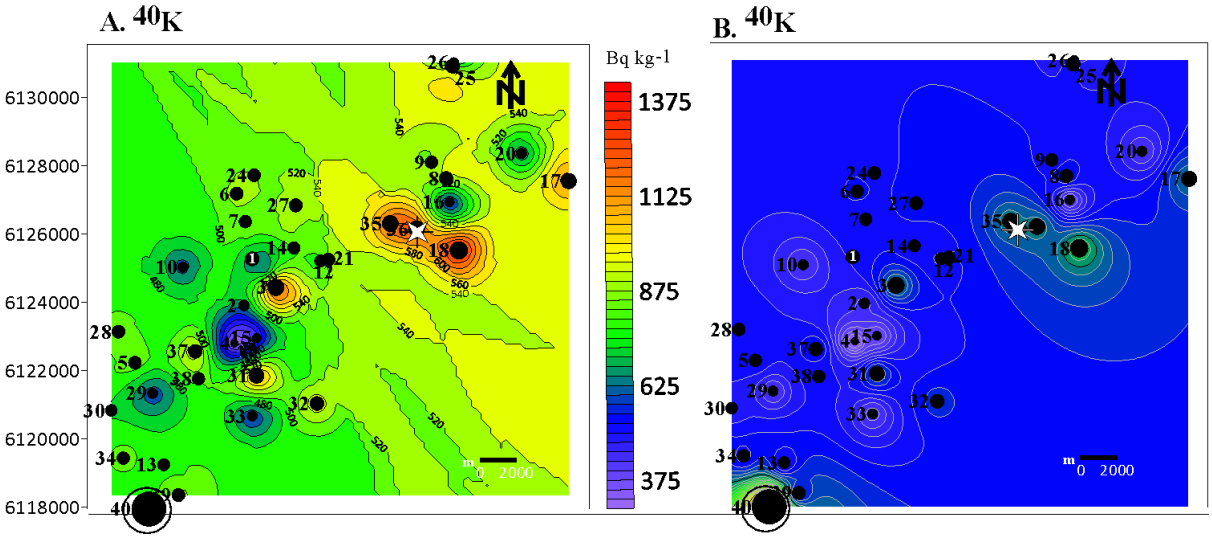

Figure 30. Spatial distribution of ^{40}K radionuclides in attic dust obtained through applying inverse distance weighting to data from the Salgótarján study area. Diameters of filled black circles are proportional to activity concentrations of ^{40}K. (A) The outlier attic dust STN40AD family house sample was excluded, (B) The outlier attic dust sample (STN40AD-family house: ^{40}K: 1382.3 $\pm$ 77.6 Bq kg^{-1}) was included. Map projection is EPSG: 3857; WGS84/Mercator projection (m).

5.5.3 Isoscapes of ^{137}Cs in Salgótarján attic dust

In general, it is accepted that noticeably higher levels of activity tend to be directly proportional to the sampling altitude. This altitude effect was observed in Transylvania after the Chernobyl accident (Begy et al., 2017) and in general in Europe after the Fukushima accident (Masson et al., (2015). To explore whether elevation (ELE*) (Table S. 1, S. 2) has a significant role in the ^{137}Cs activity values observed in Salgótarján and Ózd, OLS regression analysis (Goldberger, 1964; Freeman, 2018).) was applied with elevation as the predictor and ^{137}Cs activity as the dependent variable. For ^{137}Cs concentration activity values, the linear relationship with elevation (m) was demonstrated to be insignificant at $\alpha = 0.05$ ($r^2 = 0.09$, F (1, 17) = 1.58, $p = 0.22$) and ($r^2 = 0.07$, F (1, 16) = 1.22, $p = 0.28$), respectively. The reason behind the insignificant relationship between the ^{137}Cs activity concentration and ELE* is probably due to the relatively small elevation range (258 m and 40 m) for Salgótarján and Ózd, respectively, since after the Fukushima accident, for example, the altitude effect was determined from samples spanning a range of elevations of > 3,000 m in Europe (Masson et al., 2015).

Isotropic spherical semivariogram models were fitted to the empirical semivariograms of Salgótarján (Figure S. 5A-1) and Ózd (Figure S. 5B-1) Since the semivariograms indicate a

meaningful spatial autocorrelation structure (see e.g Chilés and Delfinier, 2012: Sect. 2.2 therein) of the ^{137}Cs activity samples, the theoretical semivariograms fitted were suitable for the application of kriging to obtain the ^{137}Cs isoscapes of the two cities (Figure S. 5).

The elevated ^{137}Cs activity concentrations in attic dust over the exterior part of urban areas in Salgótarján (Figure 31A) and Ózd (Figure 31B) display an increasing level of ^{137}Cs similar to that found in the central part of those cities. The lowest activity concentrations, found from valleys where former industrial areas had been located, might have a decrease in ^{137}Cs levels in both the areas studied, in an agreement with Outola et al. (2003). Because of less environmental degradation in attic areas, attic deposition probably contains rich heavy metal/loid dust particles which are not a preferred Cs-137 deposition location. On the other hand, ^{137}Cs is adsorbed reversibly and/or irreversibly onto the clay minerals, particularly onto illite (Lee et al., 2017).

The distribution of atmospherically derived radionuclide ^{137}Cs depends on various environmental properties and exhibits complex spatial variability (Van der Park et al., 2002; Navas et al., 2011). Apparently, Salgótarján received a larger amount of ^{137}Cs than Ózd (Figure 31A-B), where the regular cleaning and renovation of attic areas might have caused a depletion of ^{137}Cs. On the basis of geostatistical considerations, attic dust samples STN26AD (family house) and OZD54AD (church) were left out of the analysis due to their unacceptably high variance compared with their neighbouring sites (Figure 31A-B; marked in white circles). Several other factors, such as attic height changes, variable degrees of ventilation and renovation status may also be assumed to be reasons for omissions. The ^{137}Cs spatial distribution patterns arrived at herein for the two urban areas are based on a higher sampling density than previous assessments in Hungary (De Cort et al., 1998; Szerbin et al., 1999; Szabó et al., 2012).

Overall, the long-term preserved dust that had not undergone severe disturbance may well have resulted in higher levels of ^{137}Cs activity in attic areas. The studied regions had an intensive heavy-industrial history over the past two centuries, and dust accumulated from local anthropogenic activities as industrial (commonly iron and steel work processes, coal mining, transportation, and in case of Salgótarján coal-fired power plant, too), mixing with natural sources and with atmosphere derived dust particles. Taken together, these resulted in a large variability in the nature of the dust. The activity concentrations of ^{137}Cs measured in buildings of different age (Figure 23; Table S. 1; S. 2) provide a better basis for further consideration than previous studies (Cizdziel et al., 1999; Ilacqua et al., 2003). The opportunity to study

layered attic dust samples (OZD45AD-former iron and steel factory; Table S. 2; Figure S. 1) in Ózd from the former steel factory (Figure 23; Table S. 1; S. 2) sheds light on the significance of the investigation of ^{137}Cs in urban areas. All these findings confirm that attic dust apparently traps ^{137}Cs for decades, and it remains detectable. The present research is one of the first steps towards a broader-based interdisciplinary evaluation of this question.

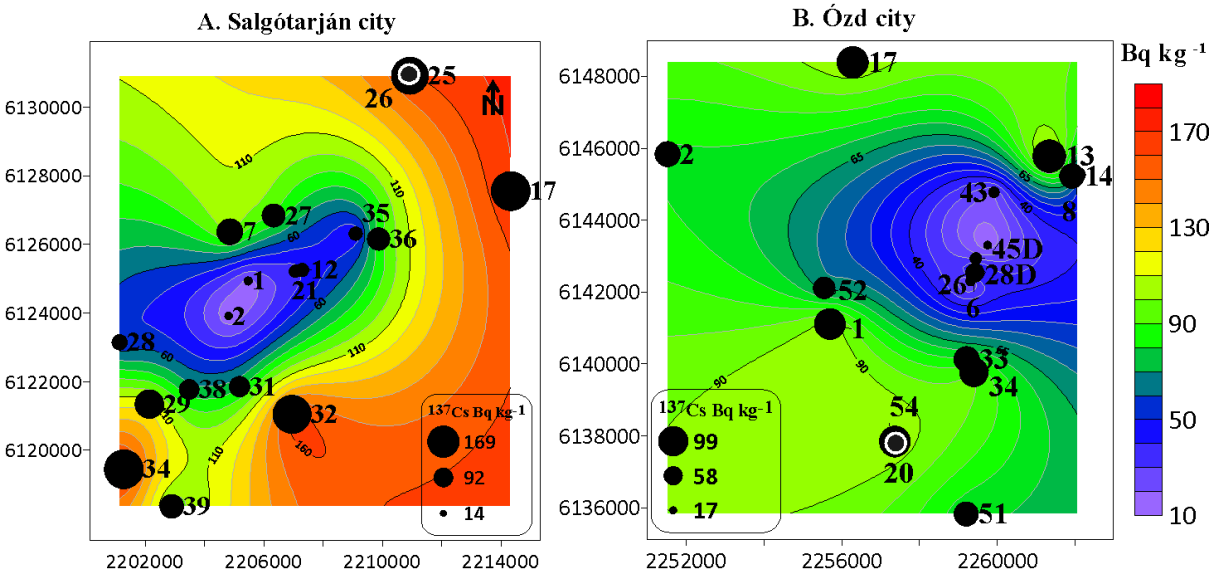

Figure 31. The kriged contour map (isoscape) (Map projection: EPSG:3857, WGS 84/Mercator projection, m) of the ^{137}Cs activity from the urban environments studied, (A) Salgótarján (*n*=17) and (B) Ózd (*n*=16). Grid resolution: 0.9 ×1 km for Salgótarján and 0.8 × 1 km for Ózd. Interpolation was performed using ordinary point kriging employing the spherical semivariogram models, (Note samples of Salgótarján AD26-family house and Ózd AD54-family house were excluded in the interpolated contour map, shown in white circles).

5.6 Human health radiological dose assessment in Salgótarján

To assess the risk the population living or working near the CFPP, and slag dumps are exposed to (Figure 5B-6), the total absorbed gamma dose rate (*D*) [Eq. 4] and the annual effective dose (*E*) [Eq. 5] were calculated for the urban soil and attic dust samples. The total absorbed gamma dose rate (*D*) ranged between 35 and 64 nGy h^{-1} with a mean value of 48 nGy h^{-1} in urban soils from Salgótarján (Figure 32; Table S. 4), which is below the worldwide population weighted average value of D outdoors from terrestrial gamma radiation (59 nGy h^{-1}; range: 1-1200 nGy h^{-1}) and below the same values in Hungary (61 nGy h^{-1}, range: 15-130 nGy h^{-1}) (Figure 32) (UNSCEAR, 2010). Although the *D* value for all urban soils is higher than for the brown forest soil (32 nGy h^{-1}), it can be stated that the samples nearest to the CFPP, namely STN09US- park,

STN20US-playground and STN29US-park (Figure 5B), exhibit the highest D values of 64, 59 and 62 nGy h^{-1}, respectively (Table S. 4). Accordingly, the CFPP in Salgótarján and its slag dumps did not result in considerable amounts of radionuclides entering the urban soils. (UNSCEAR, 2010). This means that the Salgótarján CFPP and its coal ash cone delivered relatively small amount of radionuclides to the urban soils (85 % of urban soil samples is < 58 nGy h^{-1}), whereas the nearest areas (*n*=3 US samples; STN09-park, STN20-playground and STN29-park, 15%; Figure 32; Table S. 4) to CFPPs show significant (64; 59 and 62 nGy h^{-1}, respectively) variations (Table S. 4).

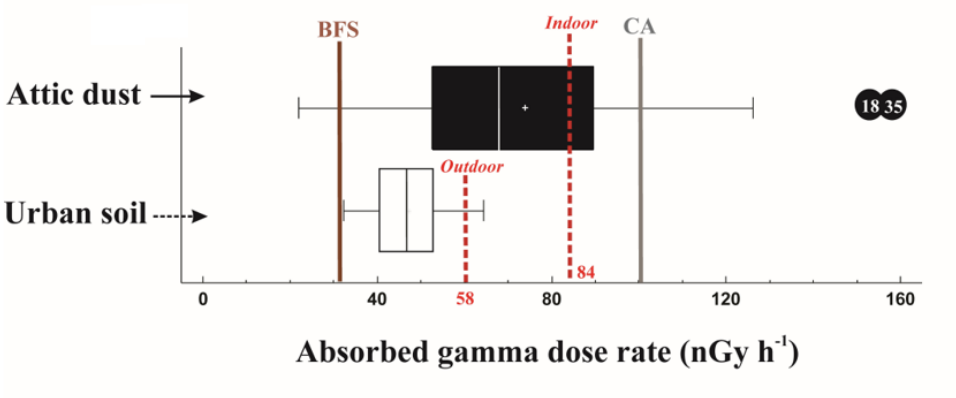

Figure 32. Box and whisker plot of calculated gamma dose rate (nGy h^{-1}) for all studied Salgótarján samples: 36 attic dust, 19 urban soil, 1 brown forest soil sample (BFS marked with a brown vertical line) and 1 coal ash (CA marked with grey vertical line). The red dashed lines indicate international outdoor and indoor World recommended values (UNSCEAR, 2010).

Absorbed gamma dose rate, D ranges between 22 and 155 nGy h^{-1} in attic dust samples with a higher mean of 74 nGy h^{-1} compared to urban soils (Figure 32; Table S. 4). Absorbed gamma dose rate, D for the coal ash is 101 nGy h^{-1}. In the absence of literature on attic dust, the calculated D values were compared to the worldwide population weighted average values concerning the absorbed dose rate in air inside dwellings (84 nGy h^{-1} with national averages ranging from 20 to 200 nGy h^{-1}) (UNSCEAR, 2010), which is rather consistent with the mean value of attic dust (74 nGy h^{-1}). Some of the attic dust samples and the coal ash have higher *D* values than the Hungarian average (95 nGy h^{-1}) but fall within its range (11-236 nGy h^{-1}) (Figure 32). However, when exact radiological doses from attic dust are calculated, the fact that attic dust can cause doses in different ways to building materials must be taken into account, since it can move into dwellings in the form of dust and be inhaled or even ingested.

Overall, it is more likely that elevated levels of activity concentrations derive from old industrialized urban areas (Salgótarján and Ózd). What is more, because attic dust can be seen as a proxy for human exposure to ambient aerial pollutants over time, the contamination found in the attic dust samples also demonstrates that residents of the community were exposed to these contaminants. Therefore, it is observed in urban sites with elevated potentially toxic elements content are mainly the result of the presence of slag debris and layers in urban soil or due to landscape change noted during urban soil sampling (Abbaszade et al., 2022). Coal ash has been used such as landfill on the sites of schools and kindergartens and as infill in playgrounds and roads, to cover stream beds, fill potholes and mining galleries and entrances, its widespread use in insulating material for houses, blocks of flats from the early 19th centuries onwards (Wirth et al., 2012; Zacháry et al., 2015). These practices were all also common in the Salgótarján study area.

Summary

In this thesis, the elemental concentrations of U, Th, Cs (mg kg^{-1}) and K (m/m %) in urban soil from Salgótarján (STN) and Ózd (OZD): kindergarten: n_{STN} =9 and n_{OZD}=15; playgrounds: n_{STN} =11 and n_{OZD}=18; parks: n_{STN} =6 and n_{OZD}=4; other sites: n_{STN} =10 and n_{OZD}=19; and in attic dust from Salgótarján (STN) and Ózd (Ózd): family houses: n_{STN} =26 and n_{OZD}=36; churches: n_{STN} =5 and n_{OZD}=5; kindergarten: n_{STN} =3 and n_{OZD}=4; blockhouses: n_{STN} =2 and n_{OZD}=7; respectively), local brown forest soil (n_{STN} =1 and n_{OZD}=1), coal ash sample (n_{STN} =1) and smelter slag samples (n_{OZD}=2) were assessed to identify distribution and possible contamination impact of former heavy industrial records in residential area of Salgótarján and Ózd.

The activity concentrations of ^{226}Ra, ^{232}Th, ^{40}K and ^{137}Cs (Bq kg^{-1}) in urban soil from Salgótarján (STN): kindergarten: n_{STN}=3, playgrounds: n=7; park: n_{STN}=4 and others: n_{STN}=5 and attic dusts from Salgótarján (STN) and Ózd (OZD): family house: n_{STN}=27 and n_{OZD}=11; church: n_{STN}=4 and n_{OZD}=5; kindergarten: n_{STN}=3 and n_{OZD}=1; blockhouse: n_{STN}=2 and n_{OZD}=7; and coal ash: n_{STN}=1 samples were studied to identify possible radionuclide contamination impact of former heavy industrial records in residential areas of both cities.

The studied Salgótarján urban soil elemental and activity concentrations were lower and comparable to those in the literature. However, the attic dusts from Salgótarján and Ózd showed higher values than the studied Salgótarján urban soil and soil data (surface and urban soils) from the literature. Also, Salgótarján attic dust activity concentration show approx. two times higher values than those from Ózd. This is highly likely related to the local coal-fired power plant acted as a local pollution source. As a result, urban soil samples from both cities can be considered as mixtures of local brown forest soil (as geogenic) and local Salgótarján coal ash/local Ózd smelter slags (as anthropogenic) components to varying degrees.

The activity concentration of ^{226}Ra and ^{232}Th and their abundances in the by-products (i.e., coal ash) of a coal-fired power plant (CFPP) increases in both media studied as a function of decreasing distance of the sampling site from the CFPP. Furthermore, attic dust and urban soil pairs shed light on their similar geochemical features. Although the CFPP at Salgótarján exercised no demonstrable influence on the radioactivity levels measured in urban soils in the area of the settlement, and does not appear to increase environmental radiation exposure in the vicinity of the plant, it should be stressed that the results of the study of attic dust show that technologically enhanced natural radioactivity a consequence of the plant operation - can indeed be identified within an area described by an approximately 3 km radius centred on the CFPP. Particularly, two attic dust samples (STN18AD-family house and STN35AD-family

house) displayed significantly higher levels of activity (Bq kg^{-1}) with ^{238}U: 145 and 143; ^{232}Th: 83 and 94, respectively, and dose rates (D (nG y^{-1}) of 151 and 155, respectively.

The average values of activity concentration of ^{137}Cs in both studied cities are highly similar: 88.5 ± 5.1 Bq kg^{-1} for Salgótarján and 87.8 ± 4.5 Bq kg^{-1} for Ózd. The activity values of ^{137}Cs in attic dust samples are commonly higher than those in urban soils from Salgótarján and soils (urban and surface) from Hungary or other countries. This finding indicates that attic dust, accumulating in enclosed and areas likely undisturbed can more efficiently preserve fingerprints of the past atmospheric ^{137}Cs pollution compared to soil (i.e., urban, street, agricultural, forest ones, etc.,) occurring in open environments.

The variation of ^{137}Cs activity concentration as a function of year of building gradually decreases towards older buildings, from the three extremely high values (223.4; 238.6 and 272.8 Bq kg^{-1}) measured in Ózd houses built between 1954 and 1978. Thus, meteorological simulations on the studied cities back during Chernobyl NPP accident showed that Ózd had earlier been contaminated by precipitation containing material the radioactive plume of the Chernobyl NPP accident than Salgótarján, which can explain the appearance of outlier values of ^{137}Cs activity concentrations in mentioned three Ózd houses. However, in both cities, houses built on the westerly orientated slopes were found to be the most loaded with ^{137}Cs, displaying elevated activity concentrations according to terrain aspect modelling.

A study of layered attic dust samples in Ózd from the former steel works sheds light on the significance of the ^{137}Cs investigation in residential areas: the older layered dust, accumulated during the operation of the former iron/steel works, displays activity concentrations one order of magnitude higher than the more recent one, which accumulated during the ~25 years after the steel works was shut down and a source of ^{137}Cs was not available in the local environment. All these findings seem to confirm that attic dust apparently traps ^{137}Cs for decades, which it remains detectable.

This work clearly shows that attic dust preserves the undisturbed fingerprints of long-termed atmospheric deposition in its chemical and physical properties and provides an indirect assessment route, as well as representing a better and more representative historical record of local air deposition than urban soil samples. For this reason, attic dust is potentially a highly useful and productive source of environmental samples in the long-term monitoring at former industrial urban environments.

Thesis Points

1/ Salgótarján coal ash has the highest U content among all studied samples from both cities, which suggest that coal ash plays a significant impact on Salgótarján n environment. In contrast, Ózd smelter slags, from the new industrial area, have higher U concentration than the majority of Ózd urban soil and lower than the majority of attic dust samples. This indicates that the new industrial site in Ózd cannot yield elevated U content in the environment. However, Ózd urban soil samples showing noticeable U content, collected at the former industry, suggests that the former industrial activity had a potential influence on elevated U content in the city center.
In both cities urban soils have consistently higher Th content than those of attic dusts, except Salgótarján coal ash and two outlier attic dust samples collected from houses close to coal fired power plant. In contrast, Ózd smelter slags have the lowest Th content. In addition, Th content in Ózd brown forest soil is at least twice higher than that of Salgótarján counterpart. Consequently, urban soil from both cities can be considered as mixtures of local brown forest soil (as geogenic component) and local Salgótarján coal ash/local Ózd smelter slag from the former industrial area (as anthropogenic component). Therefore, certain attic dust samples from Salgótarján and urban soils from Ózd play considerable impact to local contamination sources. Furthermore, Ózd and Salgótarján attic dust samples showed higher variability in their K-content compared to urban soils, local brown forest soils, coal ash and smelters slag samples. The elevated K concentration of attic dust is characteristic for agriculturally active areas, far from industrial districts, where the K fertilizer is commonly used (*Tserendorj et al., 2023).*

2/ Activity concentrations of ^{226}Ra, ^{232}Th and ^{40}K in Salgótarján majority attic dust are higher than Salgótarján urban soils and Ózd attic dust. The elevated activity concentrations of ^{226}Ra, and ^{232}Th in Salgótarján attic dust and urban soil correspond to the close distance of sampling sites to the local coal fired power plant. Furthermore, attic dust and urban soil pairs shed light on their similar features in the change of activity concentration. It is supporting that these Salgótarján environmental samples are indeed considerable as mixtures of local brown forest soil (as geogenic component) with local coal ash as by-production of the coal fired power plant, which also contributed to in long-term accumulation of attic dust materials. Low activity concentrations in Ózd attic dust samples suggest that anthropogenic components from the former and recent industrial sites was not high enough to elevate the amount of radionuclides in attic dust, hence it was regarded as an insignificant

The highest activity concentration of ^{40}K in attic dust samples is related to samples with highly elevated K content in both cities. Also, this reveals that high ^{40}K value is possibly significant input from the surrounding agricultural areas in both cities (*Tserendorj et al., 2023).*

3/ Activity concentration of ^{137}Cs in attic dust from Salgótarján and Ózd values are greater than those found in present urban soils and soils from Hungary and other countries. Study of layered attic dust samples in Ózd from the former steel factory highlights on the significance of ^{137}Cs investigation in residential area: the older attic dust layer, accumulated during operation of the former steel factory, shows one order higher activity concentration compared to the younger one, accumulated during the past ~25 years after steel factory was shut down and source of ^{137}Cs was not available in the local environment. This finding indicates that attic dust, accumulating in closed and safe area, can more efficiently preserve fingerprints of the past atmospheric ^{137}Cs pollution compared to any soil occurring in open environments, which remain still detectable (*Tserendorj et al., 2022).*

4/ The variation of ^{137}Cs activity concentration as a function of year of building gradually decreases towards older buildings, from the three extremely high values (223.4; 238.6 and 272.8 Bq kg^{-1}) measured in Ózd houses built between 1954 and 1978. This trend indicates that ^{137}Cs activity concentration reaches back to a background value of 0 if there is no unknown sources to create an overprint on it. Thus, meteorological simulations on the studied cities back during Chernobyl NPP accident showed that Ózd had earlier been contaminated by rain precipitation containing material the radioactive plume of the Chernobyl NPP accident than Salgótarján which can explain the appearance of outlier values of ^{137}Cs activity concentrations in mentioned three Ózd houses. Also, in both cities, houses built on the westerly orientated slopes were found to be the most loaded with ^{137}Cs, displaying elevated activity concentrations according to terrain aspect modelling (*Tserendorj et al., 2022).*

5/ The radiological dose assessments (absorbed gamma dose rate and annual effective dose rate) on Salgótarján urban soil indicate that the 82 years long operation of the coal-fired power plant in Salgótarján and different slag dumps do not cause increased levels of background radiation in city. However, our findings outlined that elevated radioactive levels at the surrounding area of the coal-fired power plant, especially on two family houses (STN18AD and STN35AD) where the attic dust have high enough coal ash component, to produces

potential risk. Therefore, potential concern not only the in the vicinity where industrial activities took place but also disperse the contaminants all around the cities and pose the health treat over decade, particularly, risk assessment performed on kindergarten, family houses, church, and playgrounds.

It was concluded that attic dust provides an indirect evaluation and serves as a highly adequate historical record of local airborne dust deposition when compared to soil, and it is also an excellent environmental media for monitoring long-term, particularly in industrial urban environments (*Tserendorj et al., 2022; 2023; Abbaszade et al., 2022)*

Acknowledgements

First and foremost, I would like to express my sincere appreciation to my supervisor, Professor Csaba Szabó Ph. D, who has been a guiding light, a source of continuous encouragement and invaluable knowledge, and his patience support throughout the long road to my Ph. D. Moreover, I am very grateful to my advisor, Katalin Zsuzsanna Szabó Ph. D, for her continuous support and kind heartedness, as she went above and beyond to figure out all the data sets in meticulous details. I must also give special thanks to Peter Völgyesi, Ph. D, for allowing me access to those environmental samples in the investigation, and freely providing guidance on laboratory technique. Words cannot express my gratitude, as without their consistent guidance, support, invaluable knowledge and encouragement, this thesis would never have been completed. I am honoured to be called a student of LRG, as they taught me the ABCs of doing a Ph. D and helped me complete mine with care and meticulousness.

Sincere thanks also go to late Professor Imre Miklós Jánosi Ph. D† who helped me to work out the meteorological simulation and for answering the many queries, who sadly deceased just before finalizing my PhD thesis. Further, I am grateful to István Gábor Hatvani Ph. D for his extensive guidance on the statistical analysis components of my research. Additionally, the support I received from Zoltan Kis Ph. D and his colleagues in the Nuclear Analysis and Radiography Department at the Centre for Energy Research, who provided me with invaluable help with the gamma spectrometry analysis results. Additionally, thanks to all the LRG members particularly, Gorkhmaz, Nelson, Orsolya, Dóri, Ákos, Judith, Laci, Thomas, Tamás, Silvana, Tan, and Mona their continuous encouragement and creating an affable atmosphere to work and grow in it was a wonderful experience. I am indebted to my colleagues and friends for their constant care and all the fun we've had in these last few years.

The research work reported in this thesis would not have been possible without the financial support of the Stipendium Hungaricum Scholarship and Talent support student organisation, for which I am also grateful.

Last, but definitely not least, my family and loved ones were my greatest support. My mother, Naranchimeg Dugersuren was my guiding voice and cheerleader, who invariably helped me in all matters - and this while taking care of my three sons so often, so that I could achieve the targets I set for myself - even when she was dealing with a cancer herself. I am thankful to my cousin Naran-Erdene and her family members who always helped and supported me throughout this time. Without their help I would not even have been able to finish my

bachelor's degree, nor to be the person I am today: I owe you everything. I extend my gratitude to my friends, Chinkhulsen J, Turbold Kh, Jalsraijamts G, Tsolmon M, Tsooj E, Burenjargal and Tumendelger N, who also maintained a respecting, loving and mentally supportive atmosphere through the years.

I have been truly blessed to have had my husband, Chinzorig Tugs-Erdene, who believed in me no matter what obstacles came our way. Appreciation, too, to my three sons, Yesunge, Yesun-Erdene and Gereg, who constantly lifted my spirits and supported me through my ups and downs.

Finally, I dedicate this thesis to my father Tsegmid Tserendorj who was always behind me and supported me in achieving those dreams, far from distance.

References

Abbaszade, G., Tserendorj, D., Salazar-Yanez, N., Zacháry, D., Völgyesi, P., Tóth, E., & Szabó Cs. 2022. Lead and stable lead isotopes as tracers of soil pollution and human health risk assessment in former industrial cities of Hungary. Applied Geochemistry 145 (2022). https://doi.org/10.1016/j.apgeochem.2022.105397

Abedin, Md. J, Khan, R., 2022. NORMs distribution in the dust samples from the educational institutions of Megacity Dhaka, Bangladesh: Radiological risk assessment, Journal of Hazardous Materials Advances, Volume 8, 2022, 100155, ISSN 2772-4166, https://doi.org/10.1016/j.hazadv.2022.100155.

Ahmad, A. Y., Al-Ghouti, M. A., AlSadig, I., & Abu-Dieyeh, M. 2019. Vertical distribution and radiological risk assessment of 137Cs and natural radionuclides in soil samples. Scientific Reports, 9(1), 1 – 14. https://doi.org/10.1038/s41598-019-48500-x

Alakangas, E., Quality guidelines of wood fuels in Finland VTT-M-04712-15. 2015: Finland. p. 60

Aleksiayenak, Yu.V., Frontasyeva, M.V., Florek, M., Sykora, I., Holy, K., Masarik, J., Brestakova, L., Jeskovsky, M., Steinnes, E., Faanhof, A., & Ramatlhape, K.I., 2013. "Distributions of 137Cs and 210Pb in Moss Collected from Belarus and Slovakia." Journal of Environmental Radioactivity 117(March 2018):19 – 24. doi:10.1016/j.jenvrad.2012.01.018

Alloway, Brain J., 2013. Heavy Metals in Soils. Handb. Toxicol. Met.: Fifth Edition 2, 885 – 936

Amin, Y. M., Uddin Khandaker, M., Shyen, A. K. S., Mahat, R. H., Nor, R. M., & Bradley, D. A. 2013. Radionuclide emissions from a coal-fired power plant. Applied Radiation and Isotopes, 80, 109 – 116. https://doi.org/10.1016/j.apradiso.2013.06.014

Antovic, N. M., Vukotic, P., Svrkota, N., & Andrukhovich, S. K. 2012. Pu-239+240 and Cs-137 in Montenegro soil: Their correlation and origin. Journal of Environmental Radioactivity, 110, 90 – 97. htts://doi.org/10.1016/j.jenvrad.2012.02.001

Ashraf, M. A., Akib, S., Maah, M. J., Yusoff, I., & Balkhair, K. S. 2014. Cesium-137: Radio-chemistry, fate, and transport, remediation, and future concerns. Critical Reviews in Environmental Science and Technology, 44(15), 1740 – 1793. https://doi.org/10.1080/10643389.2013.790753

ATSDR (Agency for Toxic Substances and Disease Registry. 2017). Agency for Toxic Substances and Disease Registry 2019. https://www. atsdr.cdc.gov/SPL/#2019spl.

Balabanova, B., Stafilov, T., Sajn, R., & Bačeva, K. 2011. Distribution of chemical elements in attic dust as reflection of their geogenic and anthropogenic sources in the vicinity of the copper mine and flotation plant. Archives of Environmental Contamination and Toxicology, 61(2), 173 – 184. https://doi.org/10.1007/s00244-010-9603-5

Balabanova, B., Stafilov, T., Sajn, R., & Tănăselia, C. 2017. Long-term Geochemical Evolution of Lithogenic Versus Anthropogenic Distribution of Macro and Trace Elements in Household Attic Dust. Archives of Environmental Contamination and Toxicology, 72(1), 88 – 107. https://doi.org/10.1007/s00244-016-0336-y

Barba-Lobo, A., San Miguel, E.G., Lozano, R.L., & Bolivar, J.P. 2021. A general methodology to determine natural radionuclides by well-type HPGe detectors, Measurement, Volume 181, 109561. https://doi.org/10.1016/j.measurement.2021.109561.

Barnett, M.O., Jardine, P.M., Brooks, S.C., & Selim, H.M., 2000. Adsorption and transport of uranium(VI) in subsurface media. Soil Sci. Soc. Am. J. 64 (3), 908 – 917. doi: 10.2136/ss-saj2000.643908x.

Bem, H., Wieczorkowski, P., & Budzanowski, M. 2002. Evaluation of technologically enhanced natural radiation near the coal-fired power plants in the Lodz region of Poland. Journal of Environmental Radioactivity, 61(2), 191 – 201. https://doi.org/10.1016/S0265-931X(01)00126-6

Beretka, J., & Mathew, P. J. 1985. Natural radioactivity of australian building materials, industrial wastes and by-products. Health Physics, 48(1), 87 – 95. https://doi.org/10.1097/00004032-198501000-00007

Begy, R.Cs., Simon, H., Vasilache, D., Kelemen, Sz., & Cosma, C., 2017. ^{137}Cs Contamination over Transylvania Region (Romania) after Chernobyl Nuclear Power Plant Accident. Science of the Total Environment 599 – 600:627 – 36. http://dx.doi.org/10.1016/j.scitotenv.2017.05.019.

Beresford, N.A., Fesenko, S., Konoplev, A., Skuterud, L., Smith, J.T., & Voigt, G., 2016. Thirty Years after the Chernobyl Accident: What Lessons Have We Learnt? Journal of Environmental Radioactivity 157:77 – 89. http://dx.doi.org/10.1016/j.jenvrad.2016.02.003

Bihari, Z., Babolcsai, G., Bartholy, J., Ferenczi, Z., Kerényi, J.G., Haszpra, L., Ujváry, K.H., Kovács, T., Lakatos, M., Németh, A., Pongrácz, R., Putsay, M., Szabó, P., & Szépsyó, G 2018. Éghajlat. Magyarorsyág Nemzeti Atlasza: Természeti Környezet 58 – 69.

Bógnar. I, Á., 2019. Salgótarjáni környzeyeti minták radioaktiv elementartalma. In Hungarian, Master thesis. School of Environmental Science, ELTE university.

Bourdon, B., Henderson, G. M., Lunderstrom, C. C., & Turner, S. P., 2003. Uranium - Series Geochemistry. Reviews, in Mineralogy and Geochemistry. Turner, S.P. (Eds.), ISBN: 13 978-0-939950-64-5. 656 pages.

Bossew, P., Ditto, M., Falkner, T., Henrich, E., Kienzl, K., & Rappelsberger, U., 2001. Contamination of Austrian Soil with Caesium-137. Jounral of Environmental Radioactivity 55(2):187-94.

Brandt, J., Christensen, J.H., & Frohn, L.M., 2002. Modelling Transport and Deposition of Caesium and Iodine from the Chernobyl Accident Using the DREAM Model. Atmospheric Chemistry and Physics 2(5):397 – 417.

Buccolieri, R., & Sandberg, M., 2008. Study of the Effects of Building Density and Overall Shape of a City on Pollutant Dispersion by Combination of Wind Tunnel Experiments and CFD Simulations. Hrvatski Meteoroloski Casopis 43 PART 2(June 2014):651 – 55.

Canberra, 2017. Ultra Low-Background Cryostats (ULB). CSP0173 – 02/08

Chilés, J., & Delfiner, P., 2012. Geostatistics: Modeling Spatial Uncertainty. Vol. 2nd editio. Canada: Wiley.

Cevik, U., Damla, N., Koz, B., & Kaya, S. 2008. Radiological characterization around the Afsin-Elbistan coal-fired power plant in Turkey. Energy and Fuels, 22(1), 428 – 432. https://doi.org/10.1021/ef700374u

Charro, E., Pardo, R., & Peña, V. (2013a). Chemosphere Chemometric interpretation of vertical profiles of radionuclides in soils near a Spanish coal-fired power plant. Chemosphere, 90(2), 488 – 496. https://doi.org/10.1016/j.chemosphere.2012.08.008

Charro, E., Pardo, R., & Peña, V. (2013b). Statistical analysis of the spatial distribution of radionuclides in soils around a coal-fired power plant in spain. Journal of Environmental Radioactivity, 124, 84 – 92. https://doi.org/10.1016/j.jenvrad.2013.04.011

Cizdziel, J.V., Hodge, V.F., & Faller, S.H., 1998. Plutonium Anomalies in Attic Dust and Soils at Locations Surrounding the Nevada Test Site. Chemosphere 37(6):1157 – 68. https://doi.org/10.1016/S0045-6535(98)00107-6

Cizdziel, J.V., Hodge, V.F., & Faller, S.H., 1999. Resolving Nevada Test Site and Global

Fallout Plutonium in Attic Dust and Soils Using $^{137}Cs/^{239+240}Pu$ Activity Ratios. Health Physics 77(1):67–75.

Cizdziel, J.V., & Hodge, V.F., 2000. Attics as Archives for House Infiltrating Pollutants: Trace Elements and Pesticides in Attic Dust and Soil from Southern Nevada and Utah. Microchemical Journal 64(1):85–92.

Cinelli, G., De Cort, M. & Tollefsen, T. (Eds.), 2019. European Atlas of Natural Radiation, Publication Office of the European Union, Luxembourg, 2019. ISBN 978-92-76-08259-0 doi:10.2760/520053

Coronas, M. V., Bavaresco, J., Rocha, J. A. V., Geller, A. M., Caramão, E. B., Rodrigues, M. L. K., & Vargas, V. M. F. 2013. Attic dust assessment near a wood treatment plant: Past air pollution and potential exposure. Ecotoxicology and Environmental Safety, 95, 153–160. https://doi.org/10.1016/j.ecoenv.2013.05.033

Currie, L. A. 2004. Detection and quantification limits: Basic concepts, international harmonization, and outstanding ("low-level") issues. Applied Radiation and Isotopes, 61(2–3), 145–149. https://doi.org/10.1016/j.apradiso.2004.03.036

Cressie, N., 1990. "The Origins of Kriging." Mathematical Geology 22(3):239–52

Dai, L., Wei, H., & Wang, L. 2007. Spatial distribution and risk assessment of radionuclides in soils around a coal-fired power plant: A case study from the city of Baoji, China. Environmental Research, 104(2), 201–208. https://doi.org/10.1016/j.envres.2006.11.005

Dai, S., Seredin, V.V., Ward, C.R., Jiang, J., Hower, J.C., Song, X., Jiang, Y., Wang, X., Gornostaeva, T., Li, X., Liu, H., Zhao, L., & Zhao, C. 2014. Composition and modes of occurrence of minerals and elements in coal combustion products derived from high-Ge coals. Int. J. Coal Geol., 121, 79–97, doi:10.1016/j.coal.2013.11.004.

Davis, J. J., & Gulson, B. L. 2005. Ceiling (attic) dust: A "museum" of contamination and potential hazard. Environmental Research, 99(2), 177–194. https://doi.org/10.1016/j.envres.2004.10.011

Davis, C.J., 2002. Statistics Data analysis in Geology. Third edition. ISBN 0-471-17275-8. John Wiley & Sons, Inc.

De Cort, M., Dubois, G., Fridman, Sh.D., Germenchuk, M.G., Izrael, Yu.A., Janssens, A., Jones, A.R., Kelly, G.N., Kvasnikova, E.V., Matveenko, I.I., Nazarov, I.M., Pokumeiko, Yu.M., Sitak, V.A., Stukin, E.D., Tabachny, L.Ya., Tsaturov, Yu.S., & Avdyushin, S.I., 1998. Atlas of Caesium 137 Deposition on Europe after the Chernobyl Accident. EUR-19801- EN-RU.

Dimovska, S., Stafilov, T., & Šajn, R., 2011. Radioactivity in Soil from the City of Kavadarci (Republic of Macedonia) and Its Environs. Radiation protection dosimetry 107–20. doi:10.1093/rpd/ncq60

Demetriades, A., & Birke, M. 2015. URBAN GEOCHEMICAL MAPPING MANUAL: Sampling, Sample preparation, Laboratory analysis, Quality control check, Statistical processing and Map plotting. Brussels, Belguim: EuroGeoSurveys.

Dragović, S., & Onjia, A. 2006. Classification of soil samples according to their geographic origin using gamma-ray spectrometry and principal component analysis. Journal of Environmental Radioactivity, 89(2), 150–158. https://doi.org/10.1016/j.jenvrad.2006.05.002

Eisenbud, M., & Petrow, H. G. 1964. Radioactivity in the Atmospheric Effluents of Power Plants That Use Fossil Fuels. Science, 144, 288–289. https://doi.org/10.1126/science.144.3616.288

EPA (Environmental Protection Agency). 2006. Technical Report on Technologically Enhanced Naturally Occurring Radioactive Materials from Uranium Mining Volume 1 :

Mining and Reclamation Background. U . S . Environmental Protection Agency Office of Radiation and Indoor Air Radiation Protection Divisi, 1(2006), 1 – 225.

Flues, M., Moraes, V., & Mazzilli, B. P. 2002. The influence of a coal-fired power plant operation on radionuclide concentrations in soil. Journal of Environmental Radioactivity, 63(3), 285 – 294. https://doi.org/10.1016/S0265-931X(02)00035-8

Finkelman, R.B. 1993. Trace and minor elements in coal. In Organic Geochemistry; Engel, M.H.; Macko, S., Eds.; Plenum: New York, NY, USA, pp. 593 – 607.

Freeman, J. V., 2018. Scope Papers (collection of statistical papers first published in Scope)

Gabersek, M., Watts, M. J., & Gosar, M. (2022). Attic dust: an archive of historical air contamination of the urban environment and potential hazard to health? Journal of Hazardous Materials, 432(November 2021), 128745. https://doi.org/10.1016/j.jhazmat.2022.128745

Garnier, L., Colle, C., & Morello, M., 2001. Natural Uranium and the environment. radionuclide fact sheet. IRSN.

Ghasemi, A., & Zahediasl, S. (2012). Normality tests for statistical analysis: A guide for non-statisticians. International Journal of Endocrinology and Metabolism, 10(2), 486 – 489. https://doi.org/10.5812/ijem.3505

Goldberger, Arthur S., 1964. Classical Linear Regression. Econometric Theory. John Wiley & Sons, New York, p. 158, 0-471-31101-4.

Gosar, M., Šajn, R., & Biester, H. 2006. Binding of mercury in soils and attic dust in the Idrija mercury mine area (Slovenia). Science of the Total Environment, 369(1 – 3), 150 – 162. https://doi.org/10.1016/j.scitotenv.2006.05.006

Gilmore. R., 2008. Practical Gamma-ray Spectrometry - 2nd edition. ISBN 978-0-470-86196-7. John Wiley & Sons Ltd, The Atrium, Southern Gate, Chichester, West Sussex PO19 8SQ, England

Giardina, M., Buffa, P., Cervone, A., & Lombardo, C., 2019. "Dry Deposition of Particle on Urban Areas." Journal of Physics: Conference Series 1224(1). doi:10.1088/1742-6596/1224/1/012050

Habib, M. A., Basuki, T., Miyashita, S., Bekelesi, W., Nakashima, S., Phoungthong, K., Khan, R., Rashid, M. B., Reza M. A., Islam, T., & Techato, K. 2019. Distribution of naturally occurring radionuclides in soil around a coal-based power plant and their potential radiological risk assessment. Radiochimica Acta, 107(3), 243 – 259. https://doi.org/10.1515/ract-2018-3044

Hatvani, I.G., Leuenberger, M., Kohán, B., & Kern, Z. 2017. Geostatistical analysis and isoscape of ice core derived water stable isotope records in an Antarctic macro region. Polar Science, 13, 23 – 32. https://doi.org/10.1016/j.polar.2017.04.001

Hatvani, I.G., Erdélyi, D., Vreča, P., & Kern, Z., 2020. "Analysis of the Spatial Distribution of Stable Oxygen and Hydrogen Isotopes in Precipitation across the Iberian Peninsula." Water (Switzerland) 12(2). doi:10.3390/w12020481

Hatvani, I. G., Leuenberger, M., Kohán, B., & Kern, Z. (2017). Geostatistical analysis and isoscape of ice core derived water stable isotope records in an Antarctic macro region. Polar Science, 13, 23 – 32. https://doi.org/10.1016/j.polar.2017.04.001

Hollander, M. & Wolfe, D.A. (1973) Nonparametric Statistical Methods. John Wiley and Sons, New York.

HORIBA - A guidebook to particle size analysishttps://www.horiba.com/fileadmin/uploads/Scientific/eMag/PSA/Guidebook/pdf/PSA

IAEA (International Atomic Energy Agency). 2006. Environmental Consequences Ofthe

Chernobyl Accident and Their Remediation: Twenty Years of Experience. In:Radiological Assessment Reports Series. Report of the Chernobyl Forum Expert Group “Environment” Assessment Reports Series No. 8, IAEA, Vienna (2006)

IAEA (International Atomic Energy Agency). 2003. Extent of Environmental Contamination by Naturally Occurring Radioactive Material (NORM) and Technological Options for Mitigation, (Technical reports series No. 419).

ICRP (International Commision on Radiological Protection. 1990. Recommendations of the international commission onradiological protection). ICRP Publication 60. PergamonPress, Oxford .

Ilacqua, V., Freeman, N. C. J., Fagliano, J., & Lioy, P. J. 2003. The historical record of air pollution as defined by attic dust. Atmospheric Environment, 37(17), 2379 – 2389. https://doi.org/10.1016/S1352-2310(03)00126-2

Kalina, J., & Tichavský, J., 2020. On Robust Estimation of Error Variance in (Highly) Robust Regression. Measurement Science Review 20(1):6 – 14. doi: 10.2478/msr-2020-0002

Kercsmár, Z., Budai, T.G., Csillag, G.I., Selmeczi, I., & Sztanó, O., 2010. Surface Geology of Hungary. Geological and Geophysical Institute of Hungary.

Kabata-Pendias, A., 2011. Trace Elements in Soils and Plants (4th editio). CRC PRESS, Taylor & Francis Group.

Kercsmár, Z., Budai, T.G., Csillag, G.I., Selmeczi, I., & Sztannó, O., 2010. Surface Geology of Hungary. Geological and Geophysical Institute of Hungary. Retrieved from http://www.dnr.wa.gov/ResearchScience/Topics/GeosciencesData/Pages/gis_data.aspx

Kis, Z., Völgyesi, P., & Szabó, Zs. 2013. DÖME: Revitalizing a low-background counting chamber and developing a radon-tight sample holder for gamma-ray spectroscopy measurements. Journal of Radioanalytical and Nuclear Chemistry, 298(3), 2029 – 2035. https://doi.org/10.1007/s10967-013-2691-8

Kolo, M.T., Abdul Aziz, S.A.B., Khandaker, M.U., Asaduzzaman, K., & Amin, Y.M., 2015. Evaluation of radiological risks due to natural radioactivity around Lynas advanced material plant environment, Kuantan, Pahang, Malaysia. Environ. Sci. Pollut. Res. 22 (17), 13127 – 13136. doi: 10.1007/s11356-015-4577-5

Konert, M., & Vandenberghe, J., 1997. Comparison of laser grain size analysis with pipette and sieve analysis: A solution for the underestimation of the clay fraction. Sedimentology 44, 523 – 535.

Kovács, J., Tanos, P., Korponai, J., Kovács, I., Gondor, K., Gondor-Sőregi, K., & Gábor, I., 2012. Analysis of Water Quality Data for Scientists. Water Quality Monitoring and Assessment. https://doi.org/10.5772/32173

Knoll Glenn. F., 2008. Radiation Detection and measurement, third edition. Wiley New York. ISBN 0-471-07338-5.

Laborie, J.M., Le P.,G., Abt, D., & Girard, M. 2000. Monte Carlo calculation of the efficiency calibration curve and coincidence-summing corrections in low-level gamma-ray spectrometry using well-type HPGe detectors. Applied Radiation and Isotopes, 53(1 – 2), 57 – 62. https://doi.org/10.1016/S0969-8043(00)00114-7

Lauer, E.N., Hower, C.J., Hsu-Kim, H., Taggart, K.R., & Vengosh, A., 2015. Naturally Occurring Radioactive Materials in Coals and Coal Combustion Residuals in the United States. Environ. Sci. Technology journal. DOI: 10.1021/acs.est.5b01978

Le T., D., Abbaszade, G., Tserendorj, D., Salazar-Yanez, N., Völgyesi, P., Falus, Gy. & Szabó Cs., 2021. A study on the accumulation of 55 elements in attic dust at two former industrial cities-Ózd and Salgótarján Hungary. Goldschmidt2021• Virtual• 4-9 July

Lee, J., Park, S., Jeon, E., & Baek, K. (2017). Applied Geochemistry Selective and irreversible adsorption mechanism of cesium on illite. Applied Geochemistry, 85, 188 – 193. https://doi.org/10.1016/j.apgeochem.2017.05.019

Lilley, J.S., 2001. Nuclear Physics: Principles and Applications, first. ed. Wiley, Manchester. ISBN: 0-471-97936-8. 393 pages.

Lioy, P. J., Freeman, N. C. G., & Millette, J. R. 2002. Dust: A metric for use in residential and building exposure assessment and source characterization. Environmental Health Perspectives, 110(10), 969 – 983. https://doi.org/10.1289/ehp.02110969

Llorens, J., Fernández-Turiel, J. & Querol, X. 2001. The fate of trace elements in a large coal-fired power plant. Environmental Geology 40, 409 – 416. https://doi.org/10.1007/s002540000191

Lottermoser, B.G., 2002. Mobilization of heavy metals from historical smelting slag dumps, North Queensland, Australia. Mineral. Mag. 66 (4), 475 – 490. https://doi. org/10.1180/0026461026640043.

Lu, X., Zhao, C., Chen, C., & Liu, W. 2012. Radioactivity level of soil around Baqiao coal-fired power plant in China. Radiation Physics and Chemistry, 81(12), 1827 – 1832. https://doi.org/10.1016/j.radphyschem.2012.07.013

Luksienė, B., Puzas, A., Remeikis, V., Druteikienė, R., Gudelis, A., Gvozdaitė, R., Buivydas, S., Davidonis, R., & Kandrotas, G., 2015. Spatial Patterns and Ratios of ^{137}Cs, ^{90}Sr, and Pu Isotopes in the Top Layer of Undisturbed Meadow Soils as Indicators for Contamination Origin. Environmental Monitoring and Assessment 187(5):1 – 16. doi:10.1007/s10661-015-4491-9

Mabit, L., & Bernard, C., 2007. Assessment of Spatial Distribution of Fallout Radionuclides through Geostatistics Concept. Journal of Environmental Radioactivity 97(2 – 3):206 – 19. doi:10.1016/j.jenvrad.2007.05.008

Masson, O., Baeza, A., Bieringer, J., Brudecki, K., Bucci, S., Cappai, M., Carvalho, F.P., Connan, O., Cosma, C., Dalheimer, A., Didier, D., Depuydt, G., De Geer, L.E., De Vismes, A., Gini, L., Groppi, F., Hammond, À.D., Hanley, O.O., Hole, K., Gudnason, K., Gurriaran, À.R., Hainz, D., Homoki, Zs., Ioannidou, A., Isajenko, K., Jankovic, M., Katzlberger, C., Kettunen, M., Kierepko, Q.R., Kontro, R., Kwakman, P.J.M., Lecomte, M., Leon Vintro, L., Lepp, A., Lind, X.B., Lujaniene, G., Ginnity, P.Mc., Mahon, C. Mc., Mal, H., Manenti, S., Manolopoulou, M., Mattila, A., Mauring, A., Mietelski, J.W., Møller, B., Nielsen, S.P., Nikolic, J., Overwater, R.M.W., Reis, M.C., & Ringer, W., 2011. Tracking of Airborne Radionuclides from the Damaged Fukushima Dai-Ichi Nuclear Reactors by European Networks. 7670 – 77. doi.org/10.1021/es2017158

Masson, O., Bieringer, J., Brattich, E., Dalheimer, A., Estier, S., Penev, I., Ringer, W., Schlosser, C., Steinkopff, T., Steinmann, P., Tositti, L., Beek, P.V., & Vismes-Ott, A.D., 2016. Variation in Airborne 134Cs, 137Cs, Particulate 131I and 7Be Maximum Activities at High-Altitude European Locations after the Arrival of Fukushima-Labeled Air Masses. Journal of Environmental Radioactivity 162 – 163:14 – 22. http://dx.doi.org/10.1016/j.jenvrad.2016.05.004

Mann, H. B., & Whitney, D. R. 1947. On a Test of Whether one of Two Random Variables is Stochastically Larger than the Other. The Annals of Mathematical Statistics, 18(1), 50 – 60. https://doi.org/10.1214/aoms/1177730491

Matheron, G., & Marie, G.F.P., 1965. Les variables régionalisées et leur estimation: une application de la théorie de fonctions aléatoires aux sciences de la nature. Paris: Masson.

Mcgill, R., Tukey, J.W., & Larsen, W.A. 2016. Variations of Box Plots. Published by : Taylor & Francis , Ltd . on behalf of the American Statistical Association Stable URL :

http://www.jstor.org/stable/2683468 Accessed : 11-04-2016 05 :, 32(1), 12 – 16.
Mishra, U. C. 2004. Environmental impact of coal industry and thermal power plants in India. Journal of Environmental Radioactivity, 72(1 – 2), 35 – 40. https://doi.org/10.1016/S0265-931X(03)00183-8
Milenkovic, B., Stajic, J. M., Gulan, Lj., Zeremski, T., & Nikezic, D., 2015. Radioactivity Levels and Heavy Metals in the Urban Soil of Central Serbia. Environmental Science and Pollution Research 22(21):16732 – 41. doi:10.1007/s11356-015-4869-9
Moore, I.D., Grayson, R.B, & Ladson, A.R., 1991. Digital Terrain Modelling: A Review of Hydrological, Geomorphological, and Biological Applications. Hydrological Processes 5(1):3 – 30.
Nafee, S.S., Abdel-Moneim, A.N., Abbas, M.I., Badwi, M.S, Mahmoud, S.A., 2009. Full Energy Peak Efficiency Determination for the 4p Gamma-ray Detector by a Numerical Simulation Method. Arab Journal of Nuclear Science and Applications, 46(2), (92-106) 2013
Navas, A., Gaspar, L., López-Vicente, M., Machin, J., 2011. Spatial Distribution of Natural and Arti Fi Cial Radionuclides at the Catchment Scale (South Central Pyrenees). Radiation Measurements 46(2):261 – 69. doi:10.1016/j.radmeas.2010.11.008
Outola, I., Pehrman, R., Jaakkola, T., 2003. Effect of Industrial Pollution on the Distribution of Pu and Am in Soil and on Soil-to-Plant Transfer of Pu and Am in a Pine Forest in SW Finland. Journal of Radioanalytical and Nuclear Chemistry 257(2):267 – 74.
Morel, J.L., Schwartz, C., Florentin, L., de Kimpe, C., 2005. Urban soils. In: Hillel, D. (Ed.), Encyclopedia of Soils in the Environment. Elsevier, Oxford, pp. 202 – 208.
NEA-OECD (Nuclear Energy Agency-Organization for Economic Co-operation and Development). 1979. Exposure to radiation from the natural radioactivity in building materials. Report by an NEA group of experts. Retrieved from https://www.oecd-nea.org/rp/reports/1979/exposure-to-radiation-1979.Painecur, P., Muñoz, A., Tume, P., Melipichun, T., Ferraro, F. X., Roca, N., & Bech, J. 2022. Distribution of potentially harmful elements in attic dust from the City of Coronel (Chile). Environmental Geochemistry and Health, 0123456789. https://doi.org/10.1007/s10653-021-01164-x
Papaefthymiou, H. V., Manousakas, M., Fouskas, A., & Siavalas, G. 2013. Spatial and vertical distribution and risk assessment of natural radionuclides in soils surrounding the lignite-fired power plants in megalopolis basin, Greece. Radiation Protection Dosimetry, 156(1), 49 – 58. https://doi.org/10.1093/rpd/nct037
Papp, Z., & Daróczy, S. 1997. Measurement of radon decay products and thoron decay products in air by beta counting using end-window Geiger-Muller counter. Health Physics, 72(4), 601 – 610. https://doi.org/10.1097/00004032-199704000-00012
Papp, Z. 1998. Estimate of the annual per capita surplus dose due to the elevated indoor exposure to 222Rn progeny caused by the use of slag and spoil of uranium rich coal for building purposes in Ajka Town, Hungary. Health Physics, 74(3), 393 – 397. https://doi.org/10.1097/00004032-199803000-00013
Papp, Z., Dezső, Z., & Daróczy, S. 2002. Significant radioactive contamination of soil around a coal-fired thermal power plant. Journal of Environmental Radioactivity, 59(2), 191 – 205. https://doi.org/10.1016/S0265-931X(01)00071-6
Papp, Z., & Dezső, Z. 2003. Estimate of the dose-increment due to outdoor exposure to gamma rays from uranium progeny deposited on the soil around a coal-fired power plant in Ajka town, Hungary. Health Physics, 84(6), 709 – 717. https://doi.org/10.1097/00004032-200306000-00003
Parzentny, H.R. & Róg, L. 2019. The role of mineral matter in concentrating Uranium and

Thorium in Coal and combustion residues from power plants in Poland. Minerals 9, 13 – 15. doi:10.3390/min9050312

Prăvălie, R. (2014). Nuclear Weapons Tests and Environmental Consequences: A Global Perspective. Ambio, 43(6), 729 – 744. https://doi.org/10.1007/s13280-014-0491-1

Reimann, C., Filzmoser, P., Garrett, R. G., & Dutter, R. 2008. Statistical Data Analysis Explained: Applied Environmental Statistics with R. John Wiley & Sons, Ltd.

Reimann, C., Demetriades, A., Eggen, O. A., & Filzmoser, P. (2009). EuroGeoSurveys Geochemistry Expert Group The EuroGeoSurveys Geochemical Map- ping of Agricultural and Grazing Land Soils Project (GEMAS) e Evaluation of Quality Control Results of Aqua Regia Extraction Analysis 049, 92 Norges Geologiske Undersøkelse Report.

Ritchie, J, C. & McHenry, J, R., 1990. Application of Radioactive Fallout Cesium-137 for Measuring Soil Erosion and Sediment Accumulation Rates and Patterns: A Review. Journal of Environmental Quality. 19:215-233.

Richard V. Pouyat, Tara L.E., 2019. Chapter 10 - Climate change and urban forest soils: in book of Developments in Soil Sciences, Editor(s): Matt Busse, Christian P. Giardina, Dave M. Morris, Debbie S. Page-Dumroese, Elsevier, Volume 36, Pages 189-211, https://doi.org/10.1016/B978-0-444-63998-1.00010-0.

Rudnick, R. L., & Gao, S. 2004. Composition of the Continental Crust. Treatise on Geochemistry, 3, 1-64. Elsevier, Oxford.

Quennehen, B., Schwarzenboeck, A., Matsuki, A., Burkhart, J.F., Stohl, A., Ancellet, G., Law, & K.S., 2012. Anthropogenic and forest fire pollution aerosol transported to the Arctic: observations from the POLARCAT-France spring campaign. Atmos. Chem. Phys. 12, 6437 – 6454. https://doi.org/10.5194/acp-12-6437-2012.

Querol, X., Fernández-Turiel, J., & López-Soler, A. 1995. Trace elements in coal and their behaviour during combustion in a large power station. Fuel, 74, 331 – 343, doi:10.1016/0016-2361(95)93464-O.

Sajn, R. 2005. Using attic dust and soil for the separation of anthropogenic and geogenic elemental distributions in an old metallurgic area (Celje, Slovenia). Geochemistry: Exploration, Environment, Analysis, 5(1), 59 – 67. https://doi.org/10.1144/1467-7873/03-050

Salazar-Yanez, N., Abbaszade G., Tserendorj, D., Völgyesi, P., Zacháry, D., Szabó , K.Zs., & Szabó , Cs. 2021. Assessment of 15 heavy metals in urban soils of former industrial city (Salgótarján n, Hungary). 16th Carpathian Basin Conference for Environmental Sciences, 30th March - 1st April, Budapest Hungary. 88. https://www.researchgate.net/publication/358214503_XVI_K ÁRPÁT-MEDENCEI_KÖRNYEZETTUDOMÁNYI_KONFERENCIA

Salminen, R., (Chief-editor), Batista, M.J., Bidovec, M., Demetriades, A., De Vivo, B., De Vos, W., Duris, M., Gilucis, A., Gregorauskiene, V., Halamic, J., Heitzmann, P., Lima, A., Jordan, G., Klaver, G., Klein, P., Lis, J., Locutura, J., Marsina, K., Mazreku, A., O'Connor, P.J., Olsson, S.A., Ottesen, R.T., Petersell, V., Plant, J.A., Reeder, S., Salpeteur, I., Sandström, H., Siewers, U., Steenfelt, A., & Tarvainen, T., 2005. FOREGS Global Geochemical Baselines Programme. Geochemical Atlas of Europe. <http://weppi.gtk.fi/publ/foregsatlas>

Schober, P., & Schwarte, L. A. 2018. Correlation coefficients: Appropriate use and interpretation. Anesthesia and Analgesia, 126(5), 1763 – 1768. https://doi.org/10.1213/ANE.0000000000000286

Seleznev, A.A., Yarmoshenko, I.V., Ekidin. A.A., 2010. Accumulation of Cs in Puddle Sediments within Urban Ecosystem. Journal of Environmental Radioactivity 101(8):

643 – 646. doi:10.1016/j.jenvrad.2010.03.015
Shapiro, S.S., & Wilk, M. B., 1965. An Analysis of Variance Test for Normality. Source: Biometrika, Dec., 1965, Vol. 52, No. 3/4 (Dec., 1965), pp. 591-611 Published by: Oxford University Press on behalf of Biometrika Trust Stable URL: https://www.jstor.org/stable/2333709
Sven E.J., & Brian, D.F., 2008. Encyclopedia of Ecology, first ed., in: Brisban, I.L.Jr., Dallas, C.E., 2008, Radiation Ecology. London, Elsevier Science, pp. 2956-2959.
Silva, L.F.O., Ward, C.R., Hower, J.C., Izquierdo, M., Waanders, F., Oliveira, M.L.S., Li, Z., Hath, R.S., & Querol, X. 2010. Mineralogy and leaching characteristics of coal ash from a major Brazilian power plant. Coal Comb. Gasif. Prod., 2, 51 – 65
Singh, A., Ulrich, K., & Giammar, E. D., 2010. Impact of phosphate on U(VI) immobilization in the presence of goethite, Geochimica et Cosmochimica Acta,Volume 74, Issue 22, Pages 6324-6343,ISSN 0016-7037, https://doi.org/10.1016/j.gca.2010.08.031.
Spearman, C. 1904. 'General Intelligence' objectively determined and measured. American Journal of Psychology., 15, 201-293
Stefaniak, S., Miszczak, E., Szczepanska-Plewa, J. &, Twardowska, I., 2015. Effect of weathering transformations of coal combustion residuals on trace element mobility in view of the environmental safety and sustainability of their disposal and use. I. Hydrogeochemical processes controlling Ph and phase stability. J. Environ. Manag. 156, 128 – 142. https://doi.org/10.1016/j.jenvman.2015.03.046
Szabó, I. 1992. Measurements on environmental effects of sole emitted by the Ajka thermal power station, Fizikai Szemle, 42, 55-63
Szabó, K.Zs., Udvardi, B., Horváth, A., Bakacsi, Z., Pásztor, L., Szabó, J., Laczkó, L.D, & Szabó, Cs., 2012 “Cesium-137 Concentration of Soils in Pest County, Hungary.” Journal of Environmental Radioactivity 110:38 – 45. doi:10.1016/j.jenvrad.2012.01.023
Szabó, M., Zsuzsanna, A., Szabó, C., Konc, Z., Marosvölgyi K., 2007. Erőművi Salakhányók Környezeth Hatásai (Environmental Effects of power station's slag heaps) in Földrajyi Köyleménzek CXXXI. IV kötet, 2007. 4, 303-317. In Hungarian
Szerbin, P., Koblinger-Bokori, E., Koblinger,L., Végvári, I., Ugron, Á. 1999. Caesium-137 Migration in Hungarian Soils. Science of the Total Environment 227(2 – 3):215 – 27.
Tanić, M. N., Mandić, L. J. J., Gajić, B. A., Daković, M. Z., Dragović, S. D., & Bačić, G. G. (2016). Natural radionuclides in soil profiles surrounding the largest coal-fired power plant in Serbia. Nuclear technology and Radiation Protection, 31(3), 247 – 259. https://doi.org/10.2298/NTRP1603247T
Trevisi, R., Leonardi, F., Risica, S., & Nuccetelli, C. 2018. Updated database on natural radioactivity in building materials in Europe. Journal of Environmental Radioactivity, 187(February), 90 – 105. https://doi.org/10.1016/j.jenvrad.2018.01.024
Tserendorj, D., Szabó, K.Zs., Völgyesi, P. , Nguyen, T. C., Hatvani, I. G., Jánosi, I. M., Abbaszade G., Salazar-Yanez .N., & Szabó, C. 2022a. Activity concentration of 137Cs in undisturbed attic dust collected from Salgótarján and Ózd (northern Hungary), Journal of Environmental Radioactivity 251 – 252 (2022) 106950. https://doi.org/10.1016/j.jenvrad.2022.106950
Tserendorj, D., Szabó, K.Zs., Völgyesi, P., Nguyen, T.C., Abbaszade, G., Salazar-Yanez, Y.N. & Szabó, Cs. (2022b) Determination of naturally occurring radionuclides in attic dust samples from different industrialized Hungarian cities using inductively coupled plasma mass spectrometry and gamma-spectroscopy. VIII Terrestrial Radioisotopes in Environment International Conference on Environmental Protection (TREICEP), October 4-7th 2022. Vonyarcvashegy, Hungary. Abstract Book pp. 34. DOI 10.18428/TREICEP-2022

Tukey, J. W. 1977. Exploratory data analysis. Communications in Computer and Information Science. (Vol. 2, pp. 131-160). https://doi.org/10.1007/978-3-662-45006-2_9

Unno, Y., Furukawa, R., Yunoki, A., 2017. Simulation of a well-type HPGe detector for samples both in the hole and on top of the endcap. http://dx.doi.org/10.1016/j.apradiso.2017.02.011

UNSCEAR (United Nations Scientific Committee on the Effects of Atomic Radiation). 2000a. Sources and effects of ionizing radiation. Retrieved from http://www.unscear.org/docs/publications/2000/UNSCEAR_2000_Report_Vol.I.pdf

UNSCEAR (United Nations Scientific Committee on the Effects of Atomic Radiation). 2000b. SOURCES AND EFFECTS United Nations Scientific Committee on the Effects.

UNSCEAR (United Nations Scientific Committee on the Effects of Atomic Radiation) 2010. Sources and Effects of Ionizing Radiation: United Nations Scientific Committee on the Effects of Atomic Radiation UNSCEAR 2008 Report, Volume I: SOURCES. Report to the General Assembly: Annex B. Exposures of the Public and Workers from Various Sources of Radiation. United Nations. New York. ISBN 978-92-1-142274-0

USDA (United States Department of Agriculture). 2014. Soil survey field and Labotatory Methods Manual. Soil Survey Investigations Report No.51. Version 2. Nebraska, USA.

Van der Perk, M., Slávik, O., & Fulajtár, E., 2002. Assessment of Spatial Variation of Cesium-137 in Small Catchments. Journal of Environmental Quality 31(6):1930 – 39.

De Vivo, B., Ippolito, F., Capaldi, G., & Simpsom, P, R.. 1984. Uranium geochemistry, mineralogy, geology, exploration and sources. ISBN-13: 978-94-009-6062-6 001: 10.1007/978-94-009-6060-2e-ISBN-13:

Vosniakos, F.K., 2012. November. Cs-137 and K-40 concentration in soil and their transfer to plant. In Third International Scientific Symposium "Agrosym Jahorina (Vol. 10).

Vukasinović, I., Todorović, D., Životić, Lj., Kaluđerović, L., & Đorđević, A., 2018. An Analysis of Naturally Occurring Radionuclides and 137 Cs in the Soils of Urban Areas Using Gamma-Ray Spectrometry. 1049 – 60. https://doi.org/10.1007/s13762-017-1467-z

Völgyesi, P., Jordan, G., Zacháry, D., Szabó, Cs., Bartha, A., & Matschullat, J. 2014a. Attic dust reflects long-term airborne contamination of an industrial area: A case study from Ajka, Hungary. Applied Geochemistry, 46, 19-29. https://doi.org/10.1016/j.apgeochem.2014.03.010

Völgyesi, P., Kis, Z., Szabó, Zs., & Szabó, Cs. 2014b. Using the 186-keV peak for 226Ra activity concentration determination in Hungarian coal-slag samples by gamma-ray spectroscopy. Journal of Radioanalytical and Nuclear Chemistry, 302(1), 375 – 383. https://doi.org/10.1007/s10967-014-3274-z

Wheeler, A.J., Jones, P.J., Reisen, F., Melody, Sh.M., Williamson, G., Strandberg, B., Hinwood, A., Almerud, P., Blizzard, L., Chappell, K., Fisher, G., Torre, P., Zosky, G.R., Cope, M., & Johnston, F.H., 2020. Roof Cavity Dust as an Exposure Proxy for Extreme Air Pollution Events " Chemosphere 244:125537. https://doi.org/10.1016/j.chemosphere.2019.125537

Wirth, P., Černič Mali, B., & Fischer, W. 2012. Using the Potentials of Post-Mining Regions - A Good Practice Overview of Central Europe. Post-Mining Regions in Central Europe - Problems, Potencials, Possibilities.

White, M. William., Casey, H. William., Mary, B., & Yurimoto, H., 2018. Encyclopedia of Geochemistry, A comprehensive reference source on the chemistry of the earth. ISBN: 978-3-319-39311-7. Springer International Publishing AG, part of Springer Nature 2018

Webster, R., & Oliver, M, A., 2007. Geostatistics for Environmental Scientists, 2nd edition. DOI:10.1002/9780470517277.

Wilcox, R.R., & Keselman, H.J., 2012. "Modern regression methods that can substantially

increase power and provide a more accurate understanding of associations" 26(3):165-174. doi:10.1002/per.860

Wu, B., Wu, X., Shi, X., Zhang, X., Qiao, S., Hu, L., Liu, J., Liu, S., Zhang, J., Zhang, H., & Zhu, A. (2021). Lead isotopes in the Central Yellow Sea Mud: Evidence of atmospheric deposition and its implication for regional energy consumption shift. Environmental Pollution, 268, 115702. https://doi.org/10.1016/j.envpol.2020.115702

Yu, C., & Yao, W., 2017. Robust linear regression: a review and comparison. Commun. Stat. Simulat. Comput. 46 (8), 6261–6282.

Zacháry, D., Jordan, G., Völgyesi P., Bartha A., & Szabó Cs. (2015) Urban geochemical mapping for spatial risk assessment of multisource potentially toxic elements — A case study in the city of Ajka, Hungary. Journal of Geochemical Exploration 158 (2015) 186–200. http://dx.doi.org/10.1016/j.gexplo.2015.07.015

Web links

1. https://world-nuclear.org/information-library.aspx
2. https://www.env.go.jp/en/chemi/rhm/basic-info/index.html
3. https://www.ecmwf.int/

Supplementary tables

Table S. 1. Results of elemental (U, Th, K, Cs) and activity concentrations (^{226}Ra, ^{232}Th, ^{40}K, ^{137}Cs) in Salgótarján attic dust (n=40), urban soil (n=36), brown forest soil (n=1) and coal ash (n=1) samples, categories of sampling sites and their locations (x, y), elevation (m), characteristics of houses

Attic dust	**Coordinates of the sampling locations (X, Y) meter**			**Activity concentration (Bqkg^{-1})**				**Elemental concentration (mg kg^{-1})**				**Category of sampling sites**	**Characteristics of houses**			
	X	**Y**	**Elevation, m*** ****Slope ˚** **Terrain aspect ˚**	**^{238}Ra**	**^{232}Th**	**^{40}K**	**^{137}Cs**	**U**	**Th**	**K**	**Cs**		**Year of built. *****	**Roof type**	**Sampling surface**	**Construction material**
STN01AD	2205477	6124930	310 4.5 316	36.7 ± 3.5	29.4 ± 6.4	437.3 ± 28.6	15.9 ± 1.1	2.1	2.2	0.4	1.0	Church	1936	Metal	Concrete beam	Mixed stone, bricks and wood
STN02AD	2204815	6123910	324 3.6 278	39.8 ± 3.3	31.2 ± 6	442.5 ± 29.4	13.0 ± 1.3	2.1	4.5	0.3	1.4	Church	1914	Tile	Fiberglass Envelope	Bricks
STN03AD	2205749	6124438	309 2.3 186	35.8 ± 6.9	23.5 ± 6.6	658.7 ± 55.0	91.7 ± 6.0	3.4	3.0	1.0	2.0	Family house	1957	Tile	Wooden beam	Bricks
STN04AD	2204534	6122799	270 1.2 78	23.3 ± 2.7	24.6 ± 5.3	309.2 ± 21.7	57.8 ± 3.1	1.4	3.1	0.2	1.4	Kindergarten	1980	Slate and tile	Concrete and Wooden beam	Cement and brick
STN05AD	2201621	6122238	254 1 176	42.9 ± 4.2	37.4 ± 6.9	518.5 ± 34.1	49.6 ± 3.1	2.9	3.7	0.6	2.1	Kindergarten	1990	Tile	Wooden beam	Tile
STN06AD	2204602	6127185	267 2.2		29.1	529.3	162.3	2.9	2.7	0.6	2.5	Family house	1960	Tile	Wooden beam	Blocks

			276	44.0 ± 5.4	± 8.7	± 40.9	± 8.8									
STN07AD	2204855	6126365	273 7.9 92	33.7 ± 5.2	27.8 ± 7.1	511.4 ± 42.4	104.1 ± 6.2	2.0	2.5	0.4	1.6	Family house	1944	Tile	Wooden beam	Slag blocks (natural stones included)
STN08AD	2210734	6127634	351 5 103	71 ± 5.4	49.9 ± 8.1	546.5 ± 35.9	126.5 ± 7.1	3.5	5.6	0.5	2.2	Kindergarten	1960	Slate	Wooden beam	Wood
STN09AD	2210308	6128102	349 3.8 77	20.5 ± 4.7	25.4 ± 12.1	513.9 ± 41.6	101.5 ± 5.6	2.5	3.4	0.5	1.6	Family house	1961	Slate	Wooden beam	Adobe
STN10AD	2203028	6125036	287 1.5 264	22.0 ± 2.6	15.5 ± 5.8	422.2 ± 27.3	5.5 ± 0.9	1.0	2.1	0.2	1.1	Family house	1980	Slate	Wooden beam	Blocks
STN11AD	2203059	6124156	276	-	-	-	-	1.3	1.6	0.5	1.2	Family house	1972	Slate	Wooden beam	Mixed wood, cement bricks
STN12AD	2207059	6125216	307 9.4 17	16.4 ± 4.0	24.7 ± 9.5	486.2 ± 37.3	35.4 ± 2.5	1.9	2.9	0.8	1.3	Family house	1890	Slate	Wooden beam	Mixed wood, cement bricks
STN13AD	2202467	6119246	233 1.1 35	34.9 ± 3.5	32.0 ± 6.8	487.5 ± 33.5	54.8 ± 3.4	1.8	3.8	0.3	1.0	Family house	1965	Slate	Wooden beam	Bricks
STN14AD	2206280	6125594	275 3 177	16.7 ± 4.1	19.6 ± 2.6	501.5 ± 38.8	115.8 ± 6.7	2.0	3.3	0.7	1.5	Blockhouse	1950	Slate	Wooden beam	Concrete and wood
STN15AD	2205184	6122957	308 6.8 212	> dl	8.0 ± 2.6	368.1 ± 34.1	36.7 ± 2.7	4.1	1.3	0.7	2.1	Blockhouse	1965 (2006)	Tile with iron structures	Wooden beam and Steel	Bricks
STN16AD	2210836	6126935	337 1.3		21.7	391.3	93.9	2.5	3.6	0.6	2.1	Family house	1970	Slate	Wooden beam	Blocks

			120	21.3 ± 2.8	± 6.5	± 26.6	± 5.3									
STN17AD	2214330	6127551	495 8.3 182	91.6 ± 6.4	61.0 ± 9.6	621.7 ± 43.3	169.8 ± 8.8	2.7	5.0	0.4	1.8	Family house	1922	Tile	Wooden beam	Wood
STN18AD	2211109	6125522	314 3.5 279	145.6 ± 8.3	83.9 ± 8.0	708.2 ± 41.4	35.7 ± 2.2	4.8	8.8	0.6	3.3	Family house	1970	Slate	Wooden beam	Bricks
STN19AD	2211393	6127328	340	-	-	-	-	1.6	2.0	0.4	1.6	Family house	1981	Tile	Wooden beam	Mixed wood, cement bricks
STN20AD	2212946	6128359	507 7.8 226	50.3 ± 8.2	20.1 ± 5.5	427.7 ± 55.6	123.4 ± 7.6	1.5	1.8	0.4	1.5	Family house	1960	Slate and tile	Wooden beam	Adobe
STN21AD	2207291	6125248	305 6.5 341	56.0 ± 4.3	47.1 ± 6.5	533.5 ± 34.5	41.8 ± 2.6	2.9	4.8	0.4	2.0	Family house	1916	Tile	Wooden beam	Bricks
STN22AD	2211559	6126111	322	-	-	-	-	2.0	0.4	0.4	1.6	Family house	1950	Slate	Wooden beam	Mixed wood, cement bricks
STN23AD	2208265	6126797	284	-	-	-	-	2.1	1.1	0.6	1.4	Family house	2005	Tile	Wooden beam	Mixed wood, cement bricks
STN24AD	2205113	6127722	276 1 205	17.9 ± 3.3	21.8 ± 8.2	522.8 ± 37.7	100.5 ± 5.6	1.4	2.7	0.3	1.3	Family house	1970	Slate	Wooden beam	Blocks
STN25AD	2210931	6130914	492 1.7 265	31.0 ± 4.5	37.1 ± 8.9	568.6 ± 41.2	159.6 ± 8.4	2.0	3.4	0.6	0.9	Church	1930	Metal	Wooden beam	Bricks
STN26AD	2210963	6131022	496 3 261	21.8 ± 2.4	24.5 ± 5.0	395.6 ± 25.7	41.3 ± 2.2	1.6	3.8	0.5	0.9	Family house	1920	Metal	Wooden beam	Bricks
STN27AD	2206333	6126840	331		16.3	537.6	90.3	2.4	1.8	1.2	1.8	Family house	1940	Tile		Adobe

			2.5 90	18.1 ± 3.4	± 5.3	± 38.2	± 5.2								Wooden beam	
STN28AD	2201138	6123143	275 1.8 209	12.0 ± 6.0	24.5 ± 7.6	524.6 ± 38.5	51.0 ± 3.3	2.2	3.3	0.5	1.3	Church	1934 (2013)	Slate	Wooden beam	Wood and bricks
STN29AD	2202141	6121341	245 1.4 203	15.7 ± 5.3	18.8 ± 7.4	417.6 ± 30.3	117.8 ± 6.6	1.7	3.0	0.4	1.4	Family house	1936	Tile	Wooden beam	Bricks
STN30AD	2200930	6120839	253 4.5 80	38.7 ± 5.4	28.7 ± 9.2	477.4 ± 38.8	70.7 ± 4.5	2.1	3.0	0.5	1.4	Family house	1950	Slate	Wooden beam	Wood and bricks
STN31AD	2205184	6121852	267 2.8 56	85.5 ± 7.4	47.0 ± 13.1	607.7 ± 49.9	77.1 ± 5.1	2.2	4.1	0.4	1.5	Family house	1910	Slate and wood	Wooden beam	Blocks
STN32AD	2206954	6121042	412 5.6 284	92.5 ± 7.8	42.8 ± 12.4	563.6 ± 45.8	165.8 ± 8.9	2.4	2.4	0.4	1.9	Family house	1900	Tile	Wooden beam	Bricks
STN33AD	2205060	6120675	299 6.2 74	13.6 ± 3.8	21.2 ± 9.4	411.4 ± 35.2	137.8 ± 7.9	1.9	2.2	0.5	1.8	Family house	1955	Tile	Wooden beam	Bricks
STN34AD	2201280	6119441	261 7.8 303	42.8 ± 6.5	30.3 ± 13.6	514.6 ± 48.9	169.3 ± 9.4	2.0	2.2	0.6	1.5	Family house	1936	Tile	Wooden beam	Adobe
STN35AD	2209100	6126310	306 5.3 213	143.5 ± 8.1	94.3 ± 9.6	649.9 ± 43.2	41.6 ± 2.5	5.6	10.5	0.6	3.2	Family house	1946	Slate	Wooden beam	Bricks
STN36AD	2209873	6126154	306 2.8 254	63.5 ± 5.9	63.1 ± 11.2	649.8 ± 47.8	87.3 ± 5	3.6	6.0	0.6	2.4	Family house	1940	Tile	Wooden beam	Brick and blocks
STN37AD	2203389	6122568	253 3.9 66	69.2 ± 5.2	44.1 ± 7.8	559.9 ± 38.2	124.7 ± 6.5	3.2	4.0	0.5	1.7	Family house	1961	Tile	Wooden beam	Bricks
STN38AD	2203483	6121767	245 3.9 284	35.3 ± 3.5	39.0 ± 7.8	510.0 ± 36.0	73.9 ± 4.3	1.7	3.5	0.3	1.4	Family house	1880 (1984)	Tile and wood	Wooden beam	Bricks

STN39AD	2202896	6118359	237 4.9 301	32.6 ± 3.4	32.6 ± 6.7	530.0 ± 33.8	93.6 ± 5.0	1.5	2.6	0.4	1.2	Family house	1880	Tile	Wooden beam	Adobe
STN40AD	2202031	6117952	230 2.7 71	27.2 ± 4.0	27.7 ± 8.4	1382.3 ± 77.6	149.0 ± 7.7	2.2	1.7	2.7	1.4	Family house	1964 (1991)	Tile	Wooden beam	Blocks

***the height of building (m) is added; ** Slope of the ground below the building; *** renovation; dl: detection limit of ^{226}Ra: 0.9 Bq kg^{-1}**

Urban soil	X	Y	Elevation, m	^{226}Ra	^{232}Th	^{40}K	^{137}Cs	U	Th	K	Cs	Category	Corresponding attic dust samples
STN01US	2206295	6125443	271	-	-	-	-	1.2	4.4	0.2	1.3	Kindergarten	
STN02US	2204899	6123866	257	-	-	-	-	1	4.9	0.3	1.1	Kindergarten	
STN03US	2205347	6124348	275	-	-	-	-	1.5	4.4	0.2	1.1	Kindergarten	
STN04US	2204508	6122794	241	-	-	-	-	0.9	3.9	0.2	1.0	Kindergarten	
STN05US	2202284	6119139	235	-	-	-	-	0.7	3.7	0.3	1.1	Kindergarten	
STN06US	2201685	6122038	244	18.2 ± 1.2	21.7 ± 2.4	357.8 ± 8	4.7 ± 0.4	0.9	4.4	0.2	1.0	Kindergarten	STN05AD
STN07US	2204494	6126513	305	-	-	-	-	0.7	5.6	0.2	1.3	Kindergarten	
STN08US	2205317	6127822	274	-	-	-	-	0.8	4	0.2	1.2	Playground	
STN09US	2204580	6127284	265	36.2 ± 1.5	48.8 ± 3.6	412.9 ± 8.8	6.3 ± 0.5	1.8	5.4	0.3	1.9	Park	STN06AD
STN10US	2210918	6127582	336	-	-	-	-	0.8	2.9	0.2	0.9	Playground	
STN11US	2210741	6128060	356	19.7 ± 1.3	28.0 ± 2.5	391.9 ± 8.1	6.5 ± 0.5	0.7	3.4	0.3	1.3	Park	STN09AD
STN12US	2210769	6127625	340	21.3 ± 1.4	26.5 ± 3.9	363.7 ± 9.0	7.4 ± 0.3	0.8	2.9	0.2	1.0	Kindergarten	STN08AD
STN13US	2203061	6125110	281	27.2 ±	42.8 ±	447.7 ±	3.1 ±	0.8	6.2	0.4	1.7	Kindergarten	STN10AD

				1.3	3	8.4	0.4						
STN14US	2207036	6125265	313	-	-	-	-	1.5	3.8	0.3	1.1	Playground	
STN15US	2204580	6124278	245	15.0 ± 1.3	25.0 ± 3.5	403.0 ± 8.4	2.7 ± 0.5	0.9	3.6	0.2	1.2	Playground	STN02AD
STN16US	2206684	6124811	297	33.2 ± 1.9	35.6 ± 6	347.5 ± 10.6	2.7 ± 0.7	1.2	4.5	0.3	1.3	Playground	STN21AD
STN17US	2205053	6123296	269	-	-	-	-	0.7	4.5	0.2	1.3	Playground	
STN18US	2205540	6121050	281	-	-	-	-	1.6	4	0.2	1.3	Others (cemetery)	
STN19US	2214540	6127535	492	24.8 ± 1.4	38.8 ± 2.9	404.3 ± 8.7	13.6 ± 0.6	1.8	3.9	0.3	1.1	Park	STN17AD
STN20US	2213437	6127905	540	30.4 ± 1.6	40.5 ± 5	428.5 ± 10.7	17.3 ± 0.4	1.2	3.3	0.2	1.0	Playground	STN20AD
STN21US	2211549	6125012	377	33.7 ± 1.4	34 ± 3.9	344.8 ± 9.2	7.8 ± 0.3	1.5	3.7	0.3	1.2	Others (roadside)	STN18AD
STN22US	2208343	6126379	394	24.5 ± 2.8	26.9 ± 0.7	355.7 ± 7.2	1.1 ± 0.2	0.8	4.6	0.3	1.2	Others (roadside)	
STN23US	2210832	6130849	482	17.7 ± 1.2	18.9 ± 2.3	373.2 ± 7.5	4.6 ± 0.4	1.2	4.3	0.2	1.1	Playground	STN25AD
STN24US	2203286	6122674	252	-	-	-	-	1	3.6	0.2	1.1	Playground	
STN25US	2201596	6119873	232	17.0 ± 1	26.3 ± 2.1	391.4 ± 7	2.3 ± 0.4	1.1	4.3	0.3	1.1	Playground	STN34AD
STN26US	2201146	6124102	262	-	-	-	-	0.9	4.8	0.2	1.2	Other (roadside)	
STN27US	2201139	6120790	244	-	-	-	-	1.2	4	0.4	1.5	Park	
STN28US	2207146	6121173	400	21.1 ±	34.9 ±	397.6 ±	12.8 ±	1.0	2.8	0.3	0.9	Playground	STN32AD

				1.2	2.3	7.3	0.5						
STN29US	2209527	6126021	293	38.3 ± 1.4	46.0 ± 2.6	385.4 ± 7.7	4.3 ± 0.5	2.3	5.8	0.4	1.8	Playground	STN35AD
STN30US	2202829	6124566						0.9	3.6	0.23	0.95	Others (roadside)	
STN31US	2208334	6127451	331	26.4 ± 3.3	22.3 ± 0.6	355.5 ± 10.3	0.7 ± 0.2	0.8	3.2	0.3	1.0	Others (garden)	
STN32US	2206997	6126439	274	27.2 ± 2	37.0 ± 7.4	398.6 ± 11.9	1.6 ± 0.8	1.3	5.4	0.3	1.2	Park	STN27AD
STN33US	2202802	6121139						0.9	4.8	0.3	1.1	Others (roadside)	
STN34US	2203747	6120914	245	21.3 ± 1.4	28.1 ± 3.7	409.8 ± 9	3.5 ± 0.5	1.0	4.6	0.3	1.1	Others (roadside)	STN38AD
STN35US	2202642	6118268						1.4	5.1	0.27	1.03	Others (roadside)	
STN36US	2202135	6117791	231	23.9 ± 1.1	41.4 ± 2.4	371.8 ± 6.9	3.5 ± 0.4	0.6	6.5	0.2	1.2	Others (cemetery)	STN40AD
Brown forest soil (BFS)	2200292	6131104	249	14.1 ± 1.3	16.7 ± 2.3	318.8 ± 9	18.4 ± 0.6	1.0	3.0	0.2	2.1	Undisturbed soil	
Coal ash (CA)	2210737	6125749	351	91.1 ± 1.7	69.5 ± 3.3	414.4 ± 8.9	0.09 ± 0.4	6.3	12.8	0.5	2.7	Production of “CFPP”	

Table S. 2. Results of elemental (U, Th, K, Cs) and activity concentrations (^{226}Ra, ^{232}Th, ^{40}K, ^{137}Cs) in Ózd attic dust (n=42), urban soil (n=56), brown forest soil (n=1) and smelter slags 1 and 2 samples, categories of sampling sites and their locations (x, y), elevation (m), characteristics of houses

Attic dust	**Coordinates of the sampling locations (X, Y) meter**			**Activity concentration (Bq kg^{-1})**				**Elemental concentration (mg kg^{-1})**				**Category of sampling sites**	**Characteristics of houses**			
	X	**Y**	**Elevation, m* **Slope° Terrain aspect°**	**^{226}Ra**	**^{232}Th**	**^{40}K**	**^{137}Cs**	**U**	**Th**	**K**	**Cs**		**Year of built**	**Roof type**	**Sampling surface**	**Construction material**
OZD01AD	2255695	6141110	179 7.2 297	52.2 ± 0.8	23.5 ± 2.1	483.6 ± 31.6	93.3 ± 4.7	1.5	2.1	0.4	1.8	Priest house	1897	Metal	Wooden beam	Bricks
OZD02AD	2251528	6145835	180 1.1 97	63.3 ± 0.6	27.1 ± 3.4	595.2 ± 37.5	74.1 ± 3.8	1.8	2.2	0.6	1.7	Priest house	1950	Slate	Wooden beam	Bricks
OZD03AD	2259744	6142814	173	-	-	-	-	2.1	1.8	0.3	3.6	Family house	1903	Tile	Wooden beam	Bricks
OZD04AD	2253809	6152311	196	-	-	-	-	1.9	1.7	0.5	1.3	Family house	1929	Tile	Wooden beam	Adobe
OZD05AD	2256881	6147495	185	-	-	-	-	1.8	1.5	0.3	2.4	Family house	1963	Tile	Wooden beam	Bricks
OZD06AD	2259419	6142538	192 1.1 163	31.0 ± 0.9	16.3 ± 1.6	225.5 ± 20.1	51.3 ± 2.7	2.2	2.2	0.2	4.0	Church	1903	Slate	Wooden beam	Bricks
OZD07AD	2259447	6142525		-	-	-	-	2	2.5	0.4	3.3	Family house	1900	Slate	Wooden beam	Bricks
OZD08AD	2262064	6145264	179 5.6 141	19.5 ± 1.3	14.3 ± 1.4	278.6 ± 18.6	39.7 ± 2.0	2.2	1.6	0.4	2.8	Priest house	1790	Tile	Wooden beam	Bricks
OZD09AD	2258941	6147392		-	-	-	-	1.9	1.6	0.6	2.4	Family house	1947	Metal	Wooden beam	Bricks
OZD11AD	2261619	6146517		-	-	-	-	1.8	1.4	0.5	3.1	Kindergarten	1962	Metal	Wooden beam	Bricks

OZD12AD	2257715	6142207		-	-	-	-	2.1	2.8	0.4	3.4	Family house	1980	Tile	Wooden beam	Bricks
OZD13AD	2261332	6145778	165 2.3 106	42.5 ± 0.5	20.4 ± 3.0	375.7 ± 28.2	100.8 ± 5.2	1.9	1.8	0.4	2.4	Blockhouse	1920	Tile	Wooden beam	Bricks/Adobe
OZD14AD	2261910	6145226	170 3.1 106	38.4 ± 1.6	14.4 ± 6.6	322.6 ± 24.8	72 ± 3.6	2.4	1.9	0.3	3.2	Blockhouse	1874	Tile	Wooden beam	Adobe
OZD15AD	2258591	6144336	135 3.1 228	45.5 ± 1.3	18.6 ± 3.9	334.8 ± 26.0	62.8 ± 3.3	2.8	2.2	0.3	3.2	Blockhouse	1957	Tile	Concrete beam	Concrete
OZD17AD	2256280	6148391	174 1.6 235	< dl	21.2 ± 6.9	570.2 ± 41.1	95.1 ± 5.0	1.0	0.2	0.8	2.1	Family house	1903	Tile	Wooden beam	Bricks
OZD19AD	2259019	6146228	186 2 158	11.0 ± 3.4	14.7 ± 3.0	314.9 ± 24.8	120.9 ± 5.9	1.7	1.1	0.4	2.4	Family house	1957	Tile	Wooden beam	Brick/concrete
OZD20AD	2257365	6137842	202 3.1 265	50.8 ± 1.1	12.4 ± 1.7	230.1 ± 23.3	93.3 ± 4.8	1.3	1.0	0.4	1.9	Kindergarten	1890	Wood and tile	Wooden beam	Bricks
OZD21AD	2258354	6143257	186					1.7	2.6	0.5	2.9	Church	1967	Tile	Wooden beam	Bricks
OZD22AD	2256488	6143552	187 1.2 183	62.9 ± 0.7	20.2 ± 3.1	350.3 ± 26.8	129.1 ± 6.5	1.5	1.8	0.3	2.4	Blockhouse	1951	Tile	Wooden beam	Bricks
OZD24AD	2255745	6143560	200	-	-	-	-	1.8	1.9	0.4	2.6	Blockhouse	1961	Tile	Wooden beam	Bricks
OZD25AD	2255570	6143772	203 4 270	39.1 ± 1.1	20.0 ± 4.5	437.4 ± 31.1	223.4 ± 6.5	2.2	1.4	0.5	2.4	Blockhouse	1954	Tile	Concrete beam	Bricks
OZD26AD	2259310	6142306	184 3.4 193	18.6 ± 0.7	16.2 ± 2.4	300.8 ± 21.3	21.5 ± 1.4	1.8	2.2	0.3	2.6	Blockhouse	1926	Slate	Wooden beam	Bricks
OZD28AD	2259444	6142935	184 1.5 227	34.4 ± 0.5	16.6 ± 1.1	228.1 ± 15.6	28.3 ± 1.5	2.4	2.5	0.3	4.7	Blockhouse	1945	Slate	Concrete beam	Bricks

OZD30AD	2258192	6141031		-	-	-	-	2.1	2.6	0.7	5.0	Family house	1988	Tile	Concrete beam	Bricks
OZD33AD	2259208	6140130	197 3.8 47	49.5 ± 0.6	18.2 ± 2.4	429.0 ± 28.1	74.9 ± 3.8	1.8	1.8	0.6	2.6	Family house	1950	Slate	Wooden beam	Bricks
OZD34AD	2259394	6139765	205 7.2 54	<dl	14.8 ± 2.7	414.3 ± 27.8	85.5 ± 4.3	1.5	1.5	0.6	2.2	Family house	1930	Tile	Wooden beam	Bricks
OZD36AD	2250331	6144479	194					1.8	0.6	1.4	1.9	Family house	1912	Tile	Concrete beam	Bricks
OZD37AD	2252814	6145944	197 2.8 260	35.1 ± 3.3	21.9 ± 5.2	540.8 ± 38.9	238.6 ± 11.5	1.7	1.2	0.5	2.1	Family house	1970	Tile	Wooden beam	Bricks
OZD38AD	2253931	6145249	184					1	0.9	0.5	1.7	Family house	1960	Tile	Wooden beam	Bricks
OZD39AD	2254078	6145024	180					1.5	0.3	1.8	2.9	Family house	1960	Tile	Wooden beam	Wood and cement
OZD40AD	2256587	6145293	197 2.5 199	9.54 ± 2.8	13.4 ± 1.9	1493 ± 77.9	116.7 ± 5.7	2.1	0.7	3.3	1.8	Family house	1971	Tile	Concrete beam	Bricks
OZD41AD	2256470	6144713	170					1.6	2.1	0.4	2.6	Family house	1963	Tile	Wooden beam	Bricks
OZD43AD	2259908	6144774	165 4 117	30.9 ± 1.5	12.4 ± 2.1	264.1 ± 20.5	25.5 ± 1.6	2.4	2.1	0.3	3.2	Family house	1940	Tile	Wooden beam	Bricks
OZDAD 45UL	2259746	6143306	187 3.2 333	26.3 ± 2.5	26.3 ± 2.1	358.4 ± 25.9	1.9 ± 1.0	1.2	4.5	0.2	2.2	Blockhouse*[1]	1878	Metal	Iron beam	Bricks
OZDAD 45LL	2259746	6143306	187 3.2 333	28.3 ± 1.7	15.0 ± 2.0	144.7 ± 18.8	16.0 ± 1.4	2.6	2.2	0.2	4.7	Blockhouse*[1]	1878	Metal	Iron beam	Bricks
OZD46AD	2254672	6141007	114					1.3	1.5	0.5	1.7	Family house	1970			

OZD47AD	2255796	6140258	198 5.5 262	46.0 ± 2.2	15.3 ± 6.7	484.9 ± 36.2	272.8 ± 13.0	2.5	2.6	0.7	3.9	Family house	1978	Slate	Wooden beam	Bricks
OZD48AD	2256181	6139607	206					1.5	0.8	0.7	2.2	Family house	1960	Tile	Wooden beam	Bricks
OZD49AD	2257449	6138615	266 5.1 146	25.9 ± 3.1	9.5 ± 3.3	223.5 ± 23.2	71.4 ± 3.8	2.4	1.4	0.3	2.2	Family house	1978	Tile	Wooden beam	Bricks
OZD51AD	2259197	6135827	212 3.7 214	23.8 ± 5.2	12.5 ± 5.3	403.2 ± 32.7	71 ± 3.9	2.4	1.3	0.6	2.4	Family house	1920	Tile	Wooden beam	Bricks
OZD52AD	2255547	6142116	180 7.2 127	< dl	8.1 ± 3.3	80.50 ± 20.3	62.1 ± 3.4	1.7	0.9	0.2	1.5	Family house	1940	Tile	Wooden beam	Bricks
OZD53AD	2255540	6142086	211					1.5	1.6	0.5	2.3	Family house	1940	Tile	Wooden beam	Bricks
OZD54AD	2257283	6137854	215 0.9 173	2.6 ± 1.0	8.0 ± 6.2	508.8 ± 35.2	38.4 ± 2.6	0.5	0.9	0.9	0.7	Church	1945	Slate	Wooden beam	Cements

***the height of building (m) is added; ** Slope of the ground below the building; *** renovation; dl: detection limit of ^{226}Ra: 1.6 Bq kg^{-1}; *[1]Repair hall of the former iron and steel factory**

Urban soil	X	Y	Elevation /m/	^{226}Ra	^{232}Th	^{40}K	^{137}Cs	U	Th	K	Cs	Category	
OZD01US	2253761	6152297		-	-	-	-	1.1	2.3	0.3	0.6	Playground	
OZD02US	2251545	6145643		-	-	-	-	0.6	3.9	0.3	0.8	Playground	
OZD03US	2257529	6146357		-	-	-	-	0.9	4.9	0.3	0.9	Playground	
OZD04US	2255716	6145221		-	-	-	-	1.3	4.3	0.3	1.0	Playground	
OZD05US	2259398	6144606		-	-	-	-	0.8	4.1	0.3	1.2	Kindergarten	
OZD06US	2258461	6144457		-	-	-	-	0.9	4.5	0.3	1.0	Kindergarten	
OZD07US	2257807	6143243		-	-	-	-	0.8	4.5	0.4	1.5	Kindergarten	

OZD08US	2256842	6143276	-	-	-	-	0.8	4.7	0.3	1.2	Kindergarten	
OZD09US	2261655	6146522	-	-	-	-	0.7	2.8	0.3	1.1	Kindergarten	
OZD10US	2266044	6147857	-	-	-	-	0.5	3.3	0.2	0.9	Kindergarten	
OZD11US	2267029	6149626	-	-	-	-	0.8	4.4	0.2	1.2	Playground	
OZD12US	2262017	6144962	-	-	-	-	1	3.6	0.3	1.2	Kindergarten	
OZD13US	2259497	6142878	-	-	-	-	0.9	4.1	0.3	1.8	Kindergarten	
OZD14US	2259125	6141261	-	-	-	-	0.7	5	0.3	1.0	Kindergarten	
OZD15US	2255163	6144473	-	-	-	-	0.9	4.8	0.3	1.2	Kindergarten	
OZD18US	2262031	6145225	-	-	-	-	1	2.2	0.3	1.3	Kindergarten	
OZD19US	2256581	6140364	-	-	-	-	0.7	4.4	0.4	1.1	Kindergarten	
OZD21US	2256606	6147695	-	-	-	-	1.1	4.6	0.4	1.6	Playground	
OZD23US	2257314	6137806	-	-	-	-	0.8	3.2	0.2	1.0	Kindergarten	
OZD24US	2256547	6144114	-	-	-	-	0.6	4.1	0.3	0.8	Park	
OZD25US	2255840	6143477	-	-	-	-	1	4.3	0.2	1.0	Playground	
OZD26US	2257843	6142348	-	-	-	-	0.9	3.3	0.3	1.5	Playground	
OZD27US	2258871	6140636	-	-	-	-	0.8	4.5	0.3	1.3	Playground	
OZD28US	2258626	6146878	-	-	-	-	1	2.7	0.3	1.2	Playground	
OZD29US	2257907	6144972	-	-	-	-	1	3.7	0.2	1.14	Playground	
OZD30US	2260420	6146832	-	-	-	-	1.1	2.7	0.3	1.3	Playground	
OZD31US	2261028	6145562	-	-	-	-	2.1	3.5	0.2	1.3	Park	
OZD32US	2250339	6144503	-	-	-	-	0.7	5.4	0.3	1.2	Others	
OZD33US	2253214	6145830	-	-	-	-	0.7	4.9	0.2	0.9	Others	
OZD34US	2253929	6145231	-	-	-	-	0.7	4	0.2	0.7	Others	
OZD35US	2254043	6144981	-	-	-	-	0.8	2.7	0.1	0.6	Others	
OZD36US	2256591	6145233	-	-	-	-	1.5	3.5	0.2	1.2	Others	
OZD37US	2260308	6143879	-	-	-	-	0.9	3.5	0.2	0.9	Others	
OZD38US	2259691	6143290	-	-	-	-	2.3	2.3	0.2	4.8	Others - old industry	
OZD39US	2258952	6135821	-	-	-	-	1.7	2.8	0.2	0.6	Playground	
OZD40US	2257200	6137918	-	-	-	-	3	2.6	0.2	0.4	Park	
OZD41US	2254898	6141678	-	-	-	-	0.8	4.2	0.2	0.9	Playground	

OZD42US	2255566	6141545	-	-	-	-	1.4	3.2	0.3	1.6	Playground	
OZD43US	2260285	6142847	-	-	-	-	0.8	3.7	0.2	1.0	playground	
OZD44US	2260669	6141970	-	-	-	-	4.2	3.3	0.2	1.0	Others - old industry	
OZD45US	2260232	6142983	-	-	-	-	0.7	3.7	0.4	1.1	Kindergarten	
OZD46US	2259317	6139915	-	-	-	-	1.1	3	0.2	0.4	Kindergarten	
OZD47US	2258647	6141308	-	-	-	-	0.8	3.9	0.3	1.0	Playground	
OZD48US	2258275	6136830	-	-	-	-	1	2.8	0.3	1.1	Others	
OZD49US	2256136	6139553	-	-	-	-	1.2	1.8	0.4	1.0	Others	
OZD50US	2255827	6139765	-	-	-	-	0.8	3.5	0.3	0.7	Others	
OZD51US	2253047	6152866	-	-	-	-	1.1	2.7	0.3	0.9	Park	
OZD52US	2257342	6147642	-	-	-	-	1	2.7	0.2	1.0	Others	
OZD53US	2259416	6145524	-	-	-	-	0.8	2.9	0.3	1	Others	
OZD54US	2266141	6149894	-	-	-	-	2.1	3.8	0.3	3.83	Others - new industry	
OZD55US	2264560	6147710	-	-	-	-	0.9	1.8	0.3	0.7	Others	
OZD56US	2263068	6145710	-	-	-	-	1	3.8	0.3	1.28	Others	
OZD57US	2262468	6146913	-	-	-	-	1.1	1.8	0.2	1.0	Others	
OZD58US	2261980	6143594	-	-	-	-	0.8	4.4	0.2	1.0	Others	
OZD59US	2254299	6140909	-	-	-	-	0.7	2.9	0.3	0.9	Others	
OZD60US	2257210	6138552	-	-	-	-	1.2	3.6	0.2	0.6	Playground	
Brown forest soil (BFS)							0.8	6.4	0.2	1.1	Undisturbed soil	
Smelter slag -1 (SS-1)							1.41	1	0.01	0.01	Production of iron/steel factory	
Smelter slag -2 (SS-2)							1.26	0.9	0.01	0.01	Production of iron/steel factory	

Table S. 3. Analytical precision calculated for studied elements (U, Th, K, Cs mg kg^{-1})and radionuclides (^{226}Ra, ^{232}Th, ^{40}K, ^{137}Cs) from duplicates of 6 Salgótarján attic dust, 3 Salgótarján urban soils, 6 attic dust from Ózd and 5 Ózd urban soil samples.

	Salgótarján attic dust						**Salgótarján urban soil**				
Elemental concentrations mg kg^{-1}											
	05AD	17AD	18AD	26AD	36AD	38AD	06US	12US	28US		
U	6.9	9.7	8.3	8.3	1.9	13.6	0.0	8.3	0.0		
Th	1.8	5.4	8.3	1.8	6.1	8.5	6.7	13.3	5.2		
K	15.7	0.0	7.5	1.0	6.4	2.1	0.0	3.0	15.0		
Cs	5.2	5.6	3.5	3.0	1.7	6.0	2.0	4.1	16.3		
Activity concentrations Bq kg^{-1}											
^{226}Ra	3.6	41.6	40.8	19.4	17.7	13.9					
^{232}Th	18.9	36.8	16.0	8.9	12.7	12.9					
^{40}K	8.6	11.3	3.2	31.9	24.8	1.0					
^{137}Cs	11.6	43.5	34.1	18.1	23.5	11.9					
	Ózd attic dust						**Ózd urban soil**				
Elemental concentrations mg kg^{-1}											
	02AD	13AD	15AD	28AD	43AD	45AD	02US	13US	15US	28US	43US
U	0.0	3.6	10.0	13.0	4.9	19.0	0.0	3.6	10.8	0.0	16.4
Th	11	14	10.0	1.5	0.0	0.0	11.7	14.1	10.3	5.4	0.0
K	2.5	5.8	10.0	2.3	1.0	2.2	2.5	5.8	10.8	2.4	9.4
Cs	0.0	4.8	3.6	8.1	0.0	0.0	0.0	4.8	3.6	1.5	2.0

Table S. 4. Estimated gamma dose rate D (nGy h^{-1}), annual effective dose E (mSv y^{-1}), in the study area based on the results for the activity concentrations of ^{226}Ra, ^{232}Th, ^{40}K, and ^{137}Cs in attic dust and urban soil, brown forest soil and coal ash samples.

Attic dust (n=36)	**Absorbed gamma dose rate (nGy h^{-1})**	**Urban soil (n=19)**	**Absorbed gamma dose rate (nGy h^{-1})**	**Annual effective dose E (mSv y^{-1})**
STN01AD	55	STN06US	37	0.05
STN02AD	57	STN09US	64	0.08
STN03AD	70	STN11US	43	0.05
STN04AD	46	STN12US	42	0.05
STN05AD	70	STN13US	58	0.07
STN06AD	80	STN15US	39	0.05
STN07AD	67	STN16US	52	0.06
STN08AD	101	STN19US	54	0.07
STN09AD	59	STN20US	59	0.07

STN10AD	38	STN21US	51	0.06
STN12AD	47	STN22US	43	0.05
STN13AD	63	STN23US	36	0.04
STN14AD	55	STN25US	40	0.05
STN15AD	22	STN28US	49	0.06
STN16AD	51	STN29US	62	0.08
STN17AD	126	STN31US	41	0.05
STN18AD	152	STN32US	52	0.06
STN20AD	68	STN34US	44	0.05
STN21AD	82	STN36US	52	0.06
STN24AD	56			
STN25AD	80			
STN26AD	47			
STN27AD	52			
STN28AD	49			
STN29AD	51			
STN30AD	64			
STN31AD	103			
STN32AD	113			
STN33AD	53			
STN34AD	81			
STN35AD	156			
STN36AD	105			
STN37AD	97			
STN38AD	70			
STN39AD	68			
STN40AD	105			
Brown forest soil (BFS)	32	0.04		
Coal ash (CA)	101	0.12		
UNSCEAR recommended value, outdoor	59			

Supplementary figures

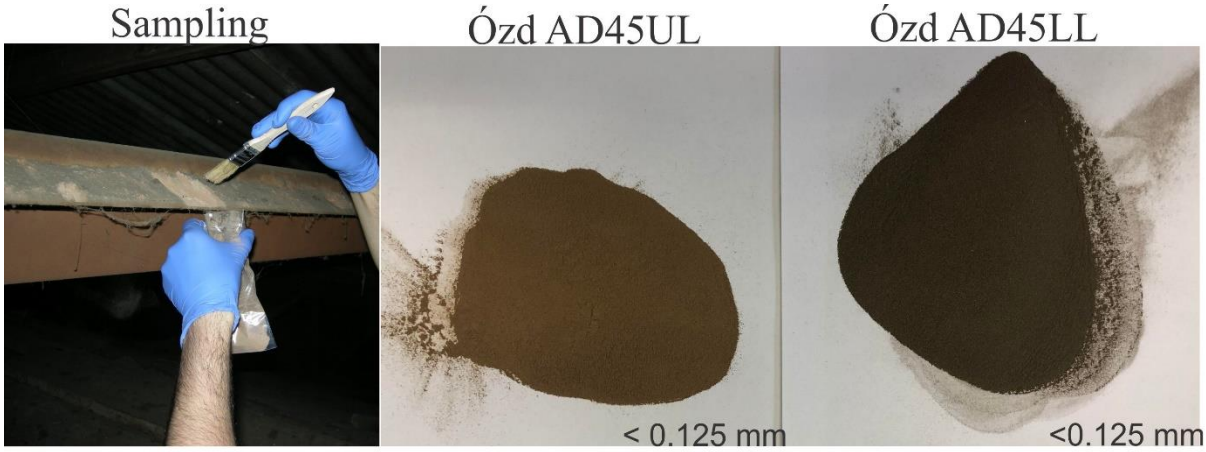

Figure S. 1. (A) Collection of layered dust sample in Ózd at the former industrial district, (B) upper layer. (OZD45ADUL) and (C) lower layer (OZD45ADLL) after sieving (<0.125 μm).

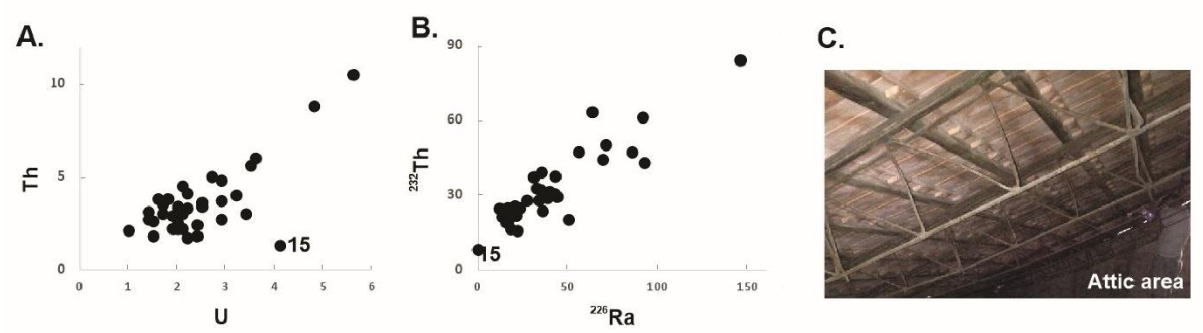

Figure S. 2. **(**A) Variation of Th vs. U (mg kg^{-1}) and (B) of ^{232}Th vs. ^{226}Ra (Bq kg^{-1}) in Salgótarján attic dust samples. Note the 15AD sample is highly distinct in elemental (A) and in activity concentration values (B) compared to the other STN attic dust samples. (C) STN15 attic space having unusual iron timber at sampling site. This attic area was also unexpectedly frequently cleaned by residents.

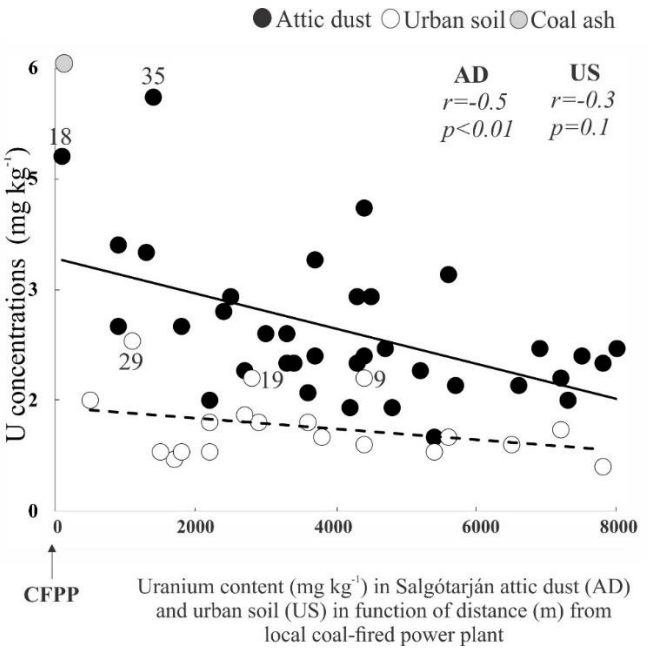

Figure S. 3. Relationship between U content (mg kg^{-1}) in attic and urban soil in function of distance from coal-fired power plant.

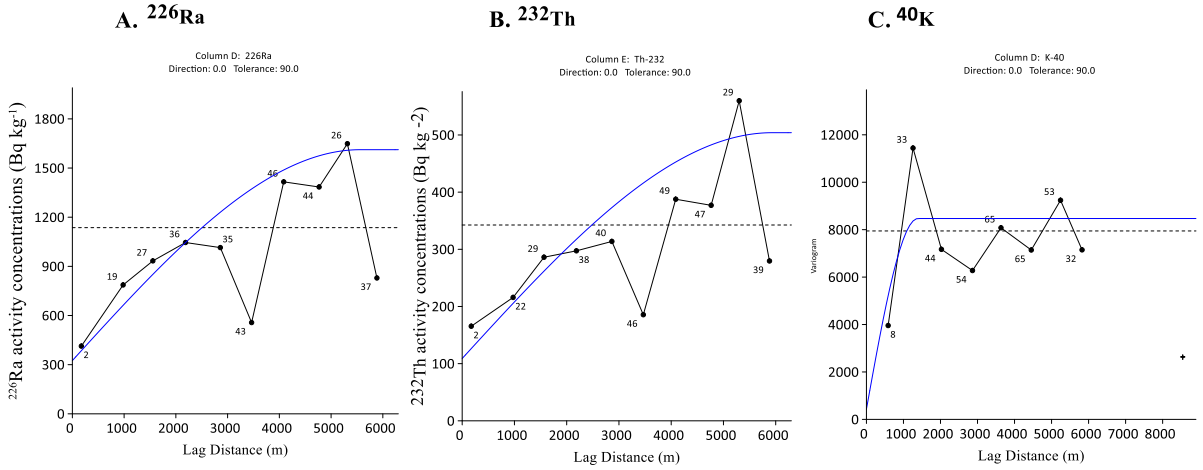

Figure S. 4. Fitted topography of studied Salgótarján urban area maps using attic dust samples (n=36) for the kriging methodology. The empirical (black dotted line) and fitted spherical semivariogram (blue line) derived ^{226}Ra, ^{232}Th and ^{40}K from activity values for Salgótarján attic dust. For Salgótarján the parameters of the spherical semivariogram model are *C_0 = 325; C_0 + C = 1287; ae = 5.5 km; r^2 = 0.4; RSS = 924360 (**A**); for ^{232}Th, C_0 = 109; C_0 + C = 398; ae = 5.9 km; r^2 = 0.5; RSS = 70705* (***B***) and *C_0 = 430; C_0 + C = 8040; ae = 8.9 km; r^2 = 0.3; RSS = 1.23E+0.7 (**C**)*. Numbers next to values of the empirical semivariogram (black numbered dots) represent the data pairs within a given distance The bin width was uniformly 630 m with a maximum lag distance of 6.3 km for ^{226}Ra and ^{232}Th and bin width was uniformly 890 m with a maximum lag distance of 8.9 km for ^{40}K. The dashed line indicates the variance.

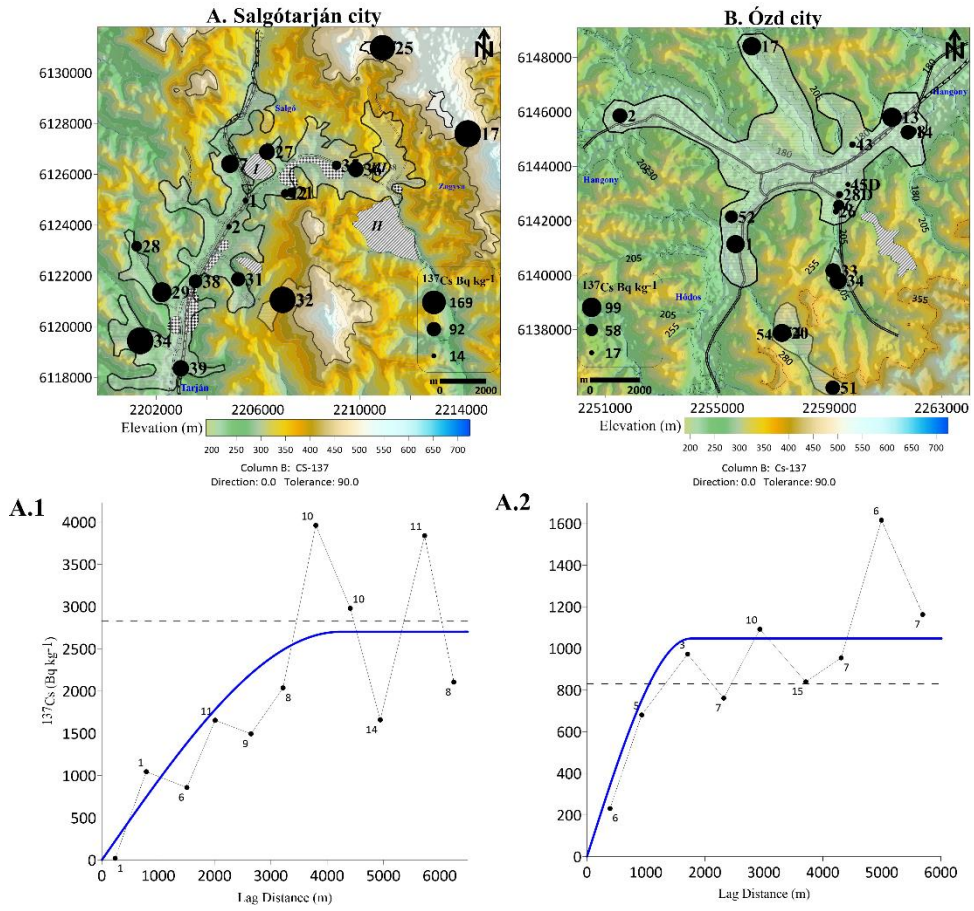

Figure S. 5. Fitted topography of studied urban area maps for the kriging methodology. The diameters of filled circles are proportional to ^{137}Cs activities (A and B), with labels; blue lines: creeks (map projection: EPSG:3857, WGS 84/Mercator projection (m)). The empirical (black dotted line) and fitted spherical semivariogram (blue line) derived from 137Cs activity values for Salgótarján (A.1) and Ózd (B.1). For Salgótarján, the parameters of the spherical semivariogram model are C0 = 1; C0+C = 2672; a = 4.2 km; r^2 = 0.72 (A.1); for Ózd, C0 = 1; C0+C = 1048; a = 1.7 km; r^2 = 0.51 (B.1). Numbers next to values of the empirical semivariogram (black numbered dots) represent the data pairs within a given distance; bin width was 590.9 m for Salgótarján and 610.0 m for Ózd. Max lag distances were 6500 m and 6010 m for Salgótarján and Ózd, respectively. The dashed line indicates the variance.